UNIVERSITÀ DEGLI STUDI DI NAPOLI FEDERICO II

Fundamentals of cell opening in polymer foaming

A dissertation submitted for the degree of Doctor of Philosophy in
Materials and Structures Engineering
coordinated by Professor Giuseppe Mensitieri

Daniele Tammaro

Tutors
Professor Ernesto Di Maio, Professor Pier Luca Maffettone, Professor Nino Grizzuti

March 2016

Contents

Abstract

Polymeric foams are ubiquitous in foods and industrial manufacturing. Since, they are used in a number of applications as thermal and acoustic insulators, in some cases it is desirable to create foams with cells not interconnected (i.e. closed cells), while in others cases an efficient interconnections between cells (i.e. opened cells) is required, as instance for culture substrates for living cells. In both cases, a fundamental understanding of the physics governing the cell opening process is needed to improve the final product and reduce the polymeric manufacturing cost.

In this dissertation, the physical mechanisms leading to cell opening in foams is investigated from a fundamental point of view. As such, the complex foaming process (i.e. involving different physical mechanisms) was studied with a bottom-up process, dividing it in four elementary steps namely: 1) cells growth, 2) cells interaction, 3) rupture and 4) retraction of the cells walls. Different experimental techniques are employed in this thesis; most of them were designed during the Ph.D. to reproduce particular experimental conditions, which are difficult to be obtained with typical foaming equipment. In fact, different new experimental apparatus were developed (i.e. Mini-batch, Interfacial bubble, Breaking bubble) and specifically designed to make unique measurements. The new apparata are particularly useful for testing theoretical predictions on some types of simplified systems useful for the study of the foaming process.

The main and novel result of this thesis is the fundamentals understanding of the entire foaming process that leads to a fundamental comprehension of how to produce a particular foam morphology, called *fully opened cell*. In the literature, there was not fundamentals understanding of the mechanisms behind the cell opening in thermoplastic foaming, since the reported foaming models stop the modeling at the rupture event in the cell walls, without considering the retraction event of the produced hole. The introduction of the retraction as the fundamental step to produce a fully open cell morphology is the novelty of this thesis. Moreover, the comprehension of the retraction step, leads to us to identify the importance of the role of the viscoelasticity for making a fully opened cell foam, that is a new concept that is unique and it was not covered earlier in the previous literature. Moreover, a model of the entire foaming process was developed and it was identified a criterion that employs the computed stresses, the elongational rate and the film thickness among the bubbles to predict the rupture of the polymeric layer between the bubbles and its retraction. As a result, the foaming process model is able to make predictions on the final foam morphology, starting from any polymer/gas solution. Independent experiments to assess the validity of each step of the proposed approach

were performed. In conclusion, the developed methodology allows to design the materials and processing conditions to control foam morphology.

In the first part of this thesis, a general overview of the foaming process is supplied, focusing the attention on the crucial points of each foaming steps pointed out by the existent literature. The main part will be occupied by the contributions published during the years of this Ph.D. because they represent the steps ahead achieved with respect to the literature.

Chapter 1: Introduction

In this chapter introduces concepts, which will be used in Chapter 2-4 to describe the current state of the art in cell opening foaming and the results achieved during the Ph.D. In effect, the reader will be introduced to the polymer foaming science focusing the attention to a particular section of the wide world of the polymer foaming: the opened cell foams. In particular, the aim of this chapter is to answer to some basic questions like, what an opened cell foam is and how it is possible to produce it.

Moreover, the objective will be fully clarified in the second paragraph and a general overview of the all manuscript will be given in the end of this chapter.

1.1 Opened cell foams and cell opening in foaming

Figure 1 compares typical microstructures of open- and closed-cell polymer foams, respectively, as seen in a scanning electron microscope (SEM). The good depth of focus allows complete cells to be seen in the interior of open-cell foams. Air can pass freely among the cells of such foams. In a typical closed-cell foamed thermoplastic, each cell is surrounded by connected faces. Partial cells, with cut faces and edges, are visible on the cut surfaces (Figure 1b), while complete cells exist in the interior of the sample. The cell faces, although thicker and stronger than those in closed-cell foams, can sometimes be split or otherwise damaged.

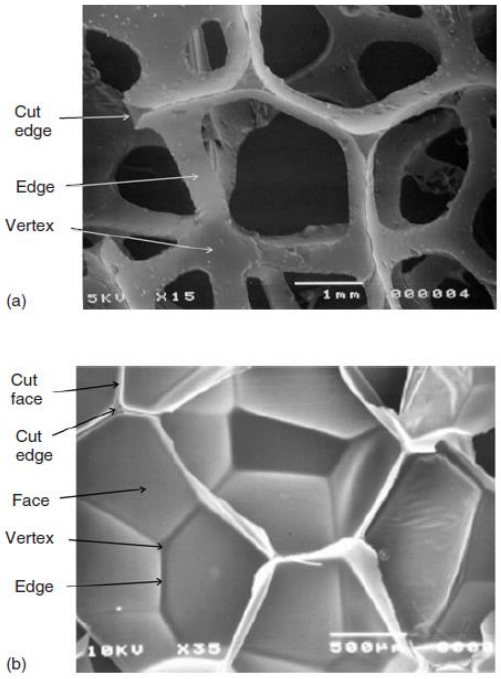

Figure 1: SEM photograph of (a) open-cell foam of density 28 kg/m^3, and (b) closed-cell foam of density 24 kg/m^3

Figure 2 shows stages in the development of foams:

(a) Isolated spherical bubbles grow in the liquid polymer. Spheres have the minimum surface area for a given volume, so the surface energy of the gas–liquid interface is minimised.

(b) When bubbles touch, their shapes distort. Equal size bubbles, packed in a face centred cubic (FCC) array, would touch when R = 0.26. Bubbles with a distribution of sizes, pack to a slightly higher density before they touch. In this wet closed-cell foam, thin, planar faces occur between the cells. Curved surfaces enclose liquid in the cell edges and vertices. The term wet was coined for soap froths, implying a significant water content. If the foam rises, while being constrained in width, the cell shapes to become anisotropic.

(c) In the limit as the foam relative density R → 0, the closed-cell foam becomes dry. This stage is never reached in polymer foams, but is a useful idealisation for modelling. When water drains from soap froths under gravity, the cell faces are stabilised by a bilayer of surfactant molecules, and the edges are of the same thickness as the faces.

(d) When the faces in a wet closed-cell foam collapse, an open-cell foam is formed. The polymerisation and crosslinking of the PU stabilise the edges and vertices.

(e) In soap froths and low viscosity polymers, the foam can collapse back to a liquid.

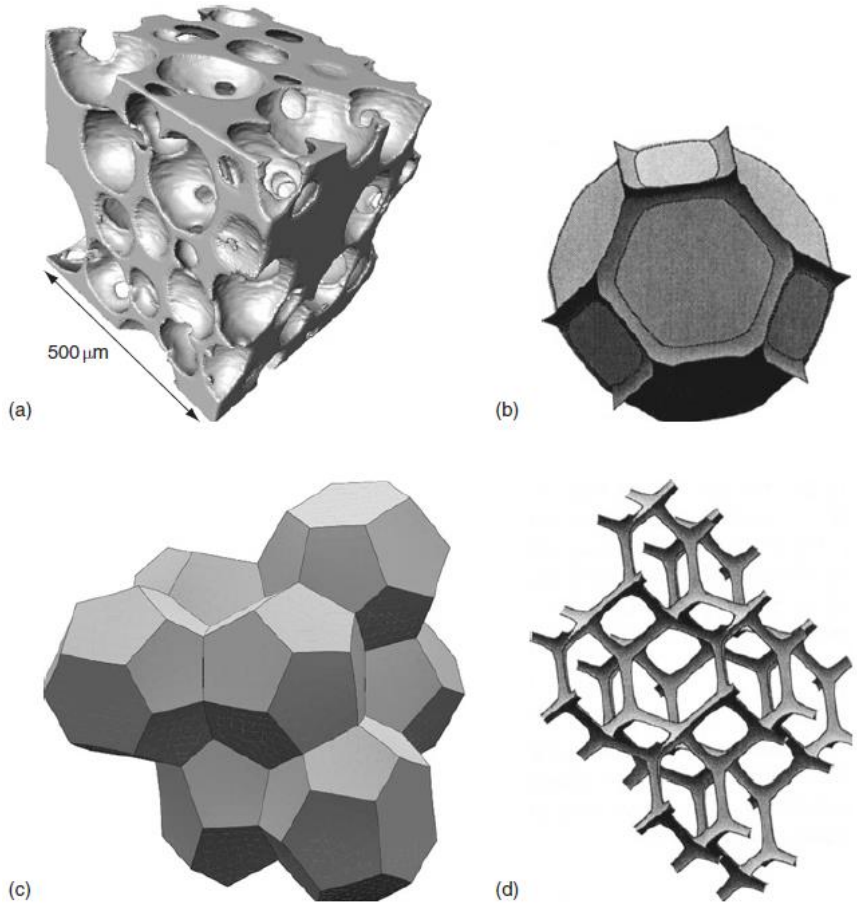

Figure 2: Stages in the development of foams: (a) isolated spherical bubbles [1], (b) a cell in a wet foam [2], (c) a dry Weaire–Phelan foam [3], and (d) an open-cell foam [4].

We will see in Chapter 2 that there are a lot of strategies to produce opened cell foams, and it will be clear that the great majority of foamed thermoplastics to be closed-cell because of the intrinsic properties of the these polymer respect to a typical polyurethane. In this thesis, for the first time with respect to the current foaming literature, it is presented a novel mechanism to help the cell opening in thermoplastic polymers.

Foam structures contain three main elements.

1) Foam – edges

Cell edges are usually straight in unloaded foams. In dry closed-cell foams, the edges have shrunk to lines; if the surface energy is minimised, three faces meet at each edge, with interface angle of 120°. In open celled foams the Plateau border edges have three cusps. The angles

between these cusps, seen along the edge, are close to 120° (Fig. 1a). The edges are usually relatively stubby, with lengths being only a small multiple of their width. The variation in edge width was characterised by Gong et al. [5]; there is a minimum value midway between vertices (Fig. 3). Edges are sometimes incorrectly described as struts; this implies that their main mechanical role is to resist axial compression, which is rarely the case. Plateau [6] described the shape of edges in soap froths, in which gravitational forces are negligible compared with the surface tension of the water–air interface (a constant). Minimisation of froth surface energy, hence minimisation of its surface area, determines the equilibrium shape of the liquid–gas interface. Since the viscosity of water is low ($1.5*10^{\wedge 3}$ Ns m^{-2}), a soap froth achieves its equilibrium geometry almost instantaneously. The cross-section of a Plateau border consists of three, touching, circular arcsine Smith [7] considered the shape of a second phase existing at the boundaries between three grains in a metal. He showed that the cusp angle θ at the corners, where the circular arcs met, was given by

$$\theta = 2 * cos^{-1}\left(\frac{\gamma_{\alpha\beta}}{\gamma_{gb}}\right)$$

where γ_{gb} and $\gamma_{\alpha\beta}$ are the surface energies of the grain boundary and the phase boundary, respectively. For open-cell foams γ_{gb} becomes the surface energy of the faces prior to collapse, and $\gamma_{\alpha\beta}$ the surface energy between the edge polymer and air. These two quantities should be equal, so θ should be 0°, as in a Plateau border. Open-cell foams have cusp angles θ < 10° [5].

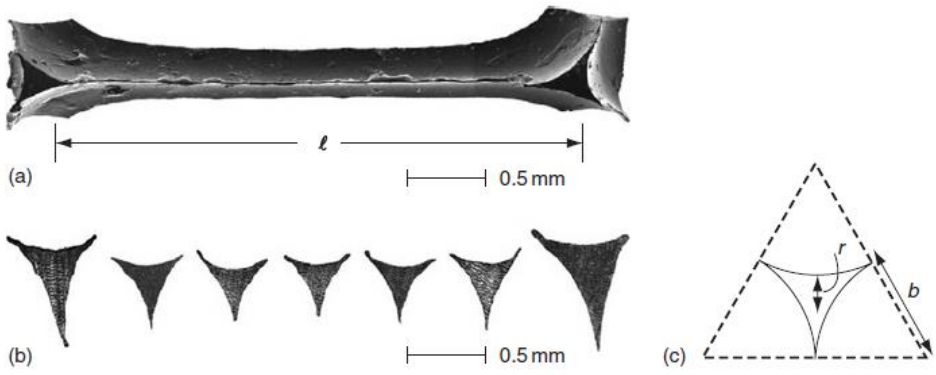

Figure 3: a) edge from a large cell size foam, b) section of the edge, c) idealised cross-section of a Plateau border.

2) Foam – vertices

Vertices connect edges in a similar way to cast metal nodes connecting tubes in a space–frame structure. Ideally, four cells and four edges meet at each vertex. Figure 4 shows a vertex and four half edges in a Kelvin foam, computed with the Surface Evolver software, available free from the University of Minnesota at www.geom.umn.edu/ software/ evolver/. The process starts with a dry Kelvin closed-cell foam. A command file, wetfoam.cmd, with an edge spread parameter (S), creates edges of constant isosceles-triangle cross-section; one side has length S/2 and the others are about (3/4) S/2. The value of S determines the foam relative density. The edge surfaces are tiled with a small number of triangular facets. A series of steps moves the locations of the facets to reduce the surface area of the foam, refines the triangular faces by dividing them into four, and calculates the minimum surface energy.

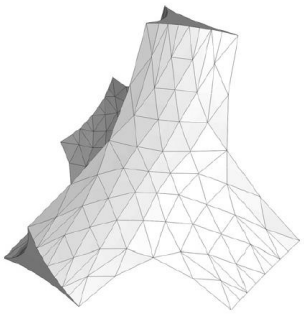

Figure 4: a vertex plus half of four edges, modelled using Surface Evolver software, with R = 0.0276

3) Foam – walls

In a foam, ususally, the face centres are thinner than the outer regions, and the thickness is typically about 1 μm. They behave as thin membranes, wrinkling under in-plane compressive forces. Rhodes et al. [8] used optical reflection microscopy to obtain interference fringes from the faces, hence the thickness distribution. Even here, the thinnest part is significantly thicker than a soap film face, which can be the length of two surfactant molecules. Faces are usually planar in undeformed polymer foams, since there is no pressure difference between the cells. SEM of some sectioned closed-cell thermoplastic foams shows that the face centres are thinner than the outer regions (Figure 5). However, there are no published thickness profiles. The face thicknesses are much greater than in foams, since the highly viscous polymer melt resists the effects of the extensional flow.

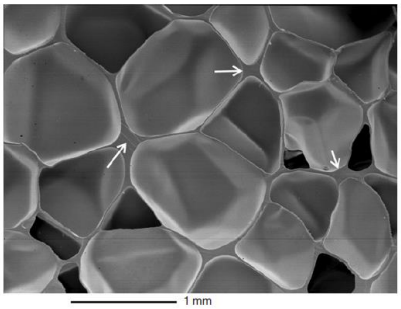

Figure 5: SEM of a closed cell foam of a high density polyethylene (HPDE) with higher order vertices arrowed, showing the variation of face thickness.

1.2 Objective of the thesis

In many industrial fields, open celled foams are used for their mass and energy transport, acoustic absorption, catalytic properties as well as templating structures for ceramic foams. They are also used in tissue engineering, as open celled foams serve as culture substrates for living cells. In the literature, there are many works on the relation among the processing parameters (e.g. saturation temperature and pressure and pressure drop rate) and the final foam morphology (e.g. open/ close celled foam) [9-15]. During my Ph.D., I conducted an extensive review of literature of the foaming mechanisms (focusing on the cell opening mechanisms), and I collaborated in a experimental study of the pressure drop rate effect on the foam morphology [16]. I believe, nevertheless, that there is a lack in the modeling of the whole foaming process, from nucleation and growth, to cell impingement, up to the opening of the cell walls. The goals of this thesis, that could be resumed with these two points:

- development of validated model of bubble growth, cell impingement and membrane rupture,
- design of experimental setups for the study of the foaming process of thermoplastic polymers with physical blowing agents, in order to validate the model developed.

In the recent years, a number of publication and review papers reported about the possible strategies to achieve cell opening, i.e. the rupture of the thin polymeric film dividing two growing bubbles. The strategies can be grouped in: a) achieving large volume expansion, b) using non-homogeneous melts by cross-linking, polymer blending, nucleating agent or crystallization and c) plasticization of the cell walls with a secondary blowing agent [17-20]. In the first strategy, the cell-wall thickness is brought to its limit by increasing the expansion ratio of the foam, while maintaining the molten, soft state of the polymer occupying the walls and

by avoiding gas loss by cooling down the external surface (skin) of the foamed part [11-12]. In the second strategy, a structural non-homogeneity, e.g. a hard/soft interface, is introduced in the expanding matter. In this context, Park et al. [11], for example, achieved a high open-cell content (up to 98%) with a low-density polyethylene/polystyrene blend. In this case, the soft sections easily opened up the cell walls during cell growth while the hard sections maintained the cell structure. Kohlhoff et al. [12] used an interpenetrating network structure to induce heterogeneities. Lee et al.[13] utilized two semi-crystalline polymers with different crystallization temperatures (T_c). In this case, at foaming temperatures intermediate between the two T_c's, the soft sections (i.e., the low-T_c polymer) would be almost liquid-like, and the hard sections (i.e., a high-T_c polymer) would be almost solid-like, and their interface becomes the weak point for cell opening. Miyamoto et al. [15] used a crystalline nucleating agent for polypropylene to form three-dimensional network of highly connected nano-fibrils by foaming, while Gong et al. [17] focused on the effect of different interfacial energies between two polymers forming the expanding blend to induce cell opening. In the third strategy, a secondary blowing agent, with a lower diffusivity into the polymer and, hence, longer diffusion time, induces a secondary bubble nucleation within the cell wall with consequent cell-opening [16].

In fact, while those strategies of cell wall rupture led to foams which, by definition, are open celled ones, a close observation of the foam morphology, and, in particular of the cell wall dividing two neighboring cells, usually still shows some presence of cell walls, yet broken. In this case, then, some of the properties may not conform to fully open celled foams, in which the polymer is solely confined to the struts. Figure 6 shows a clarifying example of a closed-celled foam, a closed celled foam with broken walls and a fully open celled foam.

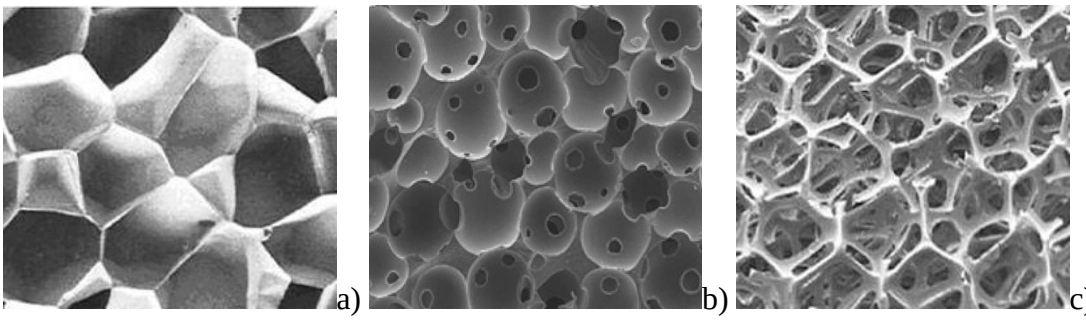

Figure 6: possible morphologies in thermoplastic foams: a) closed cells, b) open cells with plenty of polymer occupying open cell walls; c) fully open cells with polymer occupying the struts.

In order to have a fully open cell morphology where no material occupies the cell walls, then, it is not sufficient to produce a small hole or a fracture within the wall, even if the foam rise or bubble growth has not come to an end. In the latter case, the bubble growth continues to elongate the broken wall, with a corresponding increase of the hole size (like an affine deformation of the broken wall). To have a fully open celled foam, such as the one reported in Figure 6c, then, an additional mechanism has to be invoked, the *cell wall retraction*. In metallic foams, the low viscosity and high surface energy are straightforward conditions for wall retraction, which can be very fast and easy (see, for instance, Banhart, Metal Foams: Production and Stability, Advanced Engineering Materials, (2006) 781–794). In thermoplastic polymers, conversely, the large viscosity and the low surface tension often limit cell wall retraction, thereby allowing the observation of morphologies such as the one reported in **Figure** b.

In this thesis, a comprehensive analysis of the sequence of events leading to the formation of the foam and to the formation, rupture and retraction of the thin film separating the bubbles is accomplished. We gained, then, a complete picture of the cell opening phenomenon and the possibility to design the material and the process to drive the foam to a closed, partially open or fully open morphology. The approach has been tested on poly(ε-caprolactone), PCL, foamed with CO_2, and closed as well as open structures with material in the cell wall or solely in the struts, respectively, were achieved. The entire approach and the validation will be described in the first part of result section (Chapter 3).

The theoretical study of the cell opening foaming sequence was supported by experimental work to supply the input and the evidences to the model. In the second part of result section (Chapter 3), I will presents a novel batch foaming apparatus that possess *three important functions* to study the foaming process, namely: i) it allows a wide PDR range, in particular towards very high PDR; ii) it allows a very fast foamed sample extraction; iii) it has a view cell to observe the foaming "on air". Furthermore, it is very simple, cheap, versatile, since it allows multiple configurations, and environmentally friendly, for the very limited use of CO_2 and thermal energy for operation.

1.3 Overview of the thesis

The current thesis is divided in five Chapters named: introduction, background and focus of research, results and discussion, results and discussion: focus boxes, summary and conclusions.

In the first Chapter a brief introduction to the world of the polymer opened cell foams is given. The definition and all the general details of an opened cell foams are discussed in order to supply all the instruments to understand the following Chapters. Moreover, the mechanism of cell opening (i.e. the process leads to a typical opened cell structure) in thermoplastic and thermosetting polymers is explained. In the final part of the first Chapter, the objective of the thesis is described. In this part, it is clarified what kind of the foam is of the interest in the current thesis. A fully opened cell is defined and pointed out as the main objective of the current thesis work.

In the "background and focus of research" Chapter a complete analysis of the current literature concerning the cell opening field is discussed. All the technology utilized to obtain an open celled foam are described focusing the attention on the fully open celled foam. Then it is explained the lack in the current literature that concerns the study of the evolution of the hole in the cell wall after the rupture of itself. In the second part of the Chapter 2, how to model a foaming process is discussed. All the authors that studied the modeling of a foaming process are resumed and the lack of a complete model to predict a cell opening in thermoplastic foaming is evidenced.

In the Chapter 3, titled "results and discussion", the results of the complete modeling of the foaming process are reported using one of the publications born during this thesis work.

In the Chapter 4, titled "results and discussion, focus boxes", the results obtained in parallel with the development of the model are reported. In particular, all the supplementary works done in parallel with the main course of this thesis (i.e. the development of a validated modeling to predict cell opening in polymer foaming), required to complete the foaming modeling, were called *focus boxes*. Each one of these focus boxes lead to an independent publication resumed in the Chapter 4 with a proper expalnation.

In the "summary and conclusions" Chapter are resumed all the main results and conclusions of the current Ph.D. work.

1.4 References

[1] Kraynik A.D. & Warren W.E. (1994) The elastic behaviour of lowdensity cellular plastics, Chapter 7 in *Low Density Cellular Plastics*, Eds. Hilyard N.C. & Cunningham A., Chapman and Hall, London.

[2] Kraynik A.D., Reinelt D.A. & van Swol F. (2003) Structure of monodisperse foam, *Phys. Rev*. E **67**, 031403.

[3] Kusner R. & Sullivan J.M. (1966) Comparing the Weaire–Phelan equal-volume foam to Kelvin's foam, *Forma* **11,** 233–242.

[4] Weaire D. & Hutzler S. (1999) *The Physics of Foams*, Clarendon Press, Oxford.

[5] Gong L., Kyriakides S. & Jang W.Y. (2005) Compressive response of open-cell foams, Part 1. Morphology and elastic properties, *Int. J. Solid. Struct.* **42**, 1355–1379

[6] Plateau J. (1873) *Statique Experimentale et Theoretique des Liquides Soumis Aux Seules Forces Moleculaires*, Gauthier-Villars, Paris.

[7] Smith C.J. (1948) Grains, phases and interfaces, an interpretation of microstructure, *Trans. AIME* **175**, 17–51.

[8] Rhodes M.B. (1994) Characterizations of polymeric cellular structures, in *Low Density Cellular Plastics*, Eds. Hilyard N.C. & Cunningham A.C., Chapman & Hall, pp. 56–77.

[9] D. I. Collias and D. G. Baird, *Polym Eng. Sci*. 36, 1178 (1995).

[10] K. A. Seeler and V. Kumar, J. Rein *Plast. Compos*., 12 (3), 359 (1993).

[11] V. Kumar, M. VanderWel. J. Weller, and K. A. Seeler. *J. Erg. Mater. Techo*. L, 116 (4). 439.

[12] J. E Martini-Vvedensky, NP Suh, FA Waldman - *US Patent* 4,473,665, 1984.

[13] C. Marrazzo, E. Di Maio, S. Iannace, L. Nicolais, *Journal of Cellular Plastics*, 44 (2008) 37-52.

[14] C. Marrazzo, E. Di Maio, S. Iannace, L. Nicolais, *Journal of Cellular Plastics*, 43 (2007) 123-133.

[15] J.S. Colton, and N.P. Suh, *Polymer Engineering & Science* 27 (1987) 500–503

[16] S. Doroudiani, & M. T. Kortschot, (2003). *Journal of Applied Polymer Science*, Vol. 90, 1412–1420 (2003).

[17] V. Kumar, (2005). *Colloids and Surfaces* A: Physicochemical and Engineering Aspects.

[18] X. Han, K. W.Koelling, D. L. Tomasko, & J. L. Lee, (2002). *Polymer Engineering & Science*, 42(11), 2094–2106.

[19] C. Marrazzo, E. Di Maio, & S. Iannace, (2007). *Journal of Cellular Plastics*, 43(2), 123–133.

[20] K.Taki, (2008). *Chemical Engineering Science*, 63(14), 3643–3653.

[21] A. Salerno, E. Di Maio, S. Iannace, P.A. Netti (2011). *The Journal of Supercritical Fluids*, 58(1), 158–167.

Chapter 2: Background and focus of research

Since the introduction of plastic foams, there has been multitude of research studies by academia and industry to explore ways to improve the properties or processability of plastic materials and foaming technologies to produce foamed parts with better quality and characteristics. These research efforts have led to the widespread application of plastic foams, and also formed a valuable knowledge base that is key for the plastic foaming industry to overcome the previous, current, and future challenges, as well as for the scientific community to continue to advance our understanding in plastic foaming processes. In this context, this chapter serves as a thorough review of the previous theoretical studies of cell nucleation, growth, and deterioration phenomena via conceptual and analytical models, numerical simulation, and experimental visualization of these processes. In this Chapter 2, the current cell opening technologies and the modeling simulations are also reviewed to lay the foundation for the discussion of visualization system development in Chapter 3. In particular, the first paragraph reviews the methods used in polymers foaming to break the cell walls and the second paragraph reviews the different models developed in literature to predict the final foam morphology.

2.1 *Cell opening in current literature and the problem statement*

In the last decays, many novel technologies has been developed from an eco-friendly perspective, to substitute the polyurethane open-cell foams (that represent the current benchmarking) with thermoplastic foams with exceptionally high open-cell contents.

For instance, some open-cell thermoplastic foams have been created by leaching a soluble filler (i.e. salt and water soluble polymer) from a polymer matrix of polylactide (PLA) or polyethylene glycol (PEG) [1, 2]. Open-cell thermoplastic foams has also been produced by

polymer resin grafting [3]. However, these techniques cannot be used with industrial application and required a more process steps to reach the final result, respect to a gas foaming process.

The basic strategies for achieving a high open-cell content in a gas foaming process of a thermoplastic polymer are: a) cell-wall thinning by a high volume expansion ratio while maintaining soft cell walls and by a high cell-population density, b) a no-homogeneous melt structure by cross-linking, through polymer blending, nucleating agent or crystallization and c) plasticization of the soft region of the cell walls with a secondary blowing agent [4-10]. Many authors combined these three basic strategies to obtain an higher content of open-cell.

As first strategy, the cell-wall thickness could be decreased by increasing the expansion ratio of the foam while maintaining the soft noncrosslinked sections of the cell walls. For instance, this strategy could be realized submerging the foam extruded into a cold water bath right after a die exit for a short time. This process provided two main advantages for cell opening by (i) maintaining a hot core melt temperature of the foam. This high core temperature lowered the melt strength of the cell walls and thereby increased the chance of the cell opening, and (ii) lowering the foam skin temperature significantly. This prevented active gas loss through the skin. The entrapped gas was utilized to increase the internal gas pressure within the cells and, consequently, to rupture the cell walls in the interior of the extrudate [4-6].

The second strategy, a structural non-homogeneity, consists of hard and soft regions, in the polymer matrix was created by crosslinking. In this context, the most prominent results were due to Park et al. achieved a high open-cell content (up to 98%) with low-density polyethylene (LDPE)/polystyrene (PS) blend [7] as a first step inducing a hard/soft melt structure and then foaming this non-homogeneous melt structure. In particular, the soft sections was easily opened up the cell walls during cell growth while the hard sections formed the crosslink maintaining the cell shapes. Kohlhoff et al. used an interpenetrating network structure to increase the stiffness contrast between the domain and matrix [10]. The strategy of creating a structural non-homogeneity (i.e., hard/soft regions) in the melt was improved by Lee et al. instead of using cross-linking, two semicrystalline polymers with different crystallization temperatures (T_c) were melt-blended in order to maximize the stiffness contrast between hard and soft regions in the polymer matrix [9]. This means that, between two Tc values, the soft sections (i.e., a low-T_c polymer) would be almost liquidlike, and the hard sections (i.e., a high-T_c polymer) would be almost solidlike, creating a great stiffness contrast. Miyamoto et al. [11] used a crystalline nucleating agent for polypropylene to form three-dimensional network of highly connected nano-fibrils by foaming. Instead of making the clear contrast between soft and hard domains in

polymer blends, Gong et al. focused on the heterogeneous interface and interfacial properties between the two domains [13].

Usually, for thin samples it is difficult to control the skin temperature separately, however in these cases the third strategy con be used obtaining an high open-cell content. In fact, a secondary blowing agent affects the cell nucleation density, the plasticization effect and expansion ratio[8]. The expansion ratio is increased during foaming and thereby increase the overall open-cell content. Since cell opening starts to occur during the initial expansion stage, the expansion ratio may increase first and then decrease back due to fast gas loss with a high open-cell content. Thus, the final expansion ratio may not be elevated once the foam has a high open-cell content even. The secondary blowing agent, with a different diffusion time, permits to induce secondary nucleation and to change the cell density with a consequent increasing of open-cell content. Another cell-opening method, with two blowing agents, was reported by Krause et al. [12]. They prepared an open cellular polysulfone film using CO_2 and tethrahydrofurane (THF) as a blowing agent. During foaming, the cell wall thickness fluctuated, and the degree of fluctuation was facilitated by THF.

Even though these previous open-cell foams yielded high open-cell contents, it was observed under a scanning electron microscope (SEM) that most cell walls contained small 'pinhole' and/or 'partial' openings or pores between bubbles.

In the following all the possible choice used in literature will be resumed.

There are a number of possible design parameters from which to choose to produce open-cell polymeric foams. To better understand the design parameters which have been chosen it is helpful to remember the higher-level goal (DP, in this case) and means to that end (PV). These are the following:

DPM = porous polymeric material is produced

PV = microcellular plastics processing techniques are applied to a binary blend of immiscible polymers.

Once it is stated that immiscible blends combined with microcellular plastics processing techniques is the selected way to achieve the goal of a porous material, the decomposition into more specific design parameters is now appropriate. One set which follows from the above overall choices is:

DP_1 = adequate mixing of the binary polymer blend occurs so that domain sizes are sufficiently small

DP_2 = polymer-gas solution is formed with proper gas concentration

DP_3 = polymer-gas solution is subjected to a thermodynamic instability of sufficient magnitude that gas precipitates from solution

DP4 = as gas leaves the solution, adhesive fracture of the polymer-polymer interfaces occurs.

Now that a set of design parameters has been established, the designer's task is to determine process variables, which provide the necessary means to control the parameters so that they fall within the acceptable range. The domain size in a binary blend is affected by these factors: state of shear, composition ratio, interfacial tension, broadly, they may be seen to arise from three factors: choice of materials, polymer processing technique used, and relative amounts of the different materials. It is desirable that material selection not be a process variable so that it can be based on other factors specific to a particular application, especially the environment in which the plastic is intended to be used, including chemical resistance, performance at elevated temperatures, and so on. Thus, it will be assumed here that a satisfactory pair of materials is given. This leaves as process variables to control DP_1 the polymer processing method and the composition ratio of the materials. To control DP_2, the formation of a high-gas-concentration solution in the polymer matrix, process variables related to the saturation process are saturation pressure and saturation time. Lastly, to control the thermodynamic instability produced and the fracture of the polymer-polymer surfaces within the material, the PVs are foaming time, foaming temperature, and saturation pressure and composition ratio, mentioned already.

To see if the above process variables may be narrowed down to a satisfactory set, the process design for microcellular open-cell foams will be presented in the form of design equations where the relative dependence of the design parameters upon the process variables will be represented by a design matrix. The matrix elements will be evaluated to determine if there exists a strong dependence between a DP and a PV (represented by an *X*), a moderately weak dependence (represented by an *x*) or a very weak dependence (represented by an *O*). Once the matrix is constructed, it will be evaluated to see if axiom one, the independence axiom, is satisfied.

The design matrix is given in equation (2.1) where the design parameters have been stated in an abbreviated form. Also it may be noted that this equation, as stated, is a redundant design; i.e., it has more process variables than design parameters. This will be corrected by rearrangement of the matrix and by elimination of redundant variables.

$$\begin{Bmatrix} \text{solution formation} \\ \text{nucleation} \\ \text{adhesive fracture} \\ \text{mixing} \end{Bmatrix} = \begin{bmatrix} O & x & X & X & O & O \\ O & O & X & O & X & O \\ O & X & X & x & x & x \\ X & x & O & O & O & O \end{bmatrix} \begin{Bmatrix} \text{foaming time} \\ \text{composition ratio} \\ \text{saturation pressure} \\ \text{saturation time} \\ \text{processing technique} \\ \text{foaming temperature} \end{Bmatrix} \quad (2.1)$$

The above design matrix is based upon the combination of results obtained by the literature analysed in the following. Mixing is strongly influenced by the type of polymer processing employed. Saturation pressure and saturation time both affect the formation of a high-gas-concentration solution. Nucleation is affected by saturation pressure and by foaming temperature. The formation of a porous microstructure was affected relatively strongly by saturation pressure and by composition ratio.

Foaming time played little role in fracture or nucleation, since these occurred almost instantaneously. Further clarification is required for the relationships denoted by an *x*. The dependence of the design parameter upon the associated process variable, in these cases, was found to not be significant over the range studied. That is to say that over a broader range, a dependence is almost certain to some degree, but that in the processing range of interest, the dependence is slight, if at all. For example, consider the dependence of adhesive fracture upon saturation time. If the saturation time is very short, so that little gas has time to diffuse into the polymer matrix, then the concentration of gas in the polymer will be low. In this case, adhesive fracture is unlikely for sufficiently low concentrations. However, if the saturation time is reduced to this small amount, solution formation is not achieved, therefore, this case is not of practical interest. Similarly, processing the samples at room temperature would adversely affect the amount of adhesive fracture; however, this also reduces the thermodynamic instability which drives gas nucleation.

By rearranging the above matrix, eliminating redundant process variables, and considering each *x* to be negligible, the design equation (2.2) is obtained.

$$\begin{Bmatrix} \text{solution formation} \\ \text{nucleation} \\ \text{adhesive fracture} \\ \text{mixing} \end{Bmatrix} = \begin{bmatrix} O & X & O & O \\ O & X & X & O \\ O & X & O & X \\ X & O & O & O \end{bmatrix} \begin{Bmatrix} \text{composition ratio} \\ \text{saturation pressure} \\ \text{foaming temperature} \\ \text{processing technique} \end{Bmatrix} \quad (2.2)$$

The above design is an acceptable one; i.e., it satisfies the first axiom that the independence of the design parameters be maintained. This is evidenced by the diagonal nature of the design matrix. By controlling the process variables in the proper sequence, in the order shown, a satisfactory product should be produced.

Looking at extrusion of microcellular plastics as an example, the saturation pressure is not a variable, which directly translates to continuous processing; instead, it is replaced by the amount of gas injected into the molten polymer field. However, the important physical consideration is the resulting concentration of gas in the polymer-gas solution, and controlling the amount of gas injected is very effective at achieving a sufficient concentration. The other variable, which does not translate, is foaming temperature because using heating as a nucleation mechanism is counterproductive for the already hot polymer-gas solution. Instead, a rapid-pressure-drop element of some sort is used. Thus, the amount of pressure drop can be used as a suitable nucleation mechanism.

Problem statement

The recovery-induced retraction, to the best of our knowledge, has not ever been applied to foaming, and in particular as a mechanism (and, hence, as a design tool) to drive closed- to open-cell morphologies. Despite the first observations of the retraction of thin liquid films were done on soap films long time ago [14, 15], only recently film rupture has been used as a mean to measure the viscosity of molten polystyrene films [16, 17].Even more recently, the rupture of soap bubbles formed from a viscoelastic solution has been investigated with slow-motion imaging and experimental observations have been justified through a storing elastic energy that

is released after the rupture, representing an additional driving force for film retraction [18]. In foaming, viscoelastic effects on foam morphology have not been considered yet. In the Chapter 3, I thoughtfully describe our approach and how to derive information on foam morphology from growth dynamics. However, before to skip to the Chapter 3, in the next paragraph a review on the literature about the foaming modeling will be presented.

2.2 *Modeling of the foaming process in current literature and the problem statement*

In the result section a complete model of the foaming process starting from the growth of a single bubble will be described. Then, in this paragraph a complete review of the literature focusing on the bubble growth is discussed.

Bubble growth and collapse in plastic foaming processes are generally driven by mass transfer of gas molecules and momentum transfer between the bubble and the surrounding polymer-gas solution. At the onset of bubble growth upon nucleation, the bubble pressure (P_{bub}) is typically quite high owing to its small radius. The large pressure difference between the gas and liquid phase causes bubble to grow. At the same time, the gas concentration gradient across the bubble interface causes gas to diffuse into the bubble. As the bubble grows in size, the P_{bub} decreases, and the bubble growth process become more diffusion-driven. Eventually, the gas concentration within the polymer-gas solution diminishes, and bubble growth ceases. In typical foaming processes, the depressurization that causes foaming to occur also exposes the unstablized foam to a low-pressure environment (e.g., the ambient pressure). This leads to a concentration gradient that causes gas diffusion from the polymer-gas solution to the surrounding. Therefore, the gas concentration in the polymer-gas solution decreases, which decreases the bubble growth rate. If the foam sample is not cooled and stabilized rapidly, the gas loss can eventually cause gas diffusion out of the bubble, hence the bubble shrinks and even collapses.

Bubble growth

In plastic foaming processes, bubbles grow simultaneously in close proximity to generate a cellular structure. In this context, Amon and Denson [14] proposed the cell model whereby a polymer-gas solution is divided in spherical units with limited amounts of dissolved gas. This

is a significant improvement over the "Single Bubble Growth Model", which model a single bubble immersed in an reservoir with unlimited supply of gas [15, 16]. Consequently, the cell model has been widely adopted in the subsequent bubble growth research in plastic foaming processes [17-19]. To analyze a bubble growth process, it is necessary to simultaneously solve a set of governing equations: the continuity, momentum balance, and gas diffusion equations for a polymer-gas solution around a bubble interface, the constitutive equation that describes the viscoelastic nature of polymer-gas solutions, and the conservation of mass equation for gas molecules. A brief summary of this analysis using the cell model is given here. It is assumed that the polymer-gas solution is an incompressible fluid, and the bubble is spherically symmetric. In this case, the continuity equation for a polymer-gas solution surrounding a bubble interface can be reduced to [17]:

$$\frac{1}{r^2}\frac{\partial}{\partial r}\left(r^2 V_f(r)\right) = 0 \tag{2.3}$$

where r is the radial position and $V_f(r)$ is the fluid velocity at r. Since the fluid velocity at the bubble interface equals the growth rate of the bubble, the $V_f(r)$ can be expressed as:

$$V_f(r) = \frac{\dot{R}_{bub} R_{bub}^2}{r^2} \tag{2.4}$$

The inertial force is assumed to be negligible since polymer-gas solution is highly viscous with a Reynold's number < 1. In this case, the momentum equation for a polymer-gas solution surrounding a bubble interface can be simplified to [14]:

$$-\frac{\partial P_{sys}}{\partial r} + \frac{\partial \tau_{rr}}{\partial r} + 2\frac{\tau_{rr} - \tau_{\theta\theta}}{r} = 0 \tag{2.5}$$

where τ_{rr} and $\tau_{\theta\theta}$ are the stress components in the radial and tangential direction, respectively. In order to relate the stresses within the fluid to the pressure of gas inside the bubble, the previous equation can be integrated from the bubble surface (i.e., $R = R_{bub}$) to the outer boundary of the shell of the polymer-gas solution surrounding the bubble (i.e., $R = R_{shell}$). By combining the resulting equation with the force balance condition at the bubble interface [14]:

$$-P_{sys}(R_{bub}) + \tau_{rr}(R_{bub}) = -P_{bub} + \frac{2\gamma_{lg}}{R_{bub}} \tag{2.5}$$

the momentum equation can be expressed as [14]:

$$P_{bub} - P_{sys}(R_{bub}) - \frac{2\gamma_{lg}}{R_{bub}} + 2\int_{R_{bub}}^{R_{shell}} \frac{\tau_{rr} - \tau_{\theta\theta}}{r} = 0 \tag{2.5}$$

In order to solve Equation 2.5, it is necessary to determine the expressions for the stress components (i.e., τ_{rr} and $\tau_{\theta\theta}$) using a constitutive equation that relate the stresses with the rate of deformation of the polymer-gas solution. In particular, Arefmanesh and Advani [14] and Leung et al. [18] have adopted the upper convected Maxwell model to describe the viscoelastic nature of the polymer-gas solution. This model has been shown to accurately describe important viscoelastic behaviour such as stress relaxation and normal stress effects [14]. The upper convected Maxwell model can be represented as [14]:

$$\tau + \lambda\tau^{0} = \eta_{0}\gamma^{0} \tag{2.6}$$

where τ is the stress tensor; λ is the relaxation time; τ_o is the upper convected time derivative of τ; η_0 is the zero-shear viscosity of the polymer-gas solution; and γ_o is the strain rate tensor. τ_o is defined as [11]:

$$\tau^0 = \frac{D\tau}{Dt} - (\tau \cdot \nabla \boldsymbol{V}) + ((\nabla \boldsymbol{V})^T \cdot \tau) \tag{2.7}$$

where $D\tau/Dt$ is the substantial derivative operator. By combining Equation 2.6, Equation 2.5, and Equation 2.4, and applying a Lagrangian coordinate transformation [13], the constitutive equation can be reduced to the following ordinary differential equations [14]:

$$\begin{aligned} \frac{d\tau_{rr}}{dt} + \left(\frac{1}{\lambda} + \frac{4\dot{R}_{bub}R_{bub}^2}{y + R_{bub}^3}\right)\tau_{rr} &= -\frac{4\eta_0 \dot{R}_{bub}R_{bub}^2}{\lambda(y + R_{bub}^3)} \\ \frac{d\tau_{\theta\theta}}{dt} + \left(\frac{1}{\lambda} - \frac{2\dot{R}_{bub}R_{bub}^2}{y + R_{bub}^3}\right)\tau_{\theta\theta} &= \frac{2\eta_0 \dot{R}_{bub}R_{bub}^2}{\lambda(y + R_{bub}^3)} \end{aligned} \tag{2.8}$$

Assuming that the accumulation of gas molecules on the bubble interface is negligible, the conservation of mass dictates that the rate of change of the gas mass within the bubble must be equal to the net mass transfer of gas molecules across the bubble interface. By further assuming that the gas molecules behave like an ideal gas, the bubble pressure (P_{bub}) can be determined based on the mass transfer through diffusion at the bubble interface [17]:

$$\frac{d}{dt}\left(\frac{P_{bub}(t)R_{bub}^3(t)}{R_G T_{sys}}\right) = 3R_{bub}^2(t)D\frac{dC(r,t)}{dr} \tag{2.9}$$

where R_G is the universal gas constant and D is the gas diffusivity in the polymer-gas solution. In order to solve this equation, it is necessary to determine the concentration gradient at the bubble interface, which can be achieved by solving the gas diffusion equation for the polymer-gas solution [17]:

$$\frac{dC}{dt} + \frac{\dot{R}_{bub} R_{bub}^2}{r^2} \frac{dC}{dt} = \frac{D}{r^2} \frac{dC}{dr} \left(r^2 \frac{dC}{dr} \right) \tag{2.10}$$

By simultaneously solving Equation 2.10 and Equation 2.9 to Equation 2.8 with appropriate initial and boundary conditions, the bubble growth dynamics for plastic foaming processes can be determined. Due to the complexity and coupling nature of the governing equations, numerical methods are generally used to obtain such solutions.

Bubble coalescence

When two neighboring cells grow, the polymer-gas solution between them (i.e., the cell wall) is subjected to an approximate biaxial stretching. Consequently, the cell wall could be ruptured due to overstretching. This is not acceptable for close-cell foams. For the production of open-cell foams, this process of cell wall rupture (i.e., cell opening) is necessary to generate interconnectivity between cells. The foam must be stabilized quickly (i.e., via cross-linking in thermoset and cooling in thermoplastics) to maintain the cellular structure. On the other hand, if the foams are not stabilized rapidly, adjacent cells can combine together, and the cellular structure collapse non-uniformly. This phenomenon is termed cell coalescence, which is undesirable to the foam quality (e.g., detrimental to its mechanical properties). Also, due to cell coalescence, gas loss to the environment is also accelerated, hence the foam expansion decreases. Due to the difficulty to control this phenomenon to generate high-quality open-cell foams, other strategies, such as salt-leeching and puncturing of stabilized foams, have also been investigated and utilized for this purpose.

To reduce or eliminate cell coalescence, attempts have been made to develop polymers with optimized the extensional properties to prevent cell wall ruptures. Many of these studies focused on linear PP due to its low melt strength that causes cell coalescence during plastic foaming processes. One common method to solve this issue is to introduce branching in PP molecules. For example, Park and Cheung [12] and Naguib et al. [22] investigated foaming with long-chain-branched PP (LCB-PP), which exhibits significant strain hardening under extension. Through extrusion foaming, they demonstrated that much higher cell densities and volume

expansion ratios could be generated with LCB-PP when compared to linear PP. Similar results were obtained by McCallum et al. [13] in batch foaming processes. All of these three studies attributed the better foaming behaviour of branched PP to its higher melt strength that lead to reduced cell coalescence during the early stage of cell growth. Spitael & Macosko [14] and Stange & Münstedt [15] characterized the uniaxial extensional viscosities of linear PPs, LCB-PPs, and their blends at foaming conditions, and attempted to relate rheological properties to cell morphology. They found that even a small amount of LCB-PP (e.g., 10% by weight) in the blend can improve the expansion and reduce the cell opening of linear PP. Stange & Münstedt [10] attributed the higher volume expansion of LCB-PP and blends containing LCB-PP to their higher strains at rupture and higher uniformity in their deformation during extension compared to linear PP. In addition to branching, other ways to suppress cell coalescence is to decrease the melt temperature [16] and to incorporate additives (e.g., nano-particles [17]) into the polymer matrix. In the cases of plastic composites, additive particles could orient along the cell walls during the foaming processes to enhance the melt strength, which is desirable for suppressing cell coalescence [17]. This strengthening effect is believed to be more significant for additives with high aspect ratio. Meanwhile, these additives can also act as nucleating agents and barrier for gas diffusion. Consequently, more cells would be nucleated while gas loss to the environment is decelerated. As a result of the increased foam expansion, the cell wall thickness might decrease at faster pace, which could ultimately cause cell opening and hence cell coalescence, so it is necessary to control the melt temperature at the same time to prevent this behaviour.

During foam processing, cell growth and collapse processes is driven by the pressure and concentration differences between a cell and its surrounding. The gas concentration in small cells is higher than bigger ones. Therefore, gas tends to diffuse from a small bubble to an adjacent bubble with a bigger size, and the small bubble shrinks and collapses eventually. This cell deterioration mechanism is termed cell coarsening. Therefore, if there exist a non-uniform cell size distribution during the stabilization stage, the larger cells would continue to grow while the smaller ones shrink, and the final stabilized foams would have highly non-uniform cellular morphology. Compounding with the fact that cell growth is thermodynamically favorable to cell nucleation, it is clear why undissolved gas pockets in plastic matrix is hugely detrimental to the resulting foam quality and must be avoided. On the other hand, even if cell coalescence and cell coarsening are suppressed, gas diffusion to the environment could still cause rapid decrease in gas concentration in a polymer. This leads to gas transfer away from bubbles, and hence they shrink and collapse. Studies in the past have investigated the mechanisms for cell coarsening and cell collapse, and developed strategies to prevent them.

To understand the cell coarsening process in plastic foaming, Zhu and Park used finite element analysis to simulate the stability of nano-sized bubbles in the presence of neighboring bubbles [14]. The simulation demonstrated that nano-sized bubbles collapse rapidly upon interaction with adjacent cells with larger sizes due to cell coarsening. This study demonstrates the difficulty in generating nanocellular foams as mentioned in Chapter 1.

Meanwhile, Xu et al. investigated the bubble growth and collapse phenomenon in the foaming of low-density polyethylene (LDPE) blown with a CBA under atmospheric pressure using computer simulation [18], and the results were compared with empirical data obtained from in situ foaming observation. It was shown that a higher gas concentration increases a bubble life span. On the other hand, an increase in elasticity or surface tension decreases the life span of a bubble. Furthermore, a bubble life span decreases with temperature due to increased gas diffusivity. Guo et al. used a high pressure batch foaming visualization system to study the effect of system pressure on bubble sustainability of LDPE/CBA foaming systems [19]. It was found that a bubble life span increases with the system pressure, which is believed to be due to the higher gas content that sustained the bubble growth.

These aforementioned studies used diffusion phenomena to explain the cell growth and collapse processes. Meanwhile, these processes can also be explained by the CNT [24]. As mentioned in Chapter 1, a bubble that is larger than R_{cr}, grows, whereas one that is smaller than R_{cr} collapses. Leung et al. [22] investigated the continuous change of R_{cr} during plastic foaming processes of LDPE with CBA and the effect of R_{cr} on bubble sizes using computer simulation. The results were also compared with in situ observation of the bubble growth and collapse phenomena in a batch process. The computer simulation shows that a lower diffusivity, a higher solubility, and a lower surface tension will enhance the sustainability of bubbles formed in CBA-based, pressure free foaming processes.

In the past, various researchers have developed methods to improve foam morphology by preventing cell coalescence, coarsening and collapse. In particular, Naguib et al. [14] demonstrated that there is an optimal foaming temperature to achieve foams with high expansion while suppressing cell coalescence. If the foaming temperature is too low, polymer foams would cool quickly and stabilize before bubbles could grow to their maximum sizes. On the other hand, if the foaming temperature is too high, the initial cell growth rate would also be high, but the bubbles would eventually shrink to smaller sizes or cell coalescences might occur before the foam stabilized. A number of previous studies have shown that the solubility of CO_2 in PDMS and PMMA is higher than that in other commodity plastics such as PS, polyethylene (PE) and PP [19]. In this context, various researches have been done to blend PDMS or PMMA into commodity plastics to increase the amount of CO_2 dissolved in the polymer matrix. It was believed that the dispersed phase (i.e.,

PDMS or PMMA) could act as gas reservoirs to promote cell nucleation, sustain cell growth, and prevent cell collapse. In particular, Wu et al. [16] observed increased cell density and better foam morphology when PDMS was added to PP and PP copolymer, respectively. A similar result was also observed by Han et al. [15] in PS/PMMA/nanoclay foams. According to the CNT, the increased gas concentration from the PMMA or PDMS would suppress the increase of R_{cr} and hence enhance the sustainability of a bubble. Therefore, more bubbles would survive up to the stabilization stage, and thus the overall cell density would increase. Furthermore, Okamoto et al. demonstrated that nanoclay particles would align along cell walls due to extensional stress [14]. It was hypothesized that the aligned particles would decrease gas diffusion from bubbles, so they are less likely to collapse due to cell coarsening or gas loss to the environment.

Numerical simulation of the foaming processing

To achieve thorough understanding of the mechanisms governing plastic foaming processes, numerous research have developed numerical simulation to model these processes. Many of these studies are based on the mathematical formulation of cell nucleation and growth detailed in previous paragraph, respectively. In particular, in regards to the modeling of cell growth in plastic foaming, various researches have adopted the cell model and demonstrated good qualitative or quantitative agreements between numerically simulated and experimentally observed cell growth profiles [20, 22] in static conditions. Meanwhile, other researchers have attempted to simultaneously simulate bubble nucleation and growth in plastic foaming processes [15-18]. For example, Han and Han [22] simulated foaming of PS/toluene solutions by assuming constant bubble growth rates. Shafi et al. [23] developed the "influence volume approach" whereby each bubble is surrounded by a thin shell of polymer-gas solution (i.e., the influenced volume) within which cell nucleation does not occur due to insufficient gas concentration as gas is diffused into the bubble. Cell nucleation was assumed to start upon an instant pressure drop and ceased when the non-influenced volume drops to zero. The initial bubble pressure was assumed to be the same for all bubbles and was determined by the initial gas concentration and the Henry's Law constant. Shimoda et al. [23] simulated cell nucleation and growth in a flow field through a rectangular channel. In their simulation profile, they accounted for the pressure drop profile in the flow channel and changes in viscosity and flow rate during the cell nucleation stage. Ramesh et al. [20] simulated plastic foaming by considering the survival and growth of microvoids in PS-rubber composites. They suggested that voids are generated in the rubber particles due to stresses generated due to a mismatch of volume contraction between PS and rubber particles during the cooling process. When the polymer-gas solution becomes supersaturated, the Rcr decreases, thus triggering the microvoids with radius bigger than Rcr to

grow. Based on a similar concept of bubble nucleation from existing microvoids and the shear-induced nucleation model by Lee [16], Feng and Bertelo [23] simulated cell nucleation and growth from the detachment of microvoids that reside on conical cavities. Leung et al. [17, 19] used the Sanchez-Lacombe Equation of State (SL-EOS) to determine the Pbub,cr inside a critical bubble, and incorporated this method to simulate bubble nucleation and growth in plastic foaming processes. In their study [20], the bubbles were assumed to be nucleated heterogeneously on conical cavities without the consideration of microvoids. A computer simulated PS foaming process blown with CO2 was compared with in situ foaming video in a batch process using a foaming visualization system developed by Guo et al. [21], and good agreement between the two results was observed.
All of these computer simulation studies contribute significantly to our understanding of plastic foaming processes as they evaluated the validity of various underlining theories, and clarified the importance of material and processing various parameters (e.g., pressure drop rate, diffusivity of gas in polymer, viscosity and elasticity of polymer-gas solution) in cell nucleation and growth via various sensitivity studies. However, discrepancy between experimental data and computer-simulated results were often observed. There are three major reasons for the discrepancy.

The first reason is the possible errors or insufficiency in the set of governing theories used in the numerical model. For example, the CNT has been criticized to overestimate the free energy needed for nucleation. While much efforts have been directed to modify the CNT to account for its shortcoming (e.g., correction for γlg variations according to cluster sizes [23]), continued advancement in this theory is necessary to close the gaps between observed and predicted results. In addition, as mentioned in Chapter 1, stresses can significantly affect cell nucleation. Therefore, it is imperative to incorporate the effect of a flow field in the simulation model. While attempts have been made in this regard, such as by Shimoda et al. [19], the models used in the previous studies might not be sufficient in various ways to completely describe the simultaneous cell nucleation and growth process under dynamic conditions.

The second reason is the possible errors in various assumptions made in the numerical model due to difficulty in devising a simulation scheme or to lighten the computation time requirement (e.g., spherical bubble and no bubble-to-bubble interaction). For example, the average gas concentration of the polymer-gas solution at each time instant ($C_{avg}(t)$) is often used to determine the termination point of cell nucleation (i.e., nucleation ceases when $C_{avg}(t)$ is sufficiently low). However, growth in existing cells affect local gas concentration and hence it is not accurate to prescribe this single boundary condition for termination of cell nucleation for the entire polymer-gas solution. Furthermore, the assumption of no bubble-to-bubble interaction is a significant simplification from actual foam processing. While this assumption can be valid at the initial stage of a foaming process when no heterogeneity exists in the polymer-gas solution, it fails to capture

the stress-induced cell nucleation mechanism whereby the grow of an existing bubble causes cell nucleation in the surrounding [105-107]. As it is further demonstrated in the latter sections of this thesis, this could be a dominant cell nucleation mechanism in typical plastic foaming processes.

The third reason is the unavailability of material parameters (e.g., θ_c, viscosity and relaxation time of polymer-gas solution), hence fitting parameters are often introduced to fit computer simulation results to experimental results. Due to the fitting procedure used, it is difficult to confirm the validity of the computer models despite good agreement between numerical and experimental results. One way to solve this challenge is to fix the fitting parameters once they have been determined from an experiment and to use these values in other simulation runs. However, discrepancy between numerical and experimental results are often observed, possibly due to changes in these parameters at different conditions that could not be accounted for accurately. While errors in some of these parameters might not significantly affect the foaming behaviour at the relevant processing conditions as demonstrated by various sensitivity analysis (e.g., relaxation time on bubble growth [19]), the opposite is also true for other parameters. For example, it has been demonstrated that the simulated cell density varied by four orders of magnitude (i.e., from 105 to 10^9 cells/cm^3) as the θ_c changed from 85.5° to 87.5° [15]. Therefore, until the sensitive material parameters are determined accurately, as well as solutions to the other two issues listed above are developed, it is challenging to achieve quantitative agreements between numerical and experiments results on a consistent basis.

In summary, despite its many merits and versatility, the applications of computer simulation in achieving thorough understanding on cell nucleation and growth behaviour remain to be challenging even with the accelerated advancement of computing power in recent years. Moreover, in order to verify the validity of a numerical model for cell nucleation and growth and to improve the underlying theories, it is imperative to compare the numerical results with experimental data. Direct comparison between numerical results with cell morphology of foamed samples might not be accurate since the interaction of cells during their growth (i.e., deformation of cells, cell coalescence, cell coarsening) are often not considered in computer simulations. Therefore, a complete model up to the rupture and the retraction of the cell walls has to be developed, in order to predict the opened cell morphology.

2.3 *References*

[1] C.R. Thomas, Br. Plastics Moulded Prod. Trader, 1965.

[2] S.G. Mosanenzadeh, H.E. Naguib, C.B. Park, N. Atalia, "Development, characterization, and modeling of environmentally friendly open-cell acoustic foams", Journal of Applied Polymer Science, 2013.

[3] K. Kaji, M. Hatada, I. Yoshizawa, and C. Kohara, "Preparation of Hydrophilic Polyethylene Foam of Open Cell Type by Radiation Grafting of Acrylic Acid", Journal Applied Polymer Science, 1989.

[4] D. Klempner and K.C. Frisch, "Handbook of Polymeric Foams and Foam Technology", Hanser, New York, 1991.

[5] C. B. Park, L. K. Cheung, S. W. Song, "The Effect of Talc on Cell Nucleation in Extrusion Foam Processing of Polypropylene with CO2 and Isopentane" Cellular Polymer, 1998.

[6] P. C. Lee, J. W. S. Lee, C. B. Park, "Improvement of Cell Opening by Maintaining a High Temperature Difference in the Surface and Core of a Foam Extrudate" Journal of Cellular Plastics, 2007.

[7] C.B. Park, V. Padareva, P.C. Lee, and H.E. Naguib, "Extruded Open-Celled LDPE and LDPE/PS Foams Using Non-Homogeneous Melt Structure", Journal Polymer Engineering, 2005.

[8] P.C. Lee, H.E. Naguib, C.B. Park, J. Wang, "Increase of Open-Cell Content by Introducing a Secondary Blowing Agent", Polymer Engineering Science, 2005.

[9] P. C. Lee, J. Wang, C. B. Park, "Extruded Open-Cell Foams Using Two Semicrystalline Polymers with Different Crystallization Temperatures", Industrial Engineering Chemistry Research, 2006.

[10] D. Kohlhoff, M Oshshima, Macromol. Mater. Eng., 2011.

[11] R. Miyamoto, M. fukumori, H. Shikuma, M Ohshima, Proceeding of the polymer processing society 28th annual meeting, Pattaya, Thailand, 2012

[12] B. Krause, M.E. Boerrigter, N.F.A. van der Vegt, H. Strathmann, M. Wessling, J. Membr.Sci., 2001.

[13] P. Gong, M. Ohshima. *Journal of chemical engineering*, 2004, 154, 12.

[14] M. A. Dupré, Sixiéme memoire sur la theorie méchanique de la chaleur, Ann. Chim. Phys., 4 (1967), 194–220.

[15] Lord Rayleigh, Some applications of photography, Nature, 44 (1891) 249–254.

[16] K. Dalnoki-Veress, B. G. Nickel, C. Roth, J. R. Dutcher, Hole formation and growth in freely standing polystyrene films, J. Fluid Mech., 59 (1999) 2153–2156.

[17] C. B. Roth, B. Deh, B. G. Nickel, J. R. Dutcher, Evidence of convective constraint release during hole growth in freely standing polystyrene films at low temperatures, Phys. Rev., 72 (2005) 021802.

[18] E. Sabadini, R. F. S. Ungarato, P. B. Miranda, The elasticity of soap bubbles containing wormlike micelles, Langmuir, 30 (2014) 727–732.

[19] M. Amon and C. D. Denson, "Study of the Dynamics of Foam Growth: Analysis of the Growth of Closely Spaced Spherical Bubbles," Polymer Engineering and Science, vol. 24, pp. 1026-1034, 1984.

[20] E. J. Barlow and W. E. Langlois, "Diffusion of gas from a liquid into an expanding bubble," IBM Journal of Research of Development, vol. 6, pp. 329-337, 1962.

[21] J. R. Street, A. L. Fricke, and L. Philip Reiss, "Dynamics of phase growth in viscous, non-newtonian liquids: Initial stages of growth," Industrial and Engineering Chemistry Fundamentals, vol. 10, pp. 54-64, 1971.

[22] J. C. Slattery, Momentum, energy, and mass transfer in continua: McGraw-Hill, 1971.

[23] S. N. Leung, C. B. Park, D. Xu, H. Li, and R. G. Fenton, "Computer simulation of bubble-growth phenomena in foaming," Industrial and Engineering Chemistry Research, vol. 45, pp. 7823-7831, 2006.

[24] N. S. Ramesh, D. H. Rasmussen, and G. A. Campbell, "Numerical and Experimental Studies of Bubble-Growth During the Microcellular Foaming Process," Polymer Engineering and Science, vol. 31, pp. 1657-1664, 1991.

[25] A. Arefmanesh and S. G. Advani, "Diffusion-induced growth of a gas bubble in a viscoelastic fluid," Rheologica Acta, vol. 30, pp. 274-283, 1991.

[26] R. B. Bird, R. C. Armstrong, and O. Hassager, Dynamics of Polymeric Liquids. New York: Wiley, 1987.

[27] C. B. Park and L. K. Cheung, "A study of cell nucleation in the extrusion of polypropylene foams," Polymer Engineering and Science, vol. 37, pp. 1-10, 1997.

[28] T. J. McCallum, M. Kontopoulou, C. B. Park, A. Wong, and S. G. Kim, "Effect of branched PP content on the physical properties and cell growth during foaming of TPOs," Journal of Applied Polymer Science, vol. 110, pp. 817-824, 2008.

Chapter 3: results and discussion

In the Chapter 1 and 2 the reader was introduced to the world of polymer foaming. It was discussed the main features of a foam morphology and the different kind of structures were presented (i.e. opened cell and closed cell). It was explained how to perform a polymer foaming experiment and to change the processing parameters to tune the foam morphology, respect to the methods reported in the literature. In this Chapter 4 the main results of the research and the key contributions of this Ph.D. are reported. In particular, the following paragraph shown the validated model developed to predict the cell opening in a thermoplastic polymer foaming developed during these 3 years of Ph.D.

3.1 *Validated modeling of bubble growth, impingement and retraction to predict cell-opening in thermoplastic foaming*

In the following paragraph, it is reported the work authored by D. Tammaro, G. D'Avino, E. Di Maio, R. Pasquino, M.M. Villone, D. Gonzales, M. Groombridge, N. Grizzuti, P.L. Maffettone, and titled "Validated modeling of bubble growth, impingement and retraction to predict cell-opening in thermoplastic foaming", published in 2015 on Chemical Engineering. Journal Vol. 3 Pag. 845-860.

Chemical Engineering Journal 287 (2016) 492–502

Contents lists available at ScienceDirect

Chemical Engineering Journal

journal homepage: www.elsevier.com/locate/cej

Validated modeling of bubble growth, impingement and retraction to predict cell-opening in thermoplastic foaming

D. Tammaro[1], G. D'Avino[1], E. Di Maio[1*], R. Pasquino[1], M.M. Villone[2], D. Gonzales[3], M. Groombridge[3], N. Grizzuti[1], P.L. Maffettone[1]

[1]*Dipartimento di Ingegneria Chimica, dei Materiali e della Produzione Industriale, University of Naples Federico II, P.le Tecchio 80, I-80125 Napoli, Italy*
[2]*Center for Advanced Biomaterials for Health Care @CRIB, Istituto Italiano di Tecnologia, Largo Barsanti e Matteucci 53, 80125 Napoli, Italy*
[3]*The Procter and Gamble Company, Newcastle Innovation Centre, Whitley Road, Longbenton, NE12 9TS, United Kingdom*

Abstract

In this work a design tool to control cell-opening in gas foaming of thermoplastic polymers is developed. The sequence of events following bubble nucleation, namely, bubble growth and impingement, are modeled to gain a comprehensive, perspective view on the mechanisms of bubble wall rupture and on the conditions for achieving a fully open-cell morphology. In particular, unlike the previously published literature, the polymer elastic recovery is recognized as an important factor for wall retraction, which is typically driven by surface tension. The new approach is experimentally validated on poly(ε-caprolactone) (PCL), foamed with CO_2, as a model polymer/gas system.

Keywords: foaming; open-cell; modeling; elastic recovery

* corresponding author: Tel.: +39 081 768 25 11; fax: +39 081 768 24 04.
E-mail address: edimaio@unina.it (E. Di Maio)

Highlights:

- The sequence of operations involved in gas foaming process is modeled
- The dynamics of bubble growth and impingement to predict rupture and retraction

- A new retraction criterion is proposed for bubble wall opening
- The model is validated with poly(ε-caprolactone) foamed with CO_2

Graphical abstract

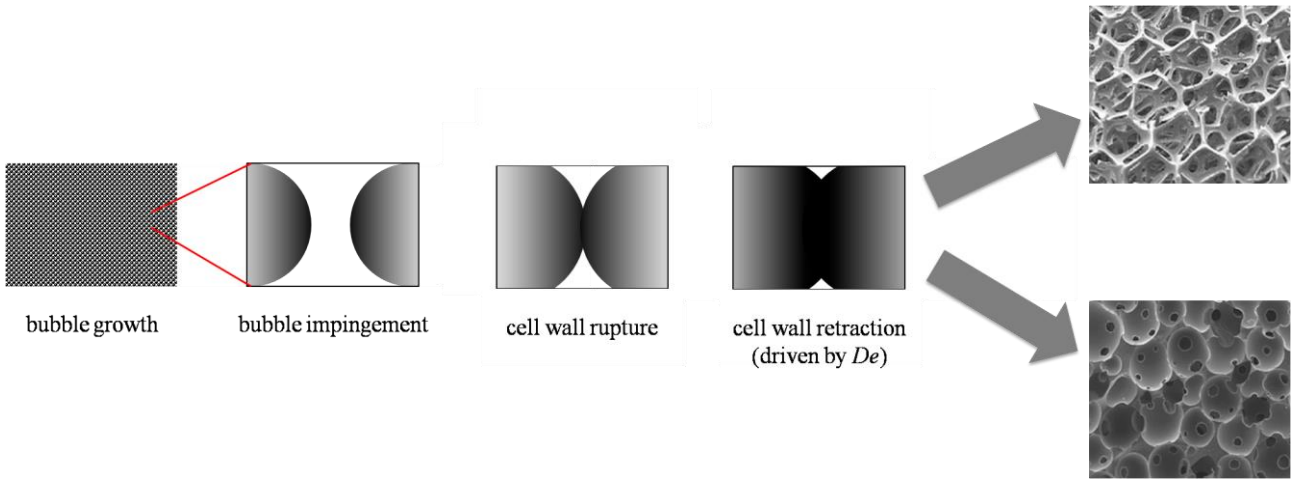

1. Introduction

Due to their mass and energy transport, acoustic absorption, catalytic, impact, and cushioning properties, open-cell polymeric foams are used in a multitude of different applications, including transportation, construction, packaging, food, extraction and separation [1], as well as in leisure, and sport. They are also used in tissue engineering, as culture substrates for living cells [2], and as templating structures for ceramic and metal foams.

The *gas foaming technology*, which makes use of a physical blowing agent (e.g., carbon dioxide or nitrogen) to form bubbles in a softened polymer, is the most used process for the making of open-cell foams, mainly because of its high productivity. The sequence of operations involved in the gas foaming technology, specifically for the case of open-cell foams, are: i) blowing gas solubilization at high pressure (to achieve a polymer/gas solution); ii) bubble nucleation induced by an instantaneous pressure quench; iii) bubble growth; iv) bubble impingement (where the growing bubbles start "feeling" each other, and the polymeric layer separating them progressively thins); and v) bubble wall rupture [1].

In the last decades, a large number of scientific papers has dealt with the modeling of the above steps, both in order to understand the underlying physic-chemical phenomena and to optimize process conditions. Today, step (i) is quite well understood, in particular how to form the polymer/gas solutions and how much the presence of the solubilized gas affects the thermal [3], mass transfer [4], sorption [5], rheological [6-10], interfacial and volumetric properties [11] of the polymer. More recently, the specific interactions occurring between the polymer and the gas molecules have been considered, opening the way to the design of novel blowing agents [12, 13].

Moving to step (ii) above, gas supersaturation is induced by imposing a rapid pressure drop on the polymer/gas solution. The subsequent bubble nucleation is typically modeled by the classical nucleation theory, where the original formulation, developed for water vapor droplets, is adapted to foaming to take into account gas solubility and the high molecular weight of the expanding material [14-16].

Bubble growth (step (iii)) is modeled by mass and momentum (and, in a few cases, also energy) balance equations. Recently, taking advantage of the improved calculating tools, the standard, purely viscous constitutive equations have been substituted by more realistic equation for viscoelastic fluids [17-20].

In some cases, in order to gain some predictive capability on the final foam structure, the nucleation and growth steps are coupled by the so-called *influence volume* approach [21], which assumes that, in the volume of the polymer/gas solution involved in the growth of a bubble, no other bubbles may nucleate as a consequence of the depleted gas concentration [22]. As the bubble keeps on growing, the subsequent step of bubble impingement has to be taken into account to consider bubble/bubble interactions. Typically, a few growing bubbles are considered and numerical models are used to investigate the evolution of the bubble wall thickness, state of stress and deformation [23-29]. Eventually, the bubble walls may rupture, due to the presence of structural inhomogeneities in the polymer matrix, either introduced from outside (e.g., solid particles) or generated inside the polymer (e.g., crystallization) [30-32]. In both cases, it is assumed that due to the presence of such inhomogeneities, a non-uniform deformation takes place, determining a high level of stress at the polymer-heterogeneity interface that, in turn, may lead to wall rupture.

The comprehensive picture of the state of the art of foaming modeling is reported in Fig. 1, as a scheme of the aforementioned sequence of operations, together with the most important scientific contributions that have dealt with the modeling of one or more of these operations.

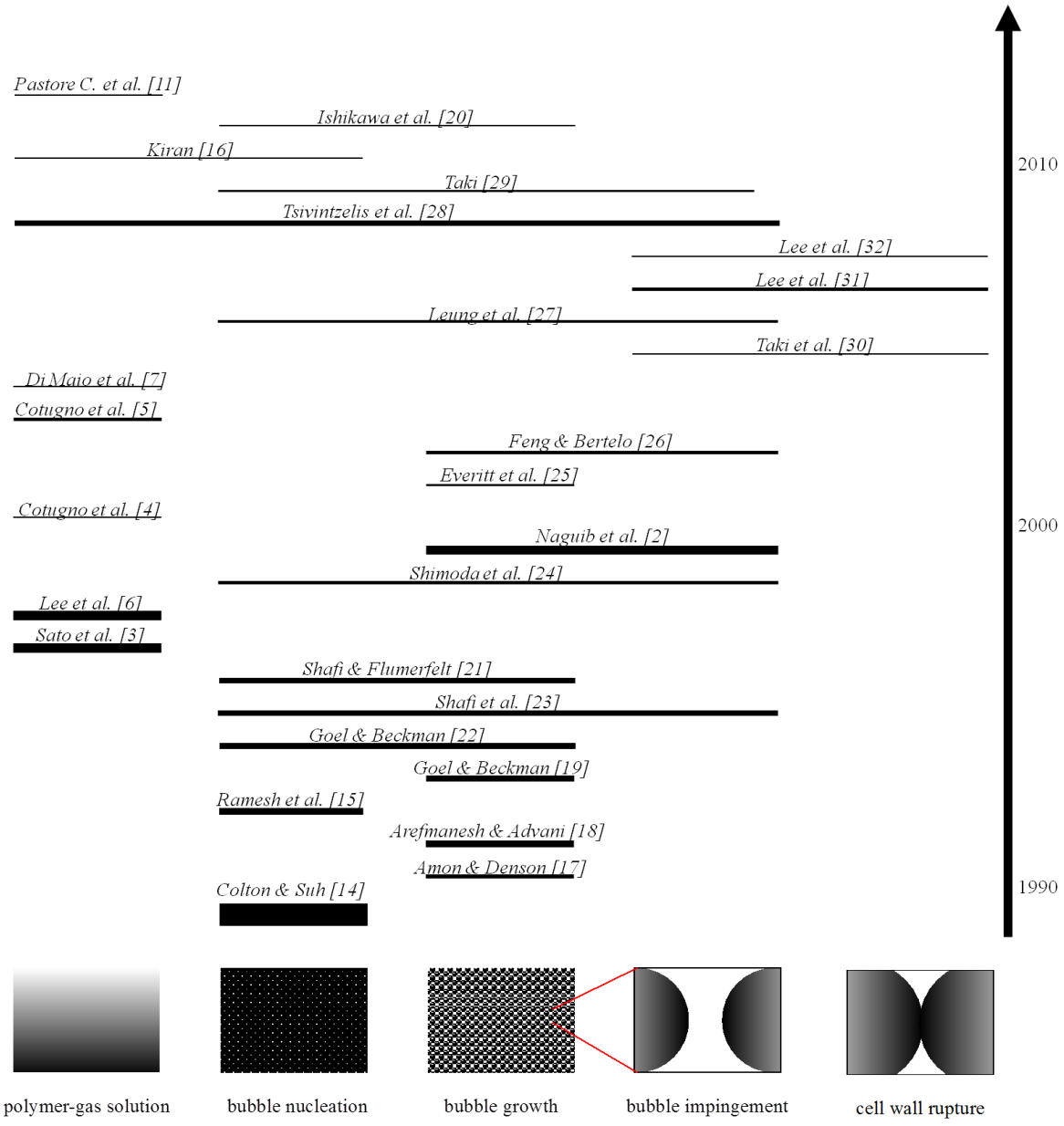

Fig. 1. Scheme of the sequence of operations leading to open-cell foams by gas foaming, together with the underlying literature that has dealt with the modeling of one of more of these operations. Lines below the references extend along the operations addressed to in the reference and line thickness is representative of its relative impact (as by the number of ISI citations as of June 2015).

Although the strategies for bubble wall rupture should lead, by definition, to open-cell foams, a close observation of the foam morphology, and, in particular, of the layer dividing two neighboring cells, usually shows that bubble walls are still present, even if broken (Fig. 2b). In this case, then, some of the properties may not conform to fully open-cell foams, in which the polymer is solely confined to the struts. Fig.2 shows a clarifying example of a closed-cell foam

(a), an open-cell foam with broken walls (b) and a fully open-cell foam, with no walls at all and with the polymer solely confined to cell struts (c).

a) 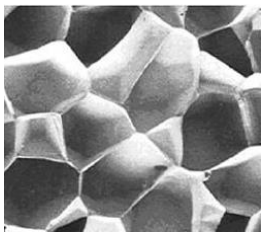 b) 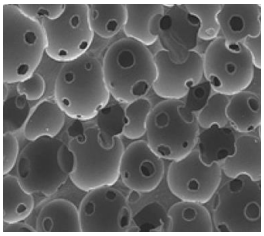 c) 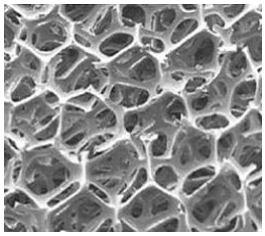

Fig.2. Possible morphologies in thermoplastic foams: a) closed cells, b) open-cells with broken bubble walls, c) fully open-cells with polymer confined to the struts.

In order to have a fully open-cell morphology, where no material occupies the bubble walls, it is not sufficient to produce a fracture within the wall, but a *bubble wall retraction* is needed. In metallic foams as well as in thermosetting polyurethane foams and soap bubbles, low viscosities and high surface energies are straightforward conditions for wall retraction, which can be very fast and easy [46-47]. In thermoplastic polymers, conversely, viscous forces can be much stronger than interfacial forces, hindering bubble wall retraction, thereby leading more easily to open-cell morphologies such as the one reported in Fig.2b [31].

In this work, in order to achieve fully open-cell foams, we conduct a comprehensive analysis, by means of experimentally-validated modeling and numerical simulations, of the sequence of events leading to the formation of the foam and to the development and rupture of the bubble walls. In particular, we investigate in details the role of the polymer elastic recovery as an additional, crucial factor in the bubble wall retraction mechanism. Finally, the developed model allows the design of the material and the process to drive the foam to a fully open-cell morphology. Both the use of the elastic recovery as an additional (actually dominant, at least in thermoplastic polymers) retraction mechanism and the resulting design tool for final foam morphology control are the main novelties of the present contribution.

The approach was validated by using a homemade apparatus with a visualization window that was designed for microcellular foaming at different processing conditions (i.e. temperature and pressure). The thermoplastic polymer used during the experiments was a poly(ε-caprolactone) (PCL) foamed with CO_2. The experimental results were compared with the theoretical analysis, as it is shown in the result section.

2. Theoretical Background and Modeling

The present approach analyzes the foaming process, from bubble growth to bubble impingement and bubble wall opening, and is divided into four operations, as described in Fig.3: single bubble growth (SBG), impingement (IM), bubbles wall rupture (RU), and bubbles wall retraction (RE). It is worth noticing, here, that we did not include the bubble nucleation stage in the model. The latter assumes that a given nuclei density is fixed and describes the growth, interaction and coalescence phenomena. In the following, we will describe in detail the different steps and their mutual interactions.

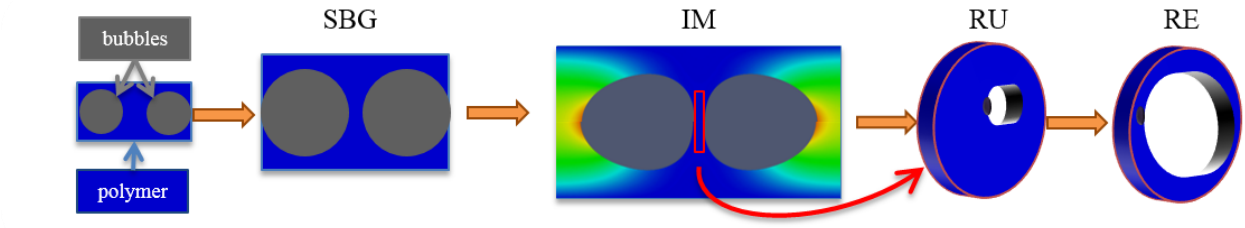

Fig.3. Schematic of the foaming process to produce open-celled foams.

SBG. The single bubble growth (SBG) model describes the growth dynamics of an isolated bubble, driven by the presence of supersaturated gas within the polymeric matrix. Single bubble growth in a viscoelastic system is modeled through a detailed 3D mathematical description, by adapting a model, initially proposed by Everitt et al. [25], to the PCL/CO_2 case at hand. All relevant properties (rheological, sorption, volumetric and interfacial) have been either taken from the literature [11] or directly measured in the present work, as described below.

We consider a single spherical gas bubble with initial radius R_0 surrounded by a spherical shell of a viscoelastic liquid containing a given quantity of dissolved gas. The initial bubble volume is $V_0 = 4/3\pi R_0^3$ and the gas pressure in the bubble is p_{g0}. Bubble growth is driven by the difference between the actual gas pressure inside the bubble, p_g, and the external ambient pressure, p_a. We assume isothermal conditions, incompressibility of the viscoelastic fluid and negligible inertia.

Under the above conditions, the bubble growth dynamics are governed by the momentum balance equation for the liquid shell and by the diffusion equation of the gas from the liquid to the bubble. Because of the spherical symmetry of the system, we choose a spherical coordinate system with the origin coinciding with the bubble center. Furthermore, due to the liquid volume conservation, we transform the radial coordinate r into a Lagrangian volume coordinate x such that $r^3 = R^3 + x$ [24], where R is the time-dependent bubble radius. Therefore, $x = 0$ is the

(Lagrangian) position of the bubble-liquid interface and $4/3\pi x$ is the liquid volume between a generic radial position inside the fluid shell and the bubble-liquid interface. We define $x = X$ the (Lagrangian) position of the outer edge of the liquid shell, thus $4/3\pi X$ is the volume of the whole shell. The boundary conditions are: i) normal stresses at the outer liquid edge equal the ambient pressure; ii) normal stresses at the bubble boundary equal the bubble pressure plus the surface tension contribution. In addition, we assume that Henry's law holds for the gas at the bubble-liquid interface. Finally, the Giesekus model [33] is chosen as the constitutive equation for the viscoelastic liquid, as it well describes the rheology of the neat PCL (see below).

We select the initial bubble radius, R_0, as length scale of the system, the ratio of the liquid viscosity, η_p, and the fluid relaxation time, λ, as stress scale, and the initial number of moles of the gas in the bubble $p_{g0}R_0^3/R_gT$, with R_g the universal gas constant and T the absolute temperature, as a scale for the number of moles of the gas in the bubble.

The following system of dimensionless equations results:

$$\frac{4}{3}\eta_r \frac{du}{dt}\left(\frac{1}{u}+\frac{1}{u+X}\right) = P_g Wi + \frac{2}{3}\int_0^X \frac{T_{rr}-T_{\theta\theta}}{x+u}\,dx - \frac{1}{\Gamma u^{1/3}} \tag{1}$$

$$\left.\begin{aligned} \frac{\partial T_{rr}}{\partial t} &= -\frac{4}{3(x+u)}\frac{du}{dt}T_{rr} - (T_{rr}-1) - \alpha(T_{rr}-1)^2 \\ \frac{\partial (T_{rr}-T_{\theta\theta})}{\partial t} &= \frac{2}{3(x+u)}\frac{du}{dt}\left[(T_{rr}-T_{\theta\theta})-3T_{rr}\right] - (T_{rr}-T_{\theta\theta}) + \alpha(T_{rr}-T_{\theta\theta})(2-T_{rr}-T_{\theta\theta}) \end{aligned}\right\} \tag{2}$$

$$\frac{\partial \phi}{\partial t} = N(x+u)^{4/3}\frac{\partial^2 \phi}{\partial x^2} \tag{3}$$

$$\left(\frac{p_a + (p_{g0}-p_a)P_g}{p_{g0}}\right)u = 1+\phi(0,t) \tag{4}$$

Equations (1)-(3) are the momentum balance for the liquid, the Giesekus constitutive equations, and the diffusion equation for the gas in the liquid, respectively. Equation (4) derives from the mass conservation in the bubble. In these equations, $u(t) = R^3(t)$ is proportional to the bubble volume, $P_g = (p_g - p_a)/(p_{g0} - p_a)$, T_{rr} and $T_{\theta\theta}$ are the *rr*- and $\theta\theta$- components of the viscoelastic

stress tensor, and ϕ is a concentration potential defined as $\partial\phi/\partial x = c - c_0$, where c and c_0 are the time dependent and initial gas molar concentration in the liquid, respectively. The quantity ϕ is introduced for numerical reasons [18]. The parameter α is a constitutive parameter of the Giesekus equation that modulates the shear-thinning behavior (in the simulation α is 0.03). Furthermore, the following set of dimensionless parameters appears in Eqs. (1)-(4):

$$
\begin{aligned}
Wi &= \frac{\left(p_{g0} - p_a\right)\lambda}{\eta_p} \\
\Gamma &= \frac{u_0^{1/3}\eta_p}{2S\lambda} \\
N &= \frac{9D\lambda}{u_0^{2/3}} \\
\Phi &= RTH \\
\eta_r &= \frac{\eta_s}{\eta_p}
\end{aligned}
\qquad (5)
$$

where the Weissenberg number, *Wi*, is the product of the rate of bubble growth and the liquid relaxation time, the capillary number, Γ, is the ratio of viscous forces and interfacial forces acting on the bubble, with S the surface tension and $u_0 = R_0^3$, the timescale ratio, N is the ratio of liquid relaxation time to gas diffusion time, with D the diffusivity, Φ is a dimensionless Henry's constant, and η_r is the ratio of solvent viscosity, η_s, to polymer viscosity, η_p, in the Giesekus model [33].

Equations (1)-(4) are supplied with initial and boundary conditions:

$$
\begin{aligned}
&u(0) = 1 \\
&T_{rr}(0) = T_{\theta\theta}(0) = 1 \\
&\phi(0) = 0
\end{aligned}
\qquad (6)
$$

$$
\begin{aligned}
&\frac{\partial\phi}{\partial x} = \Phi\frac{p_{g0} - p_a}{p_{g0}}\left(P_g - 1\right) \qquad (x = 0) \\
&\frac{\partial^2\phi}{\partial x^2} = 0 \qquad (x = X)
\end{aligned}
\qquad (7)
$$

Equations (6) are the initial conditions for the bubble volume, the stress tensor and the mass concentration of the gas in the liquid layer. Equations (7) are the boundary conditions for the gas diffusion equation at the gas-liquid interface and at the outer liquid edge. Finally, the parameter X that accounts for the fluid volume surrounding the bubble also needs to be specified. Equations (1)-(4) with conditions (6)-(7) are numerically solved through the method of lines. The output of the SBG model is the single bubble growth kinetics, namely the evolution of bubble radius and gas pressure inside the bubble.

IM. The impingement (IM) model is intended to describe the relevant fluid dynamics when two (or more) bubbles come into contact.

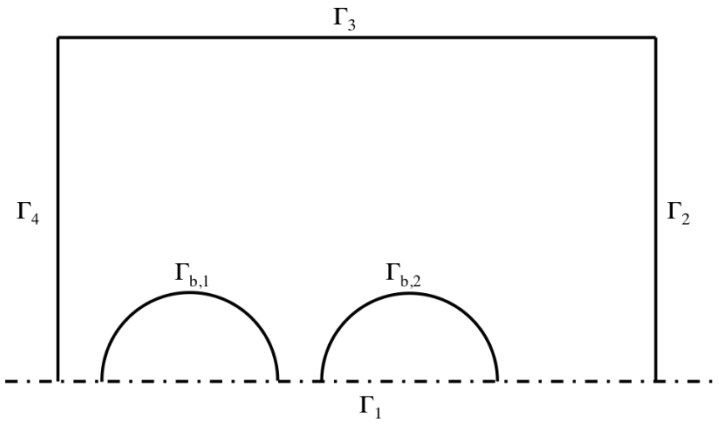

Fig. 4. Sketch of the geometry considered in the IM model.

In Fig. 4, a schematic view of two initially spherical bubbles with the same radius R_0 surrounded by the viscoelastic liquid is shown. Bubbles are collinear, i.e., their centers of mass lie on the same line. As a consequence, an axis of symmetry can be identified, thus reducing the geometry to 2Ds. The liquid motion is governed by the mass and momentum balance equations given by:

$$\left.\begin{aligned} &\nabla\cdot\boldsymbol{v}=0\\ &-\nabla p+\nabla\cdot\boldsymbol{T}=\mathbf{0}\end{aligned}\right\} \quad (8)$$

where $\boldsymbol{v}$, p and $\boldsymbol{T}$ are the fluid velocity, pressure and viscoelastic extra stress tensor fields, respectively. Axial symmetry is imposed on the boundary Γ_1, whereas symmetry is imposed on

Γ_2 and Γ_4. In other words, the system consists of an infinite array of collinear, not necessarily equidistant, initially spherical bubbles that expand in a viscoelastic liquid. Outflow conditions are set on Γ_3.

On the gas-liquid interfaces $\Gamma_{b,1}$ and $\Gamma_{b,2}$, the Young-Laplace boundary condition holds:

$$\boldsymbol{T} \cdot \boldsymbol{n} = (-p_g + K\, S)\boldsymbol{n} \tag{9}$$

where $\boldsymbol{n}$ is the outwards normal to the bubble surface, and K is the surface curvature. The gas pressure p_g is related to the mass of gas inside the bubble, m_g, through the ideal gas law:

$$p_g V_g = m_g R_g T \tag{10}$$

with V_g the bubble volume.

The gas mass m_g can be computed from a mass balance at the gas-liquid interface, which in turn would require the solution of a diffusion equation in the liquid domain. To simplify the problem, we assume that the time evolution of the gas mass inside the bubble is given by the previously described SBG model under the same conditions (i.e., same liquid, physical properties, initial radius, pressures, etc.). Such an assumption is strictly valid as long as the bubbles grow as isolated spheres, namely at the short times. However, we do not expect significant qualitative changes even when the bubble shapes become distorted due to hydrodynamic interactions with their neighbors. This greatly simplifies the model as the diffusion equation is not required, the gas mass dynamics being known as an output from the SBG model.

Equations (8) with boundary conditions (9)-(10) are solved through a finite element scheme. Outcomes of the IM model are the full stress and rate of strain tensor dynamics in the whole fluid domain, as well as the kinematic of the bubbles and, in particular, the time evolution of the liquid layer separating two bubbles.

RU. The rupture (RU) model is intended to describe the occurrence of rupture of the liquid layer separating two bubbles, therefore allowing to define specific rupture criteria. In the case of PCL, a semi-crystalline polymer, the occurrence of crystallization can be assumed as a rupture-inducing mechanism. Alternatively, rupture of the bubbles wall could be thought as triggered by the presence of solid additives.

It is known from the literature that polymer crystallization can be induced by flow. Such phenomenon, known as Flow-Induced Crystallization (FIC), affects both processing and final sample properties [34]. The enhancement of the crystallization rate is attributed to a significant enhancement of the crystal nucleation rate, which is the first step in a crystallization process. Various models, both empirical and micro-rheological, can describe and predict the FIC process [35]. Elongational flow has been demonstrated to be more effective than shear flow in orienting the polymer chains and, therefore, enhancing the crystallization rate. Under this respect, we can define a Deborah number, $De = \lambda/t_f$, where $1/t_f$ is the inverse of the flow characteristic time, equal to either the shear rate, $\dot{\gamma}$, in shear flow or to the stretching rate, $\dot{\varepsilon}$, in extensional flow. The difference in the effects of elongational and shear flow on FIC increases with *De*, showing an appreciable deviation from $De = 0.3$ (see, for example, Fig. 3 in Coppola et al. [35]).
In foaming, the polymer occupying the space between the bubbles undergoes intense extensional flows, leading to an enhanced crystallization rate. In our case, the thin polymer layer between the gas bubbles is subjected to a position-dependent extensional flow field, reaching a maximum at the shortest distance between bubbles. There, the chances to crystallize are the highest possible, with the resulting crystal nuclei acting like heterogeneous particles, thus inducing rupture of the polymer layer. Based on these considerations, two possible rupture criteria can be defined: (i) in the case of FIC, rupture is assumed upon attainment of flow-enhanced crystallization conditions (i.e. $De = 0.3$); (ii) in the case of filled polymers, where rupture is induced by the presence of heterogeneities, the attainment of a liquid thickness between bubbles equal to the significant size of the heterogeneity.

RE. As previously mentioned, the retraction of the thin film separating two bubbles is a necessary condition to achieve fully open-cell foams (see Fig. 2c). Retraction can only take place after rupture, when a "hole" is produced in the thin liquid film. Typically, retraction is imputed to the action of surface tension, which acts against the viscous forces in minimizing the interface area. In fact, the capillary number, Γ, regulates this retraction process. In some cases, such as soap bubbles, thermosetting flexible polyurethane foams or metal foams, surface forces are sufficiently larger than viscous forces [36] (i.e., $\Gamma << 1$). Bubble wall retraction is observed with the development of a fully open-cell structure, such as the one reported in Fig. 2c. In the case at hand, however, the PCL physical parameters under foaming processing conditions are such that surface tension induced retraction is not relevant. In fact, by using the following parameter values: $S = 2*10^{-2}$ N/m, $\eta = 10^5$ Pa*s, $\lambda = 0.15$ s and $R_0 = 10^{-5}$ m, one has

$\Gamma \approx 10^2 >> 1$, confirming that essentially no retraction is obtained by the action of interfacial tension. An alternative mechanism for retraction, therefore, must be considered. To this end, it is useful to remind that, depending on processing conditions, foaming can be a quite fast process, with complete expansion possibly achieved in a few seconds time. Consequently, the thinning of the liquid film separating bubbles can be very fast, too. Hence, by considering that we are dealing with a viscoelastic material, elastic recovery can be invoked as an additional mechanism for retraction, at least as long as the polymer relaxation time is longer than the foaming time. In this case, ruptured bubble walls may retract by the partial recovery of the strain in the extended polymer layer, driven by the elastic stress component.

A rough estimate of the fraction X of the area of the film separating two bubbles that can be recovered after the rupture event is given by $X = \dot{\varepsilon}_r \lambda$, where $\dot{\varepsilon}_r$ is the local stretching rate in the polymer at the rupture. To understand such an estimate, we may observe that the elastic elongational stress in the polymer film is "remembered" by the material for a time of the order of the polymer relaxation time. As a consequence, the relevant part of the recovered deformation is the one that has been built up along times shorter than λ. It is important to notice that the fraction of retracted area so defined corresponds to the Deborah number (i.e. *De*) at the rupture. This means that a retraction criterion can be defined on the basis of the *De* value reached at film rupture. The experimental availability of $\dot{\varepsilon}_r$ is not trivial, of course, since local measurements of film thickness and strain must be performed. In our case, however, the IM model yields the whole stress and strain tensor histories, thus $\dot{\varepsilon}^*$ can be easily evaluated.

The recovery-induced retraction, to the best of our knowledge, has not ever been applied to foaming, and in particular as a mechanism (and, hence, as a design tool) to drive closed- to open-cell morphologies. Despite the first observations of the retraction of thin liquid films were done on soap films long time ago [37, 38], only recently film rupture has been used as a mean to measure the viscosity of molten polystyrene films [39, 40]. Even more recently, the rupture of soap bubbles formed from a viscoelastic solution has been investigated with slow-motion imaging and experimental observations have been justified through a storing elastic energy that is released after the rupture, representing an additional driving force for film retraction [41]. In foaming, viscoelastic effects on foam morphology have not been considered yet. In the following, we thoughtfully describe our approach and how to derive information on foam morphology from growth dynamics. To clarify the interaction and flow of information among the modeled sequence of operations, Fig.5 represents a flow-chart of the whole approach.

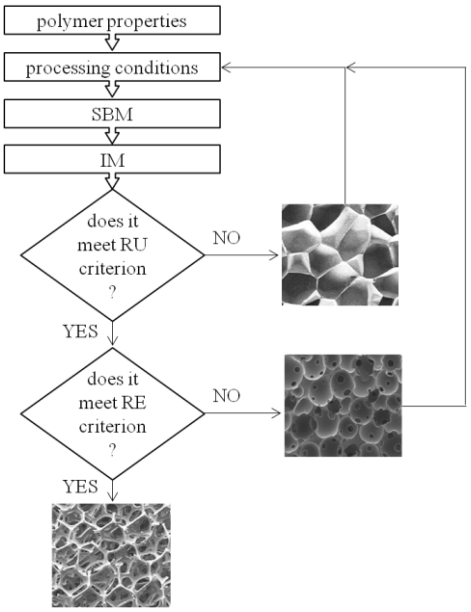

Fig. 5. Flow chart of the necessary operations for an open-cell structure.

3. Materials and Methods

3.1 Polymer and gas

PCL Capa^{TM} 6800 with a melt flow index of 3.02 g/10 min, weight average molecular weight of 120 kDa and number average molecular weight of 69 kDa, has been supplied by Perstrop Holding AB, Sweden. Linear viscoelastic moduli of the polymer have been measured in the temperature range 60-130°C under a nitrogen atmosphere using a strain-controlled Rheometric Scientific ARES rheometer (TA Instruments, USA) with parallel plates of 25 mm in diameter and a gap of about 1 mm. The strain amplitude has been set large enough to give a reliable signal while keeping the measurement in the linear viscoelastic regime (between 1% and 10%). Time sweep tests have been performed before the frequency sweep tests in order to measure the stability of the sample. A master curve has been constructed by using the horizontal shift factor with density compensation (Fig. 6b, the line is the Williams, Landel and Ferry fit). The viscoelastic response at 35°C has been obtained by using the value of the corresponding (extracted) shift factor and it is reported in Fig. 6a. At 35°C, the PCL shows a viscoelastic behavior with a relaxation time of about 0.2 seconds, calculated as the inverse of the cross over frequency in Fig. 6a.

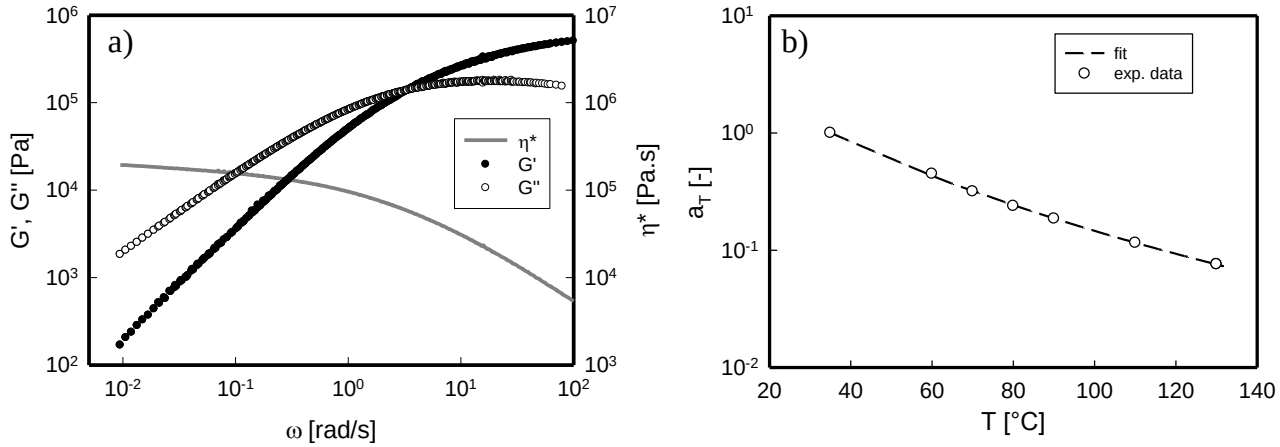

Fig.6. a) Superimposed linear viscoelastic moduli of PCL as a function of frequency at 35°C; b) horizontal shift factors as a function of temperature.

To perform the foaming experiments, a PCL film has been obtained by hot compression molding at 90°C and 10 MPa for 5 minutes. The thickness and the shape of the film have been controlled using a metal circular mold.

CO_2 (99.95% pure) supplied by Sol Group S.p.A., Italy, has been used as the physical blowing agent.

3.2 Foaming apparatus and visualization system

In order to validate the model two kind of experiments were required. On the one hand, we performed foaming experiments at different processing conditions using a novel batch foaming apparatus, called mini-batch, to obtain information on the final foam morphology. 3D rendering images of the mini-batch are reported in Fig. 7. A complete description of the foaming batch is given in [43].

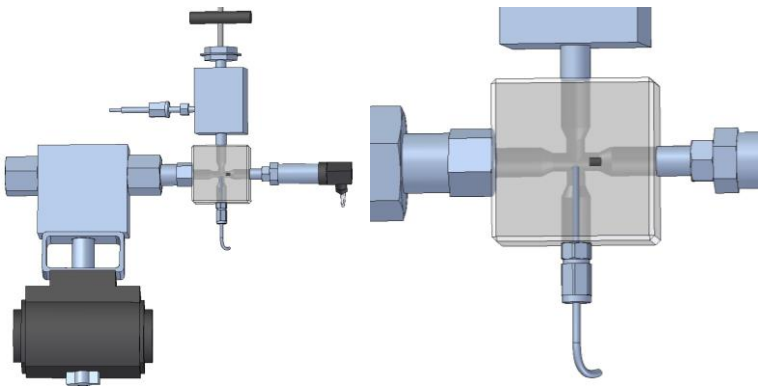

Fig.7. 3D rendering of the mini-batch in two views and magnifications.

On the other hand, based on previous apparatus for foam visualization [44, 45], we design a homemade pressurized vessel to allow the foaming visualization experiments. The pressurized vessel consists of a chamber with three transparent sapphire windows, a temperature port to control the temperature inside the vessel (as close as possible to the sample), a gas dosing/release port, and a pressure measurement port (see Fig. 8a). Two coaxial sapphire windows, placed at middle height of the vessel, are used to illuminate the chamber (light-cells), a third, smaller sapphire window, perpendicular to the other two windows, is used to visualize bubble formation in the PCL film (visualization cell). Fig. 8b shows an inside view of the chamber, where the PCL film is arranged on the bottom surface in front of the visualization cell.

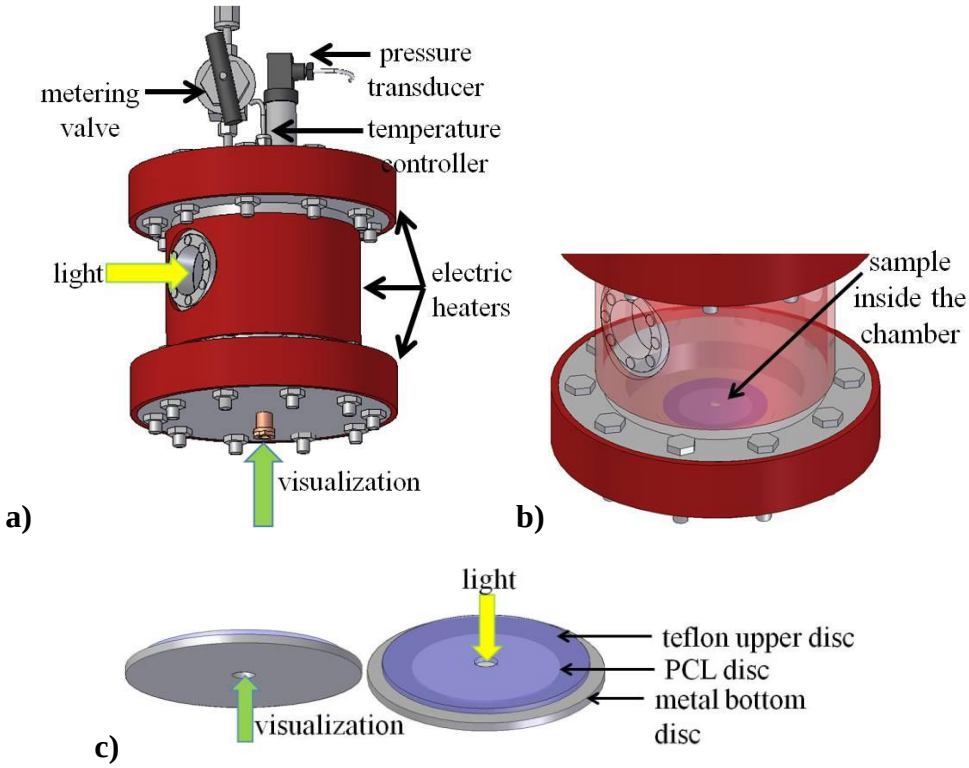

Fig.8. a) and b) 3D rendering of foaming visualization batch, in two views and magnifications. c) PCL sample between two sample-holders.

3.3 Experimental procedure

Two series of experiments were performed by means of the mini-batch (i.e. for the validation on the final foam morphology) and foaming visualization (i.e. for the validation of the SBG) system described in the previous section. Experiments were conducted by using the following procedure: PCL discs were saturated at 80°C with CO_2 at different saturation pressures (P_{sat})

for four hours. The gas was injected into the chamber via a syringe pump. In each experiment, the PCL sample was placed between two perforated holders (as shown in Fig. 8c). A stainless steel sheet (2.5 mm in thickness) with a 2 mm hole punched out in the center was placed beneath the PCL sample, so that the latter was partially suspended in air; observation of foaming process was focused upon that region. After sample loading, the vessel was, cooled to the foaming temperature T_{foam} = 35°C with a controlled, repeatable cooling history. At the foaming temperature, the sample was pressure-quenched to ambient pressure, using a Pressure Drop Rate (*PDR*) of 100 MPa/s. All experiments were performed at the same saturation and foaming temperatures and *PDR*. At the end of gas-saturation step, therefore, P_{sat} and the gas mass fraction in the polymeric matrix, C_{sat}, are univocally correlated and can be indifferently used as a unique processing variable.

The foaming process was captured by a speed camera DMK 41AUO2 by Imaging Source, Germany, placed in front of the visualization-cell. The images were analyzed through ImageJ® in order to evaluate the growth of the bubble radius in time.

4. Results and Discussion

Firstly, the SBG model has been experimentally validated. The rapid pressure drop applied in the foaming visualization system causes a thermodynamic instability within the polymer/gas solution to initiate the foaming process. Fig. 9 shows four successive snapshots taken during the foaming process, as described in §3.3. The reader may observe numerous peripheral bubbles nucleated heterogeneously at the interface with the circular sample holders, and a single central bubble, which, by chance, has nucleated sufficiently far from the others. This occurrence allowed verifying the SBG model with experimental data. In Fig. 10, we report a comparison between the experimental data and the SBG model predictions in terms of the ratio between the actual and the initial bubble radius. It is worth remarking that the theoretical curve displayed in Fig. 10 is computed by solving Equations (1)-(4) with the values of the dimensionless parameters in Equation (5) obtained from measured physical properties [11] and the operating conditions of the actual experimental system (i.e. those illustrated in § 3.3). In Table I and II, the characteristic material parameters (extrapolated from Pastore Carbone et al. [11]) and the numerical values (as described in the §2) are reported. It is clear that the SBG model predictions quantitatively agree with the experimental data in the first four seconds of the experiment.

Henry Constant (H) [mol/(N*m)]	Interfacial tension (S) [mN/m]	Diffusivity (D) [m^2/s]	Specific volume ($1/\rho$) [m^3/kg]
$5.2*10^{-5}$	19.3	$3.5*10^{-10}$	918.1

Table I. Numerical values of the physical parameters used in the model for the system PCL/CO_2, considering the processing conditions (i.e. 35°C and 5.8 MPa).

Wi	1.167
Γ	3158
N	0.0468
Φ	1.288
η_r	0
X	729

Table II. Numerical values of the dimensionless parameters used in the numerical solution of the SBG model.

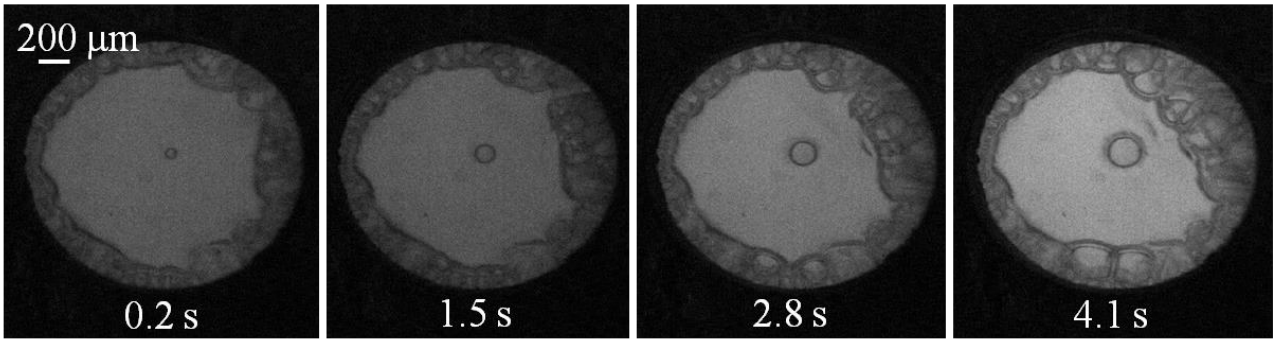

Fig. 9. Snapshots of PCL disc solubilized at P_{sat}= 5.8MPa.

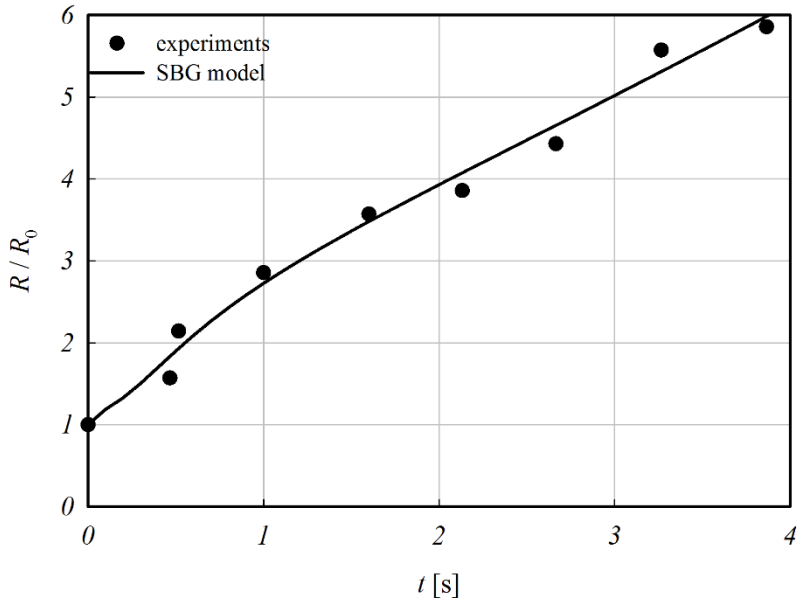

Fig.10. Growth of a CO_2 bubble in PCL: comparison between experimental data (symbols) and SBG model predictions (line). The values of the parameters are reported in Table I.

The temporal evolution of the gas pressure $p_g(t)$ and bubble radius obtained from the SBG model is, then, used as an input for the IM step. Specifically, we studied the growth of a periodic array of initially equidistant bubbles of the same size. Through numerical simulations, we investigated the shape and stress evolution in the polymer layer surrounding the bubbles. In Fig. 11, the color maps of the first normal stress difference $N_1 = T_{rr} - T_{zz}$, with r and z the radial and axial coordinates of a cylindrical reference frame centered on the line connecting the centers of the bubbles, are shown at four consecutive times. Due to the axial symmetry of the problem, in Fig. 11 a section of the 3D geometry on an rz-plane is displayed, the azimuthal coordinate being irrelevant. The parameters used in the simulation shown in Fig. 11 are the same of the SBG simulation (Table I). The initial radius of the bubble is R_0 = 10 μm, the initial thickness of the layer between the bubbles is δ_0 = 37.5 μm (δ is defined in Fig. 11). This value has been determined from SEM micrographs of the final foam morphology, by measuring the average distance among the centers of the cells and the final foam density. This is a key point in the current modeling approach and allows not to include the bubble nucleation phenomenon. As expected, when the two bubbles start to interact (see t = 1 s in Fig. 11) the maximum N_1-value is located at the middle of the line connecting the centers of the bubbles (in the point A, i.e. $N_{1,A}$). As the bubbles grow, such value increases as a consequence of the increasing stretching rate in the inter-bubble layer.

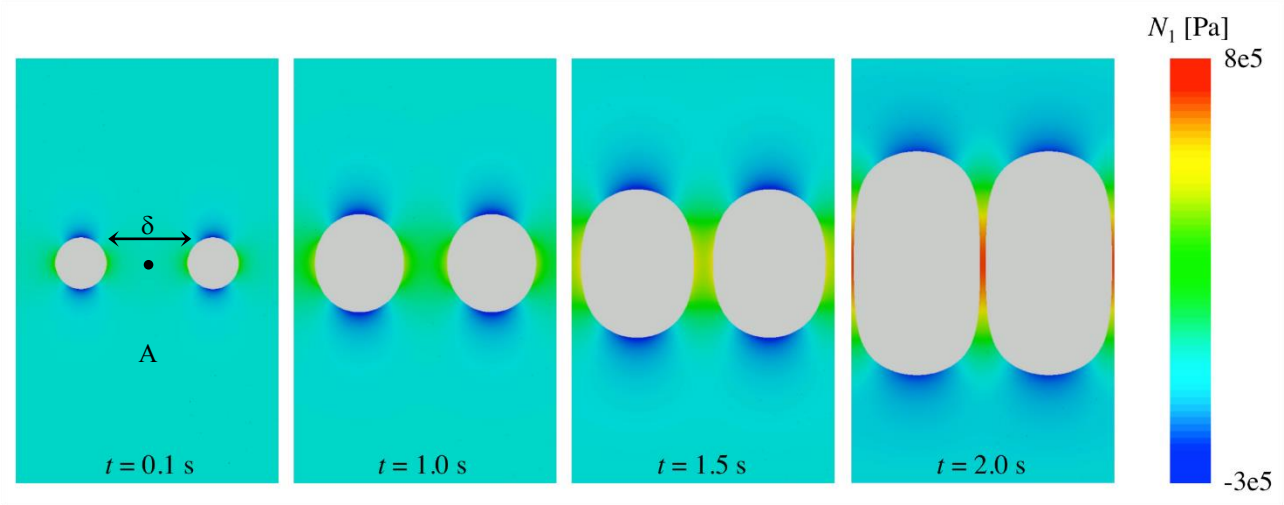

Fig.11. Color maps of the first normal stress difference N_1 in the polymer surrounding two bubbles at increasing times for R_0 = 10 μm, δ_0 = 37.5 μm and the values of the parameters in Table I. A is the middle point of the line connecting the centers of two bubbles.

The simulation results provide the temporal evolution of all quantities of interest. In particular, the thickness δ of the layer between the bubbles, plotted in Fig. 12, monotonically decreases in time from its initial value δ_0 as bubbles are approaching.

It is worth noting that the slope of δ as function of time changes passing through an inflection point between 1.5 and 2 seconds (see Figure 12). This is due to the predicted strain hardening of the fluid subjected to high stretching rates, which is an important phenomenon in the bubble coalescence process, as already reported elsewhere [49]. Due to the flow induced higher viscosity of the polymer medium between the two approaching bubbles, the thinning kinetic of the layer, consequently, slows down.

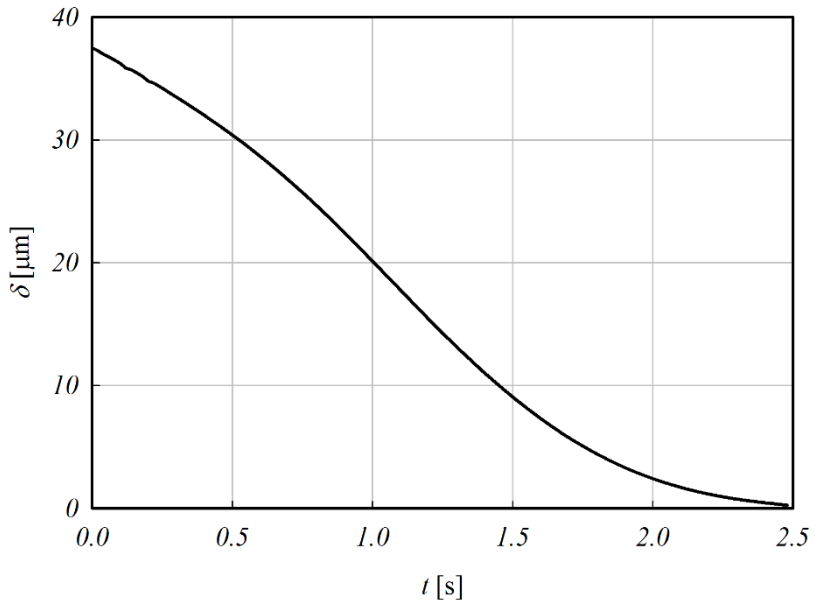

Fig. 12. Time evolution of the thickness δ of the polymer layer between an array of equidistant bubbles for R_0 = 10 μm, δ_0 = 37.5 μm and the values of the parameters in Table I.

On the basis of the results provided by SBG and IM steps, we are now in a position to evaluate the rupture of the polymer layer and its possible retraction. In this regard, we recall that it is known from the literature that, for crystallizing polymers, the crystallization event occurs when the *De* locally reaches values of about 0.3 [35]; such an event can be responsible for rupture of the polymer layer. In case the stresses in the liquid around the rupture point are sufficiently large, retraction of the polymer layer can happen.

In order to study the different morphologies that can be obtained in PCL foams, we performed two sets of experiments at different saturation pressures: $P_{sat,1}$ = 5.5MPa and $P_{sat,2}$ = 10MPa. All other processing parameters have been kept constant, i.e., temperature T = 35°C and *PDR* = 10MPa/s. The SEM images in Fig.13 confirm that different morphologies are indeed obtained. For the lower P_{sat} (Fig. 13a), a closed-cell morphology is obtained, where the gas cells are clearly separated by polymer layers. Conversely, at the higher saturation pressure (Fig. 13b), the cells are not clearly distinguishable.

a) 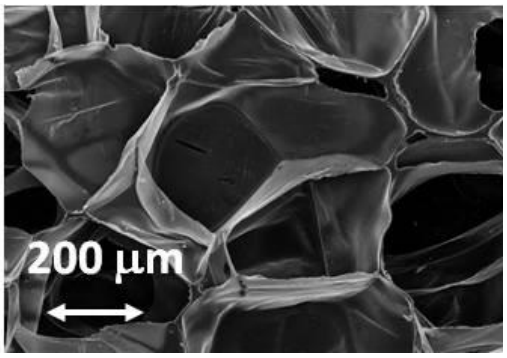

b) 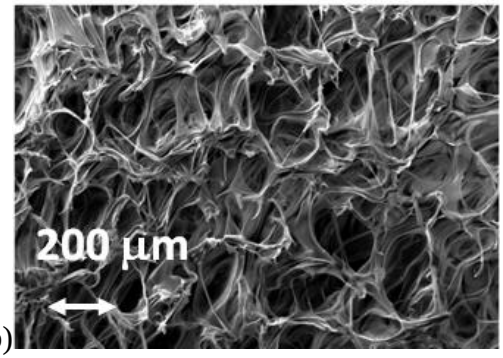

Fig.13. SEM images of PCL foams.(a) closed-cell morphology (b) open-cell morphology.

We run numerical simulations of the SBG and IM of two systems characterized by the same processing conditions as the experiments discussed above. Specifically, for the system in Fig. 13a, the initial thickness of the polymer film is δ_0 = 60 μm, whereas, for the system in Fig. 13b, it is δ_0 = 37.5 μm; in both cases, the initial radius of the bubbles is R_0 = 10 μm. In Fig. 14, we report, for the two cases, the time evolution of the maximum *De*, that is, the one evaluated at point A *(*De_A*)*. As no additive is present in the polymer and since PCL is a crystallizing polymer, we expect that rupture is caused by *FIC*. It is worth of note that, even if it is impossible to quantitatively indicate the quiescent induction time for PCL in the same operative conditions, we can speculate that the *FIC* time would be surely faster than the quiescent one [48]. The simulations end when the thickness of the film between the bubbles goes to zero. In the first case, characterized by P_{sat} = 5.5MPa, De_A does not reach the threshold value of 0.3 necessary for crystallization (red curve). Hence, in agreement with the experiments, a closed-cell structure is predicted. On the contrary, for P_{sat} = 10MPa, the De_A overcomes the threshold value at about t = 2.2s (green curve). Crystallization-induced rupture can take place, thus yielding an open-cell structure compatible with the experimental one shown in Fig. 13b.

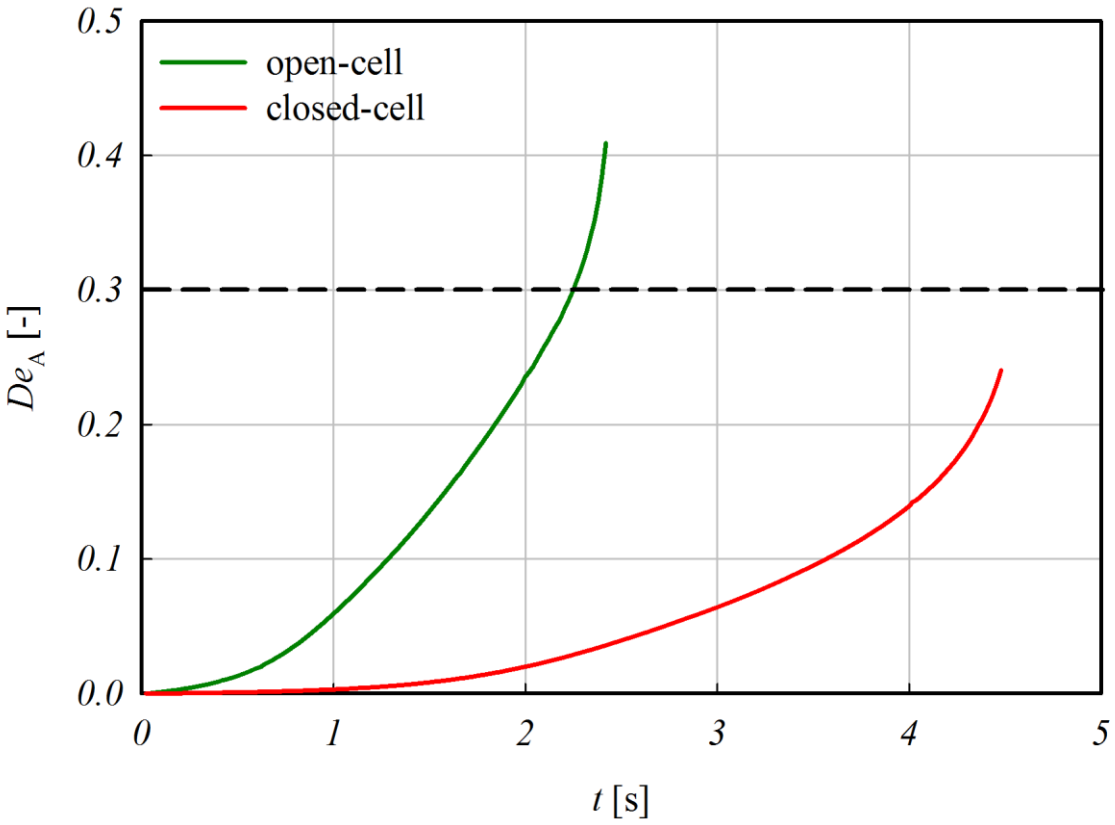

Fig.14. Temporal evolution of De_A computed at the middle point of the line connecting centers of two approaching bubbles for $P_{sat,1}$ = 5.5MPa (red curve) and $P_{sat,2}$ = 10MPa (green curve).

The procedure so far developed can be used to design materials and processing conditions to obtain desired morphologies for a pure, semi-crystalline polymeric material. In particular, the rate of bubble inflation, strictly related to the initial overpressure but also to all the material physical properties, can be used as a tool to control the morphology. In fact, when conditions are such that flow-induced crystallization takes place within the stretched bubble wall layer, rupture is expected to set in. The same basic principles can be used, however, also in the case of filled polymeric materials. Let us consider, for example, an amorphous polymer, where crystallization-induced rupture cannot take place. As previously remarked, however, the solid particle in-homogeneities embedded in the matrix can induce rupture in a very similar way when the wall bubble thickness becomes comparable to the significant particle size. In this case, obviously, the properties of the expanding polymer, which are responsible for its foaming behavior, can be severely affected by the presence of the additive. For instance, additives may work nucleating agents for the bubbles, thereby modifying the foam morphology, as well as the rheological and surface properties. Of course, it is possible to measure those properties and, as

it has been done throughout this work, adapt the starting conditions of the model (e.g. R_0 and δ_0) to the observed morphology.

In spite of the above-mentioned complication, the very final stages of bubble rupture and possible retraction is expected to be always dictated by the local interactions between the stress/strain evolution and the wall geometrical parameters. To make this point clear we may suppose, in a simplistic manner, that properties and morphologies do not change and, with reference to the foaming conditions reported in Table I, the same bubbles dynamics and interaction holds, also in case where solid particles are embedded in the polymer. Fig. 15 shows the temporal evolution of δ, the first normal stress difference at point A $N_{1,A}$, and the De_A. When a particle of 10 μm characteristic size is used, we expect that the polymeric film breaks when its thickness reaches approximately the same size. As shown in Fig.15 (blue line), this happens at t=1.4s. Here, the first normal stress difference is $N_{1,A} \approx 4*10^5$ Pa and the $De_A \approx 0.14$. Under such conditions, a certain, limited, amount of retraction will take place as predicted by described retraction criterion (see § 2 section RE). In case the solid particle is 1 μm in size, the polymeric film is expected to break after about 2.25s (vertical red line in Fig. 15). Here, $N_{1,A}$ is about $9*10^5$ Pa and De_A is about 0.3. In this latter case, due to the higher elastic energy stored in the polymer layer at rupture, a much more pronounced retraction is expected with respect to the previous case, likely leading to a morphology similar to the one shown in Fig. 13b. As a partial conclusion of this speculation on the size of the additives, while it could be erroneously thought that breaking the bubbles wall earlier (by using bigger particles) could be beneficial for achieving an open-cell morphology, we prove, conversely, that it is necessary to use smaller particles to retard the bubbles wall rupture, to allow the build-up of stresses in order to increase the elastic recovery of the bubbles wall and, in turn, to have a fully open-cell foam. It is worth to stress here that for the sake of simplicity we implicitly assumed spherical and monodispersed particles, while foaming nucleating additives are often very far from being spherical (e.g. platelets or aciculae). The inclusion of anisotropic particles in the model (both the IM and RU, but also the SBG and RE, to a lesser extent) would obviously add difficulties to the present approach. More specifically, we can speculate that the significant size for the cell opening could change during the foaming process, according to the tumbling process of the anisotropic particles. We consider this, however, out of the scope of the present contribution, and will be a matter of future work.

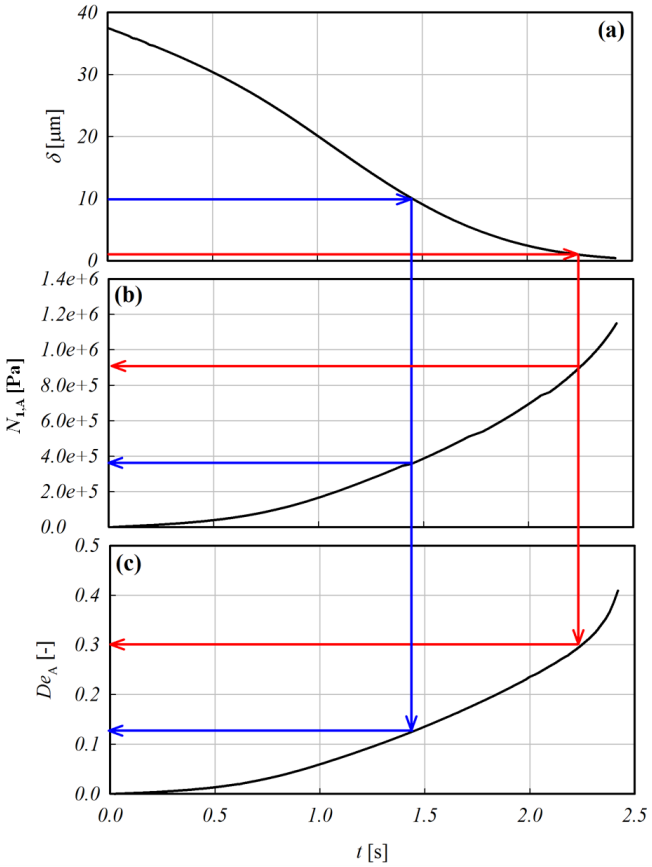

Fig. 15. Time evolution of the thickness of the layer between two consecutive bubbles δ (a), of the first normal stress difference $N_{1,A}$ (b), and of De_A(c) from numerical simulations. The operating parameters are reported in Table I, the initial radius of the bubbles is R_0 = 10 μm and the initial thickness of the polymer layer is δ_0 = 37.5 μm. The lines are guides for the eye, indicating the addition of 10μm solid particle (blue line) and 1μm solid particles (red line).

5. Conclusions

In this paper, we develop a novel approach to cell-opening in thermoplastic foams. The procedure is based on sequential steps. Single bubble growth modeling results are used as an input for the impingement model where two bubbles surrounded by a viscoelastic fluid grow and hydrodynamically interact. We identify a criterion that employs the computed stresses, the elongational rate and the film thickness to predict the rupture of the polymeric layer between the bubbles and its retraction. As a result, the model is able to make predictions on the final foam morphology, starting from the gas polymer solution properties. We performed independent experiments to assess the validity of each step of our approach. In conclusion, the

developed methodology allows to design the materials and processing conditions to control foam morphology.

As a concluding remark, it is worth of note that the current work brings three independent contributions:

- A numerical simulation approach that covers the foaming process from bubble growth to cell wall rupture and retraction was developed for a viscoelastic liquid. The result is a time evolution of bubbles and of the bubbles wall during the foaming process.
- The rupture and retraction criteria, tied at the time evolution of bubbles, were proposed to predict the final foam morphology (i.e. closed cells, open cells with broken bubble walls or fully open cells with polymer confined to the struts). The retraction criterion, introduced in the present contribution, represents a novel brick in the fundamental understanding of cell opening in thermoplastic foaming.
- The present approach allows designing the foaming process and the additives for the specific aimed morphology.

Acknowledgements

Rete di Eccellenze Mastri (MAteriali e STRutture Intelligenti, Codice 4-17-3) and Procter and Gamble Company (Newcastle Innovation Centre, Whitley Road, Longbenton, NE12 9TS, United Kingdom) are acknowledged for partial support of this work.

References

[1] S.T. Lee, C.B. Park, Foam extrusion: principles and practice, CRC Press (2014).

[2] H. E. Naguib, C. B. Park, U. Panzer, N. Reichelt, Strategies for achieving ultra-low-density polypropylene foams, Polym. Eng. Sci., 42 (2002), 1481–1496.

[3] Y. Sato, T. Takikawa, A. Sorakubo, S. Takishima, H. Masuoka, M. Imaizumi. Solubility and diffusion of carbon dioxide in biodegradable polymers, Ind. Chem. Eng. Res., 16 (1), (2000) 1029–1034.

[4] S. Cotugno, E. Di Maio, C. Ciardiello, S. Iannace, G. Mensitieri, L. Nicolais, Sorption thermodynamics and mutual diffusivity of carbon dioxide in molten polycaprolactone, Ind. Chem. Eng. Res. 42(19) (2003) 4398–4405.

[5] S. Cotugno, E. Di Maio, G. Mensitieri, S. Iannace, G.W. Roberts, R.G. Carbonell, H. B. Hopfenberg, Characterization of microcellular biodegradable polymeric foams produced from supercritical carbon dioxide solutions. Ind. Chem. Eng. Res., 44 (2005) 1795–1803.

[6] M. Lee, C.B. Park, C. Tzoganakis, Measurements and modeling of PS/Supercritical CO, solution viscosities, Polym. Eng. Sci., 39 (1999) 99–109.

[7] E. Di Maio, S. Iannace, G. Mensitieri, L. Nicolais, predictive approach based on the simha–somcynsky free-volume theory for the effect of dissolved gas on viscosity and glass transition temperature of polymeric mixtures, J. Pol. Sci., 43 (2006) 56-89.

[8] C.D. Han, C. Y. Ma, Rheological properties of mixtures of molten polymer and fluorocarbon blowing agent. I. Mixtures of low-density polyethylene and fluorocarbon blowing agent, J. Appl. Polym. Sci., 56 (1983) 28-851.

[9] L. J. Gerhardt; C. W. Manke, E. J. Gulari, Rheology of polydimethylsiloxane swollen with supercritical carbon dioxide, J. Polym. Sci. Pol. Phys., 35 (1997) 69-523.

[10] J. R. Royer, Y. J. Gay, M. Adams, J. M. De Simone; S. A. Khan, Polymer melt rheology with high-pressure CO_2 using a novel magnetically levitated sphere rheometer, J. Polym. 43 (2002) 2356-2375.

[11] M. G Pastore Carbone, E. Di Maio, G. Scherillo, G. Mensitieri, S. Iannace, Solubility, mutual diffusivity, specific volume and interfacial tension of molten PCL/CO_2 solutions by a fully experimental procedure: effect of pressure and temperature, J. Sup. Fluids, 30 (2012) 303–309.

[12] S. G. Kazarian, K. L. Andrew Chan, V. Maquet, A. R. Boccaccini, Characterisation of bioactive and resorbable polylactide/Bioglass® composites by FTIR spectroscopic imaging, Biomaterials, 25 (2004) 3931–3938.

[13] M G. Pastore Carbone, E Di Maio, P. Musto, A. Braeuer, G. Mensitieri, On the unexpected non-monotonic profile of specific volume observed in PCL/CO_2 solutions, Polymer, 56 (2015) 252–289.

[14] J. S. Colton, N. P. Suh, Nucleation of microcellular thermoplastic foam with additives: part I: theoretical considerations, Polym. Eng. Sci., 27 (1987) 485–492.

[15] N. S. Ramesh, D. H. Rasmussen, and G. A. Campbell, The heterogeneous nucleation of microcellular foams assisted by the survival of microvoids in polymers containing low glass transition particles. part I: mathematical modeling and numerical simulation, Polym. Eng. Sci., 34 (1994) 452–478.

[16] E. Kiran, Foaming strategies for bioabsorbable polymers in supercritical fluid mixtures. Part I. Miscibility and foaming of poly(l-lactic acid) in carbon dioxide + acetone binary fluid mixtures, J. Supercrit. Fluid., 54 (2010) 296–307.

[17] M. Amon, C. D. Denson, Study of the dynamics of foam growth: simplified analysis and experimental results for bulk density in structural foam molding, Polym. Eng. Sci., 26 (1986) 255–267.

[18] A. Arefmanesh, S. G. Advani, Diffusion-induced growth of a gas bubble in a viscoelastic fluid, Rheol. Acta, 283 (1991) 274–283.

[19] S. K. Goel, E. J. Beckman, Generation of microcellular polymeric foams using supercritical carbon dioxide. I: Effect of pressure and temperature on nucleation, Polym. Eng. Sci., 34 (1994) 1137–1147.

[20] T. Ishikawa, K. Taki, M. Ohshima, Visual observation and numerical studies of N_2 vs CO_2 foaming behavior in core-back foam injection molding, Polym. Eng. Sci., 56 (2012) 659-691.

[21] M. A. Shafi, R. W. Flumerfelt, Initial bubble growth in polymer foam processes, Chem. Eng. Sci., 52 (1997) 627–633.

[22] S. K. Goel, E. J. Beckman, Nucleation and growth in microcellular materials: supercritical CO_2 as foaming agent, AIChe J., 41(1995) 357–367.

[23] M. A. Shafi, J. G. Lee, R. W. Flumerfelt, Prediction of cellular structure in free expansion polymer foam processing. Polym. Eng. Sci., 36 (1996) 1950–1959.

[24] M. Shimoda, I Tsujimura, M. Tanigaki, M. Ohshima, Polymeric foaming simulation for extrusion processes, J. Cell. Plast., 37 (2001) 517–536.

[25] S. L. Everitt, O. G. Harlen, H. J. Wilson, Bubble growth in a two-dimensional viscoelastic foam, J. Non-Newton Fluid., 137 (2006) 46–59.

[26] J. J. Feng, C. A. Bertelo, Prediction of bubble growth and size distribution in polymer foaming based on a new heterogeneous nucleation model, J. Rheol., 48 (2004) 439.

[27] S. N. Leung, C. B. Park, D. Xu, H. Li, R. G. Fenton, R. G., Computer simulation of bubble-growth phenomena in foaming, Ind. Eng. Chem. Res., 45 (2006) 7823–7831.

[28] I. Tsivintzelis, A. G. Angelopoulou, C. Panayiotou, Foaming of polymers with supercritical CO_2: An experimental and theoretical study, Polymer, 48 (2007) 5928–5939.

[29] K. Taki, Experimental and numerical studies on the effects of pressure release rate on number density of bubbles and bubble growth in a polymeric foaming process. Chem. Eng. Sci., 63 (2008) 3643–3653.

[30] K. Taki, K. Tabata, S. Kihara, M. Ohshima, Bubble coalescence in foaming process of polymers, Polym. Eng. Sci., 51 (2006) 1241-1259.

[31] P. C. Lee, J. Wang, C. B. Park, Extruded open-cell foams using two semicrystalline polymers with different crystallization temperatures. Ind. Eng. Chem. Res., 45 (2006) 175–181.

[32] P. C. Lee, G. Li, J. W. S. Lee, C. B. Park, Improvement of cell opening by maintaining a high temperature difference in the surface and core of a foam extrudate, J. Cell. Plast., 43 (2007), 431–444.

[33] R.W. Kolkka, G.R. Ierley, Phase space analysis of the spurt phenomenon for the Giesekus viscoelastic fluid model, J Non-Newton Fluid, 33 (1989), 305-323.

[34] R. L. Miller, Flow Induced Crystallization in polymer systems, Ed. Gordon and Breach: London, (1979).

[35] S. Coppola, N. Grizzuti, P. L. Maffettone, Microrheological modeling of flow induced crystallization, Macromolecules, 34 (2001) 5030–5036.

[36] S. Hartland, Surface and interfacial tension. Measurement, theory, and application, Marcel Denkker Inc. (2006).

[37] M. A. Dupré, Sixiéme memoire sur la theorie méchanique de la chaleur, Ann. Chim. Phys., 4 (1967), 194–220.

[38] Lord Rayleigh, Some applications of photography, Nature, 44 (1891) 249–254.

[39] K. Dalnoki-Veress, B. G. Nickel, C. Roth, J. R. Dutcher, Hole formation and growth in freely standing polystyrene films, J. Fluid Mech., 59 (1999) 2153–2156.

[40] C. B. Roth, B. Deh, B. G. Nickel, J. R. Dutcher, Evidence of convective constraint release during hole growth in freely standing polystyrene films at low temperatures, Phys. Rev., 72 (2005) 021802.

[41] E. Sabadini, R. F. S. Ungarato, P. B. Miranda, The elasticity of soap bubbles containing wormlike micelles, Langmuir, 30 (2014) 727–732.

[42] M. L. Sentmanat, Miniature universal testing platform: from extensional melt rheology to solid-state deformation behavior, Rheol. Acta, 43 (2004), 657-669.

[43] D. Tammaro, V. Contaldi, M. G. Pastore Carbone, E. Di Maio, S. Iannace, A novel lab-scale batch foaming equipment: the mini-batch, J. Cell. Past., 2 (2015) 654.

[44] Q. Guo, J. Wang, C. B. Park, M. Ohshima, A microcellular foaming simulation system with a high pressure-drop rate, Ind. Eng. Chem. Res., 45 (2006) 6153–6161.

[45] A. Wong, R. K. M. Chu, S. N. Leung, C. B. Park, J. H. Zong,. A batch foaming visualization system with extensional stress-inducing ability, Chem. Eng. Sci., 66 (2011) 55–63.

[46] J. Banhart, Metal Foams: Production and Stability, Adv. Eng. Mater., 8 (2006) 781–794.

[47] G. Harikrishnan, T. U. Patro, D. V. Khakhar, Polyurethane foam Clay nanocomposites: Nanoclays as cell openers, Ind. Eng. Chem. Res., 45 (2006) 7126–7134.

[48] S. Acierno, E. Di Maio, S. Iannace, N. Grizzuti, Structure development during crystallization of polycaprolactone, Rheol. Acta., 45 (2006) 387-392.

[49] Y. Otsuki, T. Kanai, Numerical Simulation of Bubble Growth in Viscoelastic Fluid With Diffusion of Dissolved Foaming Agent, Polym Eng Sci, 45 (2005) 9.

Chapter 4: results and discussion, focus boxes

In this Chapter 4, all the focus boxes studied in parallel with the main research, as it was explained in introduction part, are reported. The focus box is a particular research theme required to develop the main research goal but that can be seen as an independent section of the research as well. In particular, in the first paragraph the design and the test on a novel batch foaming apparatus is reported, then, the interesting results obtained from this batch foaming are shown and explained in the second paragraph. The last paragraph resumes all the work done at University of Stanford to study the drainage of thin films.

4.1 *A novel lab-scale batch foaming equipment: The mini-batch*

In the following paragraph, it is reported the work authored by D. Tammaro, V. Contaldi, M. G. Pastore Carbone, E. Di Maio, S. Iannace, and titled “A novel lab-scale batch foaming equipment: the mini-batch”, published in 2015 on *Journal Cellular Plastic*.

Original Article

JOURNAL OF CELLULAR PLASTICS

Journal of Cellular Plastics
0(0) 1–11

DOI: 10.1177/0021955X15584654
cel.sagepub.com
SAGE

A novel lab-scale batch foaming equipment: The mini-batch

D Tammaro[1], V Contaldi[1], MG Pastore Carbone[1], E Di Maio[1] and S Iannace[2]

[1]Dipartimento di Ingegneria Chimica, dei Materiali e della Produzione Industriale, University of Naples Federico II, P.le Tecchio 80, I-80125 Napoli, Italy

[2]Istituto per iPolimeri, Compositi e Biomateriali, Consiglio Nazionale delle Ricerche,P.le E. Fermi, 1, Loc. Granatello, I-80055 Portici (Na) - Italy

Abstract

In this paper, we report the design of a new experimental apparatus for the study of the foaming process of thermoplastic polymers with physical blowing agents. The novel lab-scale batch foaming equipment is capable of achieving accurate control of the processing variables, namely, the temperature, the saturation pressure and the pressure drop rate and, furthermore, of allowing the achievement of very high pressure drop rates, the observation of the sample while foaming and the very fast extraction of the foamed sample. By recalling the considerations discussed by Muratani et al. in 2005 (Muratani et al., J. Cell. Plast 24 (2005) 15), the design converged into a simple, cheap and very small pressure vessel, thereby denoted as mini-batch. We herein describe the overall design path of the mini-batch, its characteristics, configurations, together with some examples of use with polystyrene and CO_2 as the blowing agent.

Keywords

batch foaming, pressure vessel, pressure drop rate, view cell, mini-batch

*Corresponding author,

edimaio@unina.it

Phone: +39 081 768 25 11

Fax: +39 081 768 24 04

Introduction

In the last decades, general understanding of the foaming process of thermoplastic polymers with physical blowing agents settled around the delineation of the main processing variables and of their effects on the resulting foam, in terms of foam density and cell morphology. In the 80's, in particular, the effect of the Pressure Drop Rate, PDR (i.e. the rate at which the saturation pressure is reduced to ambient pressure by blowing agent release - in fact, the rate at which super saturation of the blowing agent is achieved) was introduced as an important processing variable, being involved in the competition between the bubble nucleation and growth[2-3]. The reduction of the PDR, for instance, decreases the rate of stable nuclei formation, in turn increasing the chances for the blowing agent to inflate the formed bubbles, with a final coarsening of the cellular structure[4-7]. From the other side, since fine-celled foams possess, typically, better properties (among others, mechanical as well as thermal insulating), the correlation between the PDR and the final cell morphology were extensively studied by researchers and process designers, with the final aim of maximizing the PDR and, in turn, minimizing cell size [8-12]. In this context, numerous studies reported the design of foaming apparata allowing the possibility to release the blowing agent at several PDR. Among others, Muratani et al.[1]minimized the volume of the pressure vessel in order to increase the PDR. In fact, standing the gas discharge system, the reduction of the volume of the vessel determined an increase of the PDR by reducing the amount of gas to be evacuated from the vessel itself[13]. Furthermore, they used an hydraulic press machine to close the upper lid of the pressure vessel in order to cool and quickly take out the sample after foaming. By using this reduced-volume pressure vessel, Muratani achieved values of PDR as high as 25MPa/s, from a saturation pressure of 15MPa. Guo et al. achieved much higher PDR values, i.e. 2500 MPa/s from a saturation pressure of 27.7MPa, with a foaming system consisting of the vessel and an ad-hoc evacuating volume, characterized by optimized connections for the maximization of the PDR[14]. In particular, the apparatus proposed by Guo et al. was equipped with a sapphire window and a fast acquisition camera in order to observe the bubble nucleation. Nevertheless, unlike Muratani's apparatus, it was not possible to extract the foamed sample for further measurement. Chen et al. [15] achieved 150MPa/s from a saturation pressure of 21.1MPa with a pressure vessel capable of quick sample extraction and equipped with a tool for shearing the sample to investigate coupled effects of PDR and shear on the final foams, (actually it was not equipped with a view cell for on-line foaming observation).

This paper presents a novel batch foaming apparatus that possess all of these *three important functions* to study the foaming process, namely: i) it allows a wide PDR range, in particular towards very high PDR; ii) it allows a very fast foamed sample extraction; iii) it has a view cell to observe the foaming "on air". Furthermore, it is very simple, cheap, versatile, since it allows multiple configurations, and environmentally friendly, for the very limited use of CO_2 and thermal energy for operation. In this paper, we report on the designing process (principle of operation), the equipment characteristics (apparatus) and capabilities (results), with some foaming data using the polystyrene (PS)-CO_2 system. The miniaturization approach led us to call this new equipment as "mini-batch".

Principle of operation

The mini-batch has been developed to satisfy the aforementioned three functions and uses the pressure vessel miniaturization approach as proposed by Muratani et al. [1]. It has to possess all of the connections/ports needed to control the operations, namely, the temperature port to control the temperature inside the vessel (as close as possible to the sample), the gas dosing port, the pressure measurement port and the gas release port. Our miniaturization approach, then, was simply to *eliminate the pressure vessel itself*, by using a cross to connect the different ports. In this way, standing the gas release system, the minimization of the gas volume to be evacuated maximizes the PDR. One important feature of this design is the use of a ball valve (activated by an electromechanical actuator) as a pressure discharge system. When open, a full, see-through pipe is created, and the gas to be released does not find any obstruction on its way out of the equipment, again for PDR maximization. As a side, yet important result, the foamed sample, if sufficiently small, may be transported by the gas flow through this un-obstructed pipe, towards the outside of the system, as like an instantaneous foam extraction system. The third important feature of this design is the possibility to look inside the batch while conducting all of the sequences for foaming. To do so, a view cell can be assembled on the apparatus, as it will be seen in the following. Creative use of available connections, view windows, full-flow quick connectors, sensors, etc., allows for a full versatility of the system. Finally, the simplicity of the design and the availability of standard pieces of equipment and connections render the mini-batch extremely cheap and easy to assemble and use. We are confident it will help the development of the knowledge of the foaming process and allow more people to be involved in this fascinating subject.

Apparatus

3D rendering images of the mini-batch are reported in Figure 1. Figure 1a) shows a view of the assembled vessel with the four ports of the cross (indicated with No. 1 in the figure) occupied by the temperature sensor (No. 3), the pressure sensor (No. 4), the gas dosing system (No. 5) and the gas release (No. 6). No. 2 indicates the two square heating elements (one on the top and the other on the bottom). Figure 1b) and 1c) offer a detailed view of the assemble, with the cross rendered with a transparent material to show the sample positioning (dark colored polymer pellet) and the temperature sensor. The actual configuration is based on ½" NPT threads, but ¼" or other are possible, depending on the cross fitting. In the present case, the cross element is a mod. 15-24NFD cross from High Pressure Equipment Company, Erie, PA, USA. Temperature was controlled by a PID thermoregulator (Ascon-New England Temperature Solutions, Attleboro, MA, USA, model X1). A pressure transducer (Schaevitz-Measurements Specialties, Hampton, VA, USA, model P943) was used to measure pressures and the pressure history was registered by using a data acquisition system (DAQ PCI6036E, National Instruments, Austin, TX, USA).The pressure release system consists of a discharge valve (High Pressure Equipment Company, model 10-80 NFH ball valve) and a pneumatic electrovalve.

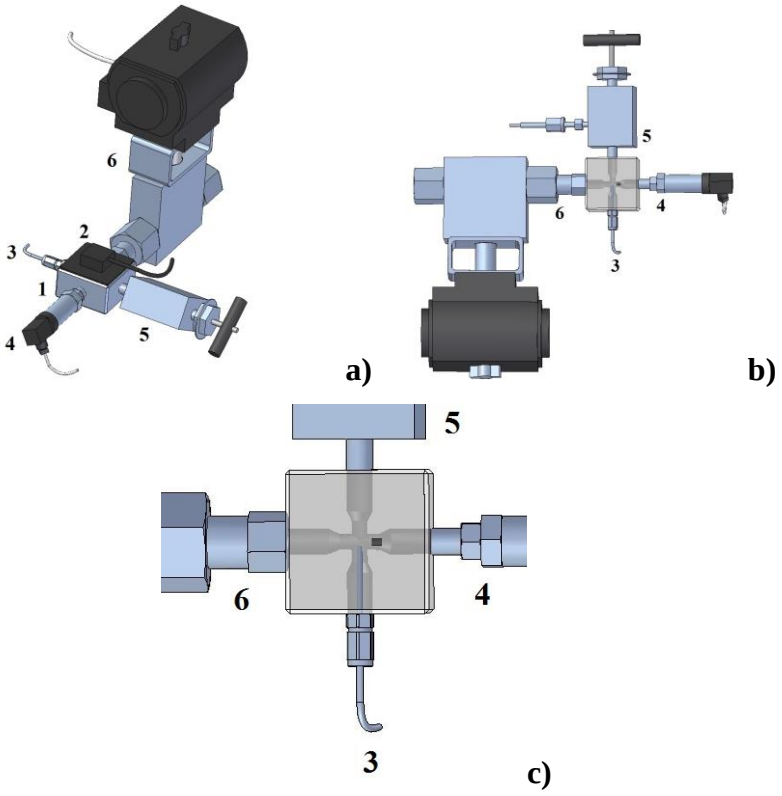

Figure 1:3D rendering of the mini-batch in three views and magnifications. a) assembled vessel, b) assemble vessel, with the cross rendered mode of transparent material. c) zoom on the sample positioning

Figure 2 shows two detailed pictures of the mini-batch. Figure 2a) shows the heating elements, and how the sample and the temperature sensor are placed within the vessel (in this case, the front port has been left open for proper observation). Figure 2b) shows again the temperature sensor and sample, but now in the "open" position of the ball valve. It is evident, in this case, the full, see-through pipe, responsible for the fast evacuation of the gas and the extraction of the foamed sample.

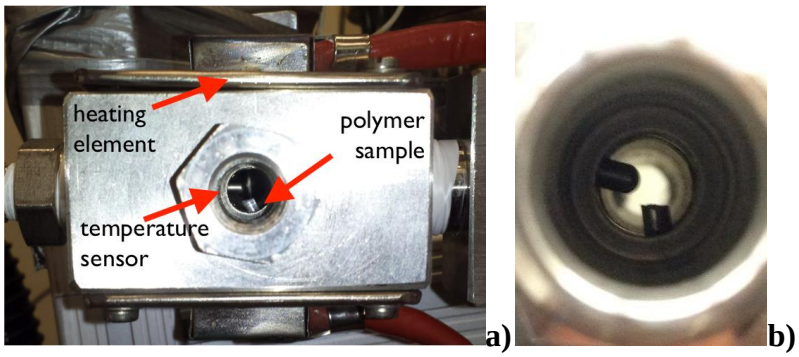

Figure 2: pictures of the details of the mini-batch; a) front view of the cross and, highlighted, some pieces; b) view of the see-through pipe with the temperature sensor and the sample.

Figure 3 shows some scheme of the possible alternative configurations of the mini-batch: a) the cross has, connected to the four ports, the gas release system, the gas dosing valve, the pressure sensor and the temperature sensor, alike in Figure 1; b) a view cell is used (the gas dosing may be done from the same port of the gas release); c) two view cells (to observe the sample in transmission, for better lighting) can be used (the pressure sensor is placed on the temperature sensor port with a T-fitting); d) a full-flow quick connector can be used on the pressure transducer side.

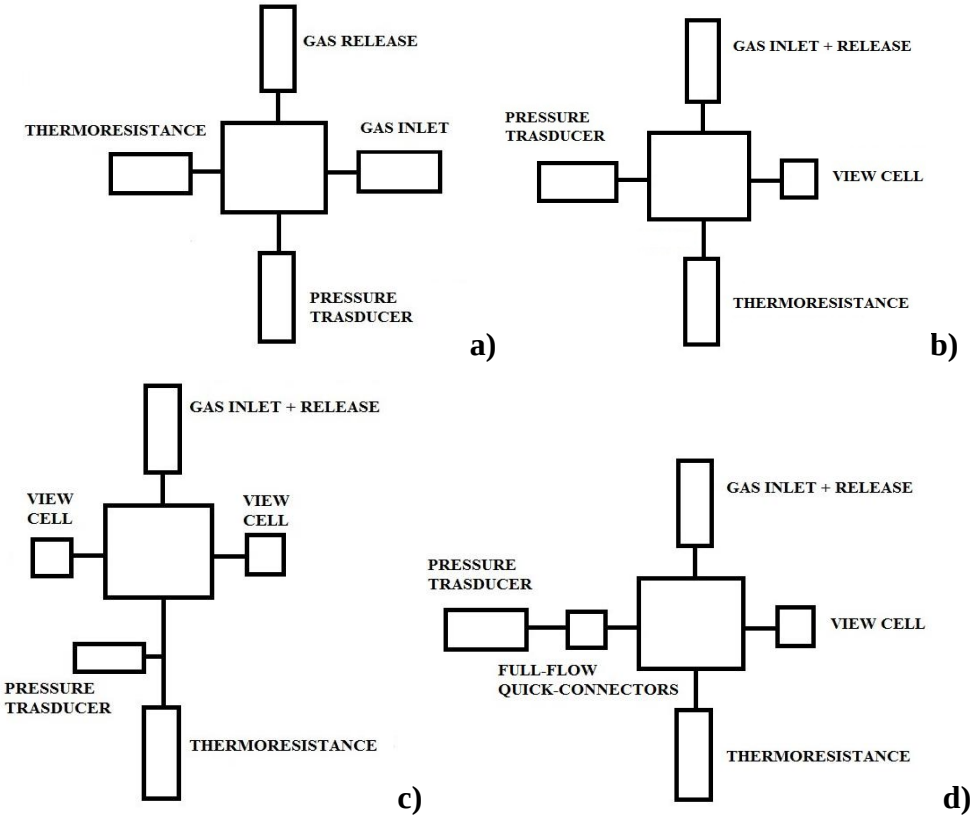

Figure 3: schemes of the possible configurations of the mini-batch.a) basicconfiguration, b) view cell configuration, c) two view cells configuration, d) a full-flow quick connector configuration.

As mentioned, a key feature of the mini-batch is the possibility tovery fast extraction of foamed sample. To tell the truth, in our case, it is a foamed sample expulsion. To clarify this point, Figure 4 shows a rendering of the details of the ball valve opening sequence: in a), the mini-batch is closed (the ball valve is closed), ready for the pressure release, with the polymer sample (dark colored) sitting in the cross; in b), the ball valve has been rotated by 90° in open position; in c), the pellet, dragged by the blowing agent evacuation, starts moving in the pipe towards the exit; in d), the foamed pellet has been expelled. It is worth of note, here, that the sample is expelled at very high speed, and a collecting net has to be used in order not to loose the sample. Finally, it comes quite trivial the consideration about how fast is the sample expulsion with respect to conventional vessel and how fast could be the temperature quench in order to set the newly formed cellular structure, a very important aspect when dealing with foams that are keen to collapse or coalesce.

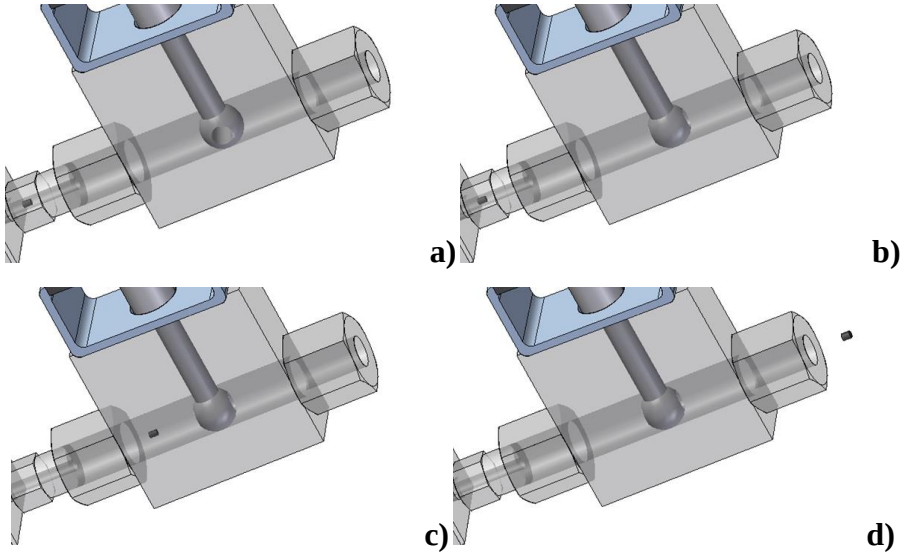

Figure 4: schematic of the sample expulsion. a), closed configuration, b), open configuration c), open configuration, with the pelletdragged by the blowing agenttowards the exit d), open configuration, with the pellets expelled.

As a possible alternative to sample expulsion, of course, it is possible to retain the sample in the mini-batch, akin in a conventional pressure vessel, and remove it after some time, for example to study aging or to perform multiple pressure treatments. In this case, it is possible to use a metallic net between the sample and the blowing agent evacuation piping, as it is shown in Figure 5. In contraposition with "*expelled*" sample (as shown in Figure 4), we will call the sample kept in this way inside the mini-batch as "*retained*".

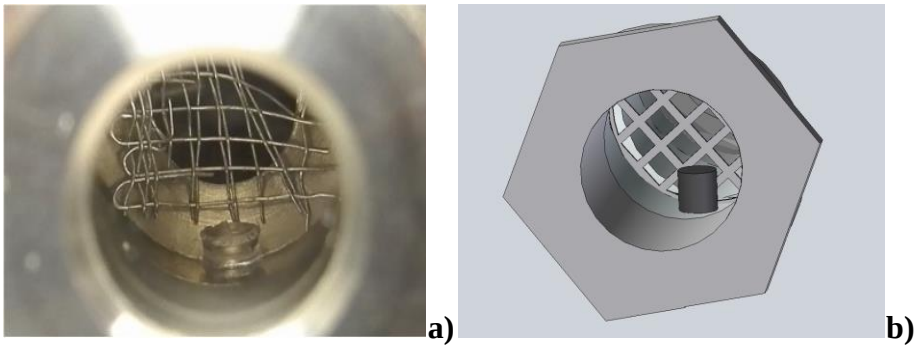

Figure 5: retained sample: a) picture of the actual configuration and b) 3D rendering

Results

The novel foam batch apparatus has been tested to verify the design by using polystyrene and CO_2 as the foaming system.The PS used in this work is PS N2380 supplied by Versalis S.p.A., Mantova, Italy, used as received. The density and melt flow index of the polymer, as

provided by Versalis S.p.A., are 1.05 g/cm^{3}and 2.0g/10 min. Technical grade CO_2 was provided by Sol, Italy. For instance, by selecting several ball valve actuator pressures and/or severaldownstreampipings, we achieved a very wide PDR range(as shown in Figure 6, namely, up to 600 MPa/s from a saturation pressure of 10 MPa, and up to 1'800 MPa/s,from a saturation pressure of 30MPa(PDR was calculated as the highest absolute value of the derivative of the pressure history as the average on 0.004s).

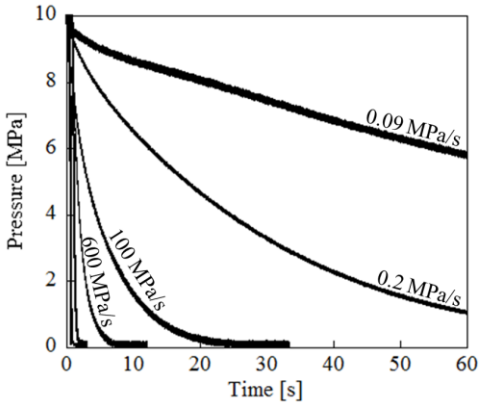

Figure 6: selected pressure histories achieved by using selecting several ball valve actuator pressures and/or several downstream pipings, from a saturation pressure of 10 MPa.

For proper comparison with other batch systems, in terms of relative pressure drop (the PDR over saturation pressure ratio), this means a maximum value of 60s^{-1}; Guo et al. [14] reached a relative pressure drop rate of 90.2s^{-1}, Chen et al. [15]of 7.1s^{-1}, and Muratani et al. [1] of 1.7s^{-1}. Figure 7 shows two pressure histories, together with their time derivative, measured during a blowing agent release in the mini-batch and in a conventional pressure vessel [4].

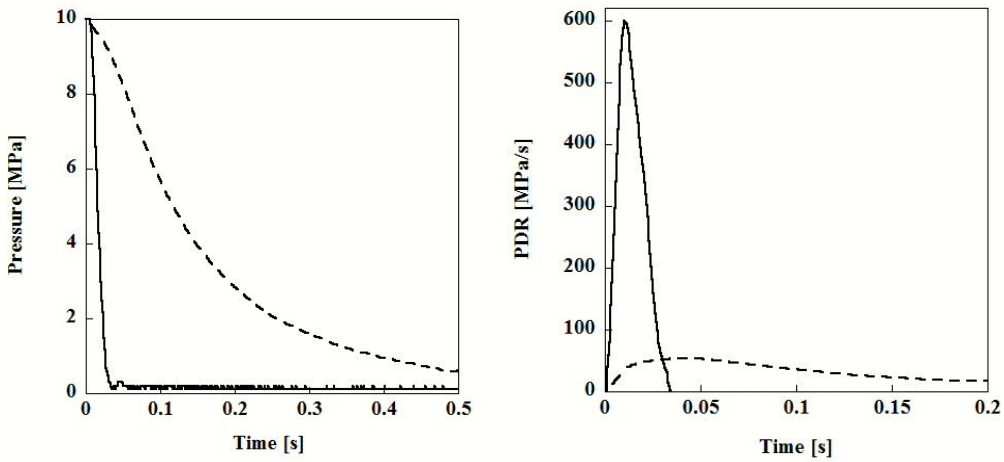

Figure 7: pressure histories during a blowing agent release event for the mini-batch and for a conventional pressure vessel: a) pressure as a function of time; b) time derivative of the pressure. Solid lines, mini-batch; dashed lines, conventional pressure vessel[4-5].

As it is possible to observe, the miniaturization approach led to a large reduction of the blowing agent evacuation time. It is worth of note, here, that we utilized the same ball valve in the two pressure vessel and that, hence, the blowing agent evacuation time is mostly due to the extremely low volume of the mini-batch (25 mL ca.).

As already reported in the *Apparatus* section, there is the possibility to both retain and expell the foamed sample. In particular, it is possible to concurrently foam two samples, one placed upstream of the separating net and one downstream. In this case, the samples would be subjected to the same foaming conditions but to different extraction conditions, one very fast and the other slower (by using the full-flow quick connection the extraction time of the retained sample could be from few seconds to any longer time). This is a key feature of the mini-batch, giving the possibility to study with some greater detail the nucleation and growth phenomena. For instance, Figure 8 reports few SEM micrographs showing the morphologies of selected foamed samples, both expelled and retained. Foaming conditions, final foam density and cell number densities (calculated with respect to the unfoamed volume[16]as $N = \left(\frac{n}{A}\right)^{3/2} \times \left(\frac{\rho_p}{\rho_f}\right)$, where n and A are the number of the cells in the micrographand area of the micrograph (in square centimeter), and ρf and ρs are the density of the foamed and solid sample, respectively) are reported in Table 1. As it is possible to observe by comparing Figure 8a) and 8b), the expelled samples show a finer morphology (cell number densities of expelled samples are 2-3 orders of magnitude higher than the corresponding retained sample) and higher densities (due to temperature quenching of the expelled samples with respect to the retained samples). While the latter result is expected, the former is not a trivial result. To explain it, we could refer to a premature cell coalescence. This subject, however, is beyond the scope of this contribution and will be discussed in a forthcoming paper.

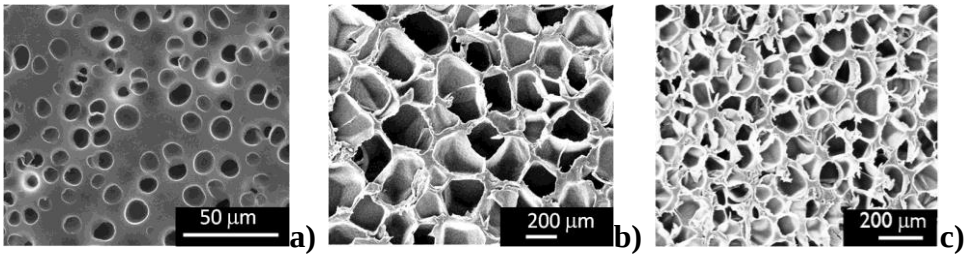

Figure 8: SEM micrographs of expelled a) and retained b) foamed samples; effect of the PDR on the foam morphology c) high PDR; refer to Table 1 for foaming conditions and foam properties (all of the samples were saturated with CO_2 at 100°C and 10MPa).

Sample	**a**	**b**	**c**
PDR [MPa/s]	270	270	600
Foam density [g/cm^3]	0.63	0.20	0.16
Cell number density [#/cm^3]	5.3*10^9	1.9*10^6	1.2*10^7
Type	expelled	retained	retained

Table 1: results of selected foaming attempt; all of the samples were saturated with CO_2 at 100°C and 10MPa; different PDR were achieved by varying ball valve actuator pressures and/or downstream piping.

As an example of the effect of the PDR on the foam morphology, Figure 8 also reports a comparison of two samples foamed at different PDR, saturated in the same conditions (see Figures 8 b) and c)). As expected, the cell number density increases and the cell diameter decreases with the increase of the PDR. A forthcoming paper will discuss about the effect of the PDR on the foam morphology of both the expelled and retained samples.

In order to show the utility of the view cell, Figure 9 reports a sequence of images of a PS sample right after foaming. It is possible to follow the relatively slow growth and the volume and density time evolution.

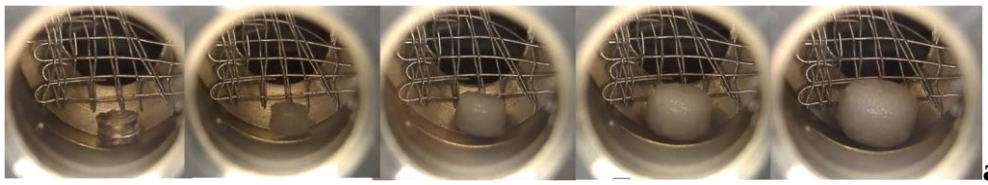
a)

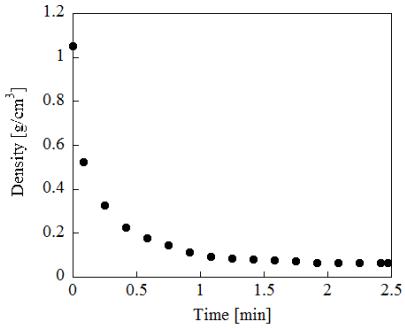

b)

Figure 9: images of PS sample foamed at 80 MPa/s after saturation with CO_2 at 100°C and 10MPa and the resulting density and volume time evolution

Conclusions

In this work, a novel batch foaming equipment has been presented, based on the idea of miniaturization of the pressure vessel, in order to maximize the pressure drop rate. The new design, however, is very versatile and cheap and it has been proved to be useful as a new tool for studying the foaming process. In fact, we achieved PDR ranging from 30 to 1'800 MPa/s, combined with the possibility to observe the sample while foaming and to expell the sample immediately at pressure release or to retain it in the pressure vessel. Several PS foams were produced by using CO_2 as blowing agent at different conditions of PDR and extraction conditions, with a wide range of final foam density and morphologies.

Acknowledgements

This work was supported by the POR CAMPANIA Rete di Eccellenza FSE. Progetto "Materiali e STrutture Intelligenti", MASTRI

References

1. Muratani K, Shimbo M, Miyano Y. Correlation of Decompression Time and Foaming

Temperature on the Cell Density of Foamed Polystyrene. *Cell Polym* 2005; 24: 1.

2. Colton JS, and Suh NP. The nucleation of microcellular thermoplastic foam with additives: Part I: Theoretical considerations.*Polym Eng Sci* 1987; 27: 2.

3. Colton JS,Suh NP. The nucleation of microcellular thermoplastic foam: Process model and experimental results. *Mater Manuf Process* 1986*;*1: 3-4.

4. Marrazzo C, Di Maio E, Iannace S, Nicolais L. Conventional and nanometric nucleating agents in poly (ϵ-caprolactone) foaming: Crystals vs. bubbles nucleation. *Polym Eng Sci* 2008;44: 37.

5. Marrazzo C, Di Maio E, Iannace S, Nicolais L. Foaming of synthetic and natural biodegradable polymers. *J Cell Plast* 2007;43: 123.

6. Doroudiani S,Kortschot MT. Polystyrene foams. II. Structure–impact properties relationships.*J ApplPolymSci*2003; 90: 14.

7. Park CB, Baldwin DF, Suh NP. Effect of the pressure drop rate on cell nucleation in continuous processing of microcellular polymers. *Polym Eng Sci*1995; 10: 7.

8. Han X, Koelling KW, Tomasko DL, Lee LJ. Extrusion of polystyrene nanocomposite foams with supercritical CO2. *Polym Eng Sci* 2002,42: 11.

9. Park CB, Xu D, Popiliev R. Effects of die geometry on cell nucleation of PS foams blown with CO_2. *Polym Eng &Sci* 2003, 7: 4.

10. Leung SN, Wong A, Park CB. Role of processing temperature in polystyrene and polycarbonate foaming with carbon dioxide. *Ind Eng Chem*2009, 48: 4.

11. Sorrentino L, Di Maio E, Iannace S. Poly(ethyleneterephthalate) Foams: Correlation Between the Polymer Properties and the Foaming Process. *J Appl Polym Sci* 2010; 116: 27.

12. Marrazzo C, Di Maio E, Iannace S,Nicolais L. Process-structurerelationships in PCL foaming. *J Cell Plast*2008;44: 37

13. Doroudiani S, Kortschot MT. Polystyrene foams. I. Processing-structure relationships. *J Appl Polym Sci* 2003; 90: 5.

14. Guo Q, Wang J, Park CB, Ohshima MA..A Microcellular Foaming Simulation System with a High-Pressure Drop Rate *Ind Eng Chem Res* 2006; 45: 18.

15. Chen L, Sheth H, Wang X. Effects of shear stress and pressure drop rate on microcellular foaming process. *J Cell Plast* 001 ;37: 4.

16. Salerno A, Di Maio E, Iannace S, Netti PA. Solid-state supercritical CO_2 foaming of PCL and PCL-HA nano-composite: Effect of composition, thermal history and foaming process on foam pore structure. *J Supercrit Fluids* 2011 ; 58 : 1.

4.2 *Polystyrene foams at high pressure drop rates*

In the following paragraph, it is reported the work authored by D. Tammaro, A. Astarita, E. Di Maio, S. Iannace, and titled “PS foams at high pressure drop rates”, submitted to *Industrial & Engineering Chemistry Research* in December 2015 Manuscript ID: ie-2015-04911y.

Polystyrene foaming at high pressure drop rates

D. Tammaro[1], A. Astarita[1], E. Di Maio[1], S. Iannace[2]*

[1]Dipartimento di Ingegneria Chimica, dei Materiali e della Produzione Industriale, University of Naples Federico II, P.le Tecchio 80, I-80125 Napoli, Italy

[2]Istituto per lo Studio delle Macromolecole, Consiglio Nazionale delle Ricerche, Via E. Bassini 15, I-20133, Milano, Italy

submitted to *Industrial & Engineering Chemistry Research* Manuscript ID: ie-2015-04911y

KEYWORDS

foam, polystyrene, CO_2, talc, bubble nucleation, pressure drop rate.

ABSTRACT

We studied the foaming of polystyrene by using the batch foaming technique, with CO_2 as the physical blowing agent, at large Pressure Drop Rates (*PDRs*) and at different foaming temperatures. In order to investigate high *PDRs*, and to easily control the foaming temperatures, a batch foaming apparatus, called "minibatch", recently developed by some of the authors, [Tammaro et al. J. Cell. Plast., 2015, DOI 10.1177/0021955X15584654)] was utilized. With respect to the *PDR* range found in the underlying literature (i.e. from 0.01 to100 MPa/s), larger *PDRs* (i.e. from 50 to 500 MPa/s) were investigated in the present work. The results show that, at each foaming temperature, the number of nucleated bubbles per unit of initial volume (*N*), increases linearly with *PDR* in a bi-logarithmic scale, with slopes increasing with the temperature. The effect of talc as nucleating agent and its role in the effect of *PDR* on bubble nucleation were also investigated. In the last part of the paper, speculating on the effect of both the *PDRs* and the foaming temperatures on *N*, a phenomenological model was developed. This approach allows to predict *N* at very high *PDR*, not accessible experimentally, and at different foaming temperatures. The approach was validated and a good agreement between the model prediction and the experimental data was obtained.

INTRODUCTION

In thermoplastic foaming with physical blowing agent, the Pressure Drop Rate, *PDR*, (i.e. the rate at which the saturation pressure is reduced to ambient pressure by blowing agent release) is an important processing variable[1], being involved in the competition between the bubble nucleation and growth. [2, 3] Many authors investigated the effect of *PDR* on the foam morphology and, to do so, designed foaming apparata capable of achieving, in similar foaming conditions, different *PDRs*. As an instance, Guo et al.[4], designed a batch foaming system to visualize "online" the nucleation phenomenon at high *PDR*. Their system was used with polystyrene (PS)/CO_2, and the results showed that, at higher *PDRs*, a finer cell morphology, i.e. more numerous pores with smaller size was achieved. From a modeling point of view, Taki[5] developed a model of bubble nucleation and growth to predict the number of nucleated bubbles per unit initial volume (*N)* as function of *PDR*, and validated it with a polypropylene (PP)/CO_2 system. Tsivintzelis et al.[6] reported observations on the final foam morphologies of PS/CO_2 obtained at different *PDR*, observing that the mean pore diameter decreases and *N* increased with the increase of *PDR*. In fact, as a general understanding, the increase of the *PDR* increases the rate of stable nuclei formation, meanwhile reducing the chances for the blowing agent to inflate the newly formed bubbles, with a correspondent refinement of the cellular structure. Classical nucleation theory can be invoked, in this context. [11] The thermodynamic instability induced by the pressure drop instantaneously nucleates a myriad of bubbles in the polymer matrix. After cell nucleation, they grow due to the diffusion of the excess gas in the bubbles. The nucleation and growth process during the foaming time compete to avail the excess gas in the system and, if the *PDR* is increased, the nucleation is favoured and a greater number of cells is formed.

In this framework, a very interesting question naturally comes out: what does it happen if the *PDR* is further increased? Is there a limit to the increase of *N* with *PDR*? Khan et al.[7] investigated the effect of *PDR* on cell size and *N* on polymethylmethacrylate and developed a validated modeling in a large range of *PDRs*. They experimentally confirmed the increase of *N* with *PDR*. In addition, they reached a certain critical *PDR* above which *N* becomes constant, reaching a threshold (at ca. 10 MPa/s). Other investigators, on other polymer/gas systems, did not find any threshold at *PDRs* far beyond 10 MPa/s (i.e. up to 100 MPa/s).[4-6] Nevertheless, it is reasonable that the presence of a *PDR* above which *N* reaches a threshold depends on the polymer/gas system. It is also clear that how *N* changes with *PDR* at high *PDR* and the possible presence of a threshold above which *N* reaches a threshold are both not well understood and are

both interesting open problems. In fact, conventional vessels for polymer foaming do not allow to reach high *PDRs*. In this context, some of the authors developed a batch foaming equipment, called "*minibatch*", to substantially increase *PDRs* with respect to conventional vessels.[8] In the present paper, we utilized the minibatch to investigate the morphology of PS foams blown with CO_2 on a wide range of *PDRs* (i.e. from 50 to 500 MPa/s). Furthermore, we studied how the effect of talc as nucleating agent influences the bubble nucleation, at different *PDRs* and foaming temperatures (T_{foam}). To describe the gathered results, a modified version of a model by Muratani et al. was used.[9] This approach allows to predict *N* at different T_{foam} and *PDRs*, with or without talc. The validation of the approach was conducted and a good agreement between the model prediction and the experimental data was obtained.

MATERIALS AND METHODS

The PS (N2380) was supplied by Versalis S.p.A., Mantova, Italy, and used as received. The density and melt flow index, are 1.05 g/cm^3 and 2.0 g/10 min at 200°C and 10 kg. Talc, supplied by Imerys Talc (Toulouse, France) with median particle size equal to 1.8 μm, was used as nucleating agent in 1% wt mixtures. The constituents (i.e. PS and talc), dried overnight under vacuum at 90 °C, were and melt compounded in a co-rotating twin-screw extruder (15 mL Micro Compounder, DSM Xplore, Geleen, The Netherlands). The extrusions were performed at 210 °C in nitrogen atmosphere. The screw speed was 150 rpm, corresponding to average shear rates of ca. 75 s^{-1}, and the residence time, accurately controlled by means of a backflow channel, was 240 s. The extrudate was granulated for subsequent foaming experiments. CO_2 (99.95% pure) supplied by Sol Group S.p.A., Monza, Italy, was used as the physical blowing agent.

The foaming equipment utilized in this study, the *minibatch*, was designed in Tammaro et al.[8] to maximize the *PDR* by minimizing the volume to be evacuated, which allowed reaching *PDRs* as high as 500 MPa/s from a saturation pressure of 10 MPa, and up to 1'800 MPa/s, from a saturation pressure of 30 MPa. The control of the processing parameters was achieved by means of a PID controller (model X1, Ascon-New England Temperature Solutions, Attleboro, MA, USA) and a syringe pump 500D (Teledyne Isco, Lincoln, NE, USA). A pressure transducer (model P943, Schaevitz-Measurements Specialties, Hampton, VA, USA,) was used to measure pressure and the pressure history was registered by using a data acquisition system (DAQ PCI6036E, National Instruments, Austin, TX, USA). *PDRs* were calculated as the highest mean value of the derivative of the pressure history on a period of 0.010s, using a data acquisition

frequency of 1000 Hz. The pressure release system consists of a discharge valve (model 10-80 NFH, High Pressure Equipment Company, Erie, PA, USA) and a pneumatic electro-valve. The pressure discharge system was designed to allow many different *PDRs*, from the same P_{sat}, by using different ball valves actuating pressure and/or different downstream piping.

In a typical experiment, two cylindrical polymeric granules (one neat and another filled with 1%wt of talc particles) were placed in the minibatch. After sample loading, the vessel was heated to the saturation temperature (T_{sat}) and the pressure was increased up to the saturation pressure (P_{sat}) of 10 MPa. After the solubilization time of 4 hours[10], during which the P_{sat} and T_{sat} were maintained constant, pressure was quenched to ambient pressure. In this procedure, in the different tests, T_{sat} was always equal to T_{foam}.

The foams were characterized to determine their densities (ρ) and *N*. ρ was measured according to ASTM D792, using an analytical balance (Mettler Toledo, Columbus, OH, USA). The cellular structure of the foams was investigated by using a Scanning Electron Microscope (SEM). The samples were first sectioned with a razor blade in liquid nitrogen and then coated with gold using a sputter coater. *N* was calculated as $N = \left(\frac{n}{A}\right)^{3/2} \times \left(\frac{\rho_p}{\rho}\right)$, where *n* is the number of the cells in the area *A* of the SEM micrograph, and ρ_p is the density of the solid sample.

As described in Tammaro et al.[8], two kinds of foamed samples may be generated with the minibatch: 1) retained samples, which are foamed within the vessel and subsequently removed after opening the vessel, and 2) expelled samples, that are dragged out by the escaping gas towards the exit of the vessel for a fast extraction and cooling. In the current work, we will only consider retained samples.

RESULTS

Three sets of experiments were performed at three different T_{foam} (i.e. 90°C, 100°C and 110°C), with *PDRs* ranging from 50MPa/s to 500 MPa/s, for samples with and without talc. The results are reported in **Figures 1-5**.

Figure 1 shows the effect of *PDR* on *N* at all of the investigated T_{foam}, for the neat PS foams. It is evident that *N* increases with *PDR*, in all the investigated range of *PDRs*, as it was expected and described in the introductory part. In fact, a linear behavior on a log-log scale is observed, indicating an exponential dependence ($N = a * PDR^b$). For instance, Taki[5] reported a similar behavior of *N* with *PDRs* (from 0.001 to 1 MPa/s) in a bi-logarithmic scale for PP foamed with CO_2 at 200°C and 11 MPa. In the current study, the linear dependence is confirmed on PS/CO_2 system at high *PDRs* (i.e. 50 to 500 MPa/s) and at three different T_{foam}. The slopes, *b*, (in

$\left[\frac{\#}{cm^3} * \frac{s}{MPa}\right]$), of the interpolating lines for *N* versus *PDR* data, increase with the T_{foam}. In particular, *b* = 0.92 at 90°C, 1.03 at 100°C and 1.10 at 110°C. In the **Figure 1** the inset shows *b* as function of *PDR* in a logarithmic scale, it was obtained with the time-temperature shift factor as it will be described in the "modelling by master curve" section. Concerning the relationship between *N* and T_{foam}, at constant *PDR*, for this specific case of CO_2 foamed PS, in the processing range explored in this contribution, *N* decreases with T_{foam}. A theoretical consideration can be invoked to explain the decrease of *N* with T_{foam}. In particular, it is thought that the number of cell nuclei decreases with the reduction of the blowing agent [10,15] solubilized in the polymer as a consequence of the increase of the saturation temperature. [2,16,18]

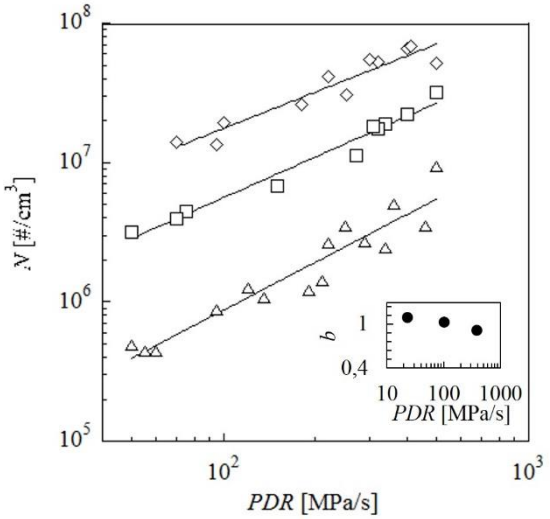

Figure 2. *N* of neat PS foams as function of *PDR* and at different T_{foam} (◇ 90°C, □ 100°C, △ 110°C). The solid lines are obtained by interpolation with $\boldsymbol{N = a * PDR^b}$ (see text for details). The inset shows *b* as a function od the *PDR*.

Figure 2 shows the effect of *PDR* on *ρ* of neat PS foams, in the *PDR* interval ranging from 50 MPa/s up to 500 MPa/s. It is evident that ρ first decreases with the *PDR*, and then it reaches a plateau value for *PDR* higher than ca. 300 MPa/s. Considering one single temperature, all of the samples were subjected to same saturation conditions (P_{sat} is the same for all the samples, see § Foaming procedure), which correspond to same equilibrium concentration of the blowing agent.

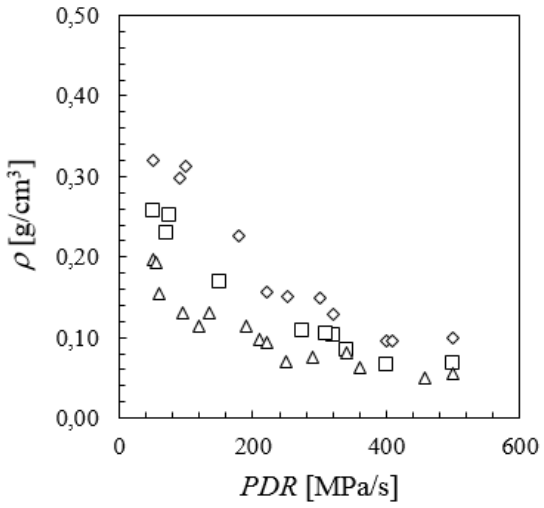

Figure 2. ρ of neat PS foams as function of *PDR* and at different T_{foam} (◇ 90°C, □ 100°C, △ 110°C).

In order to explain the effect of *PDR* on ρ, we may observe that, at lower *PDR* some gas may escape from the free surface of the polymer/gas solution being lost in the surrounding, during the bubble nucleation and growth, with a resulting density increase. With the increase of the *PDR*, instead, bubble nucleation is faster, with a corresponding increased efficiency in the use of the blowing agent. We may speculate, in these foaming conditions, that at *PDRs* of ca. 300 MPa/s and higher, the gas loss from the free surface is negligible and the minimum ρ, for the specific polymer/gas mixtures, foamed at a specific T_{foam}, is achieved.

Considering one single *PDR*, the results show a decrease of ρ with the increase of T_{foam}, due to the favoured growth of the bubbles in a less viscous medium, as also showed by Arora et al.[13]. Finally, in this range of processing conditions, the minimum achievable density is 0.06 g/cm^3.

Figure 3 shows the effect of *PDR* on *N* at all of the T_{foam} for talc-filled PS. It is well known that talc particles induce heterogeneous nucleation[19-21], and this explains the larger *N* (by ca. three orders of magnitude) with respect to the neat PS reported in **Figure 1**. Furthermore, *N* linearly increases with *PDR* for the talc-filled PS, as observed for neat PS. For talc-filled PS, however, the effect of T_{foam} and *PDRs* on *N* is smaller than neat PS: the slopes of the interpolating lines at the different T_{foam} are smaller than those calculated for PS neat. In effect, for talc-filled PS at T_{foam} equal to 110°C, 100°C and 90°C, the slopes, are, respectively, equal to 0.76, 0.64 and 0.51 (in $\left[\frac{\#}{cm^3} * \frac{s}{MPa}\right]$). In addition, a 10 fold increase of *N* is observed when T_{foam} increases from 90°C to 110°C, while, in the case of neat PS a 15 fold increase has been observed. The decreased

dependence of *N* with T_{foam} in the case of talc-filled PS has been already observed by Chen et al.[12] in a study about the effect of *PDR* on neat high density polyethylene and talc-filled high density polyethylene foamed at different saturation pressures. In particular, they observed that the *PDR* effect is larger when the activation energy for the bubble nucleation is higher, which is the case of the neat polymer.[12] In the following, the activation energy for nucleation will be defined the modeling section.

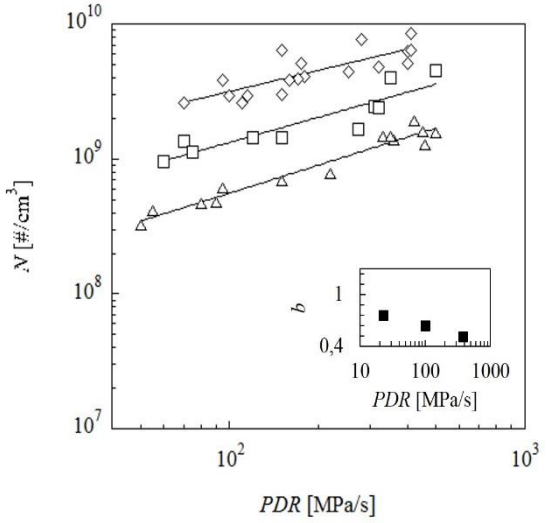

Figure 3. *N* of talc-filled PS as function of *PDR* and at different T_{foam} (◇ 90°C, □ 100°C, △ 110°C). The solid lines are obtained by interpolation with $\boldsymbol{N = a * PDR^b}$ (see text for details). The inset shows *b* as a function od the *PDR*.

In **Figure 4**, the effect of *PDR* on ρ for talc-filled PS foams is showed at different T_{foam}. As already explained for the case of neat PS as a function of *PDR*, a decrease of ρ with the increase of the *PDR* and with the increase of the T_{foam} is observed for talc-filled PS foams. In this case, the minimum achivable ρ is 0.08 g/cm^3, ca. 30% bigger than the minimum ρ achieved with neat PS. This observation is in accordance with the fact that, under the investigated processing conditions, ρ decreases with the T_{foam} since, in the testing conditions under investigation, the phenomenon governing the ρ decrease is the bubbles growth (larger for the neat PS). [13] Possibly, furthermore, a delay in the achievement of a plateau value is observed (in this case, the minimum in the density is attained at ca. 400 MPa/s and higher).

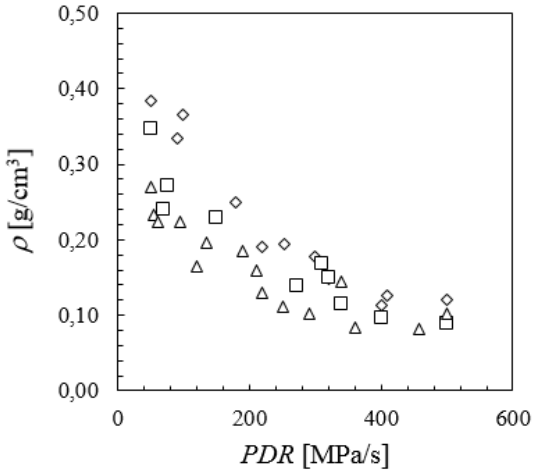

Figure 4. ρ of talc-filled PS as function of *PDR* and at different T_{foam} (◇ 90°C, □ 100°C, △ 110°C).

In **Figure 5**, characteristic SEM images of samples at different T_{foam} and *PDR* for neat and talc-filled PS foams are reported, evidencing what has been already obtained with Figure 1-4. Please note the need for using a larger magnification for the cases of talc-filled samples to properly show the foam morphology.

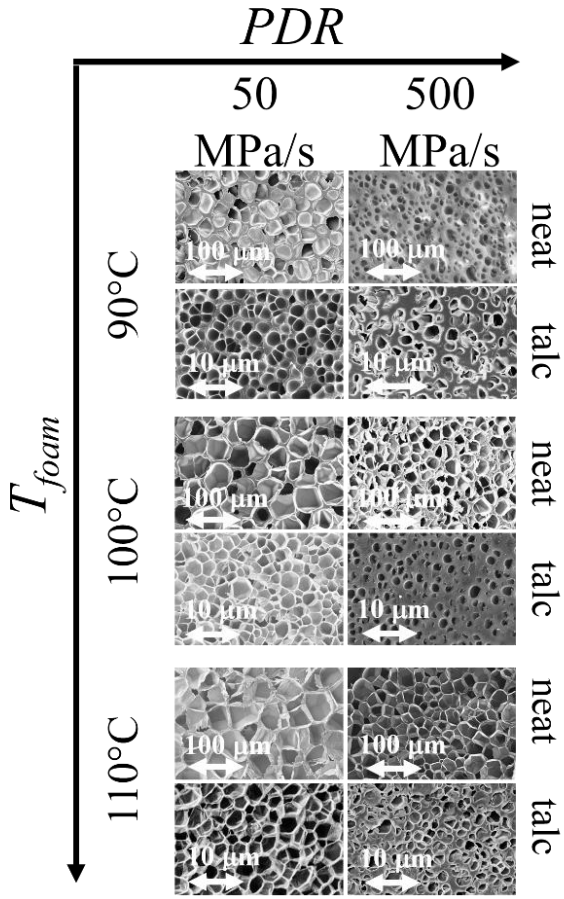

Figure 5. SEM images, showing neat and talc-filled PS foams morphologies at different *PDRs* and T_{foam}.

MODELING

The foaming experiments and the results discussed in the previous paragraphs were used to model the effect of *PDR* and T_{foam} on *N*, by recalling the considerations introduced by Muratani et al. [14] In the final part of this section, the gathered modeling tool is used and validated to design foams with target morphologies.

As it was described earlier, *N* shows both *PDR* and T_{foam} dependence, with *N* increasing with *PDR*, and decreasing with T_{foam}. Speculating on the correlation between *N* and T_{foam}, it is possible, at any *PDR* value, to describe the aforementioned dependences by an exponential law[2], as in eq. 1:

$$\dot{n}\left(T_{foam}, PDR\right) = \dot{n}(T_0, PDR)\exp\left[\frac{E_{app}}{R}\left(\frac{1}{T_{foam}} - \frac{1}{T_0}\right)\right] \quad (1)$$

Where, $\dot{n}$, T_0, E_{app}, R, are, respectively, the bubble nucleation rate (i.e. number of nucleated bubbles per unit of time and initial volume), the reference temperature, the "apparent" activation energy [17], and the ideal gas constant.

The number of nucleated bubbles per unit of initial volume, N, can be estimated by multiplying $\dot{n}$ and the characteristic time of the process, given by $\frac{P_{sat}}{PDR}$. Hence, eq. 1 now reads:

$$\dot{n}\left(T_{foam}, PDR\right) * \frac{P_{sat}}{PDR} = \dot{n}(T_0, PDR) * \frac{P_{sat}}{PDR} \exp\left[\frac{E_{app}}{R}\left(\frac{1}{T_{foam}} - \frac{1}{T_0}\right)\right] \quad (2)$$

Therefore:

$$ln\left[\frac{N\left(T_{foam}, PDR\right)}{N(T_0, PDR)}\right] = \frac{E_{app}}{R}\left(\frac{1}{T_{foam}} - \frac{1}{T_0}\right) \quad (3)$$

Using eq. 3 to fit data at the different T_{foam}, in the case of neat PS, considering 100°C as the reference temperature, T_0, and 100 MPa/s as the reference *PDR*, returns E_{app}=165 kJ/mol. The time-temperature shift factor (a_T) can be estimated by the following equation[14],

$$\ln a_T = \frac{E_{app}}{2.303R}\left(\frac{1}{T_{foam}} - \frac{1}{T_0}\right) \quad (4)$$

Figure 6 shows a_T at different T_{foam}. It is evident that $\ln a_T$ linearly decreases with $1/T_{foam}$ - $1/T_0$.

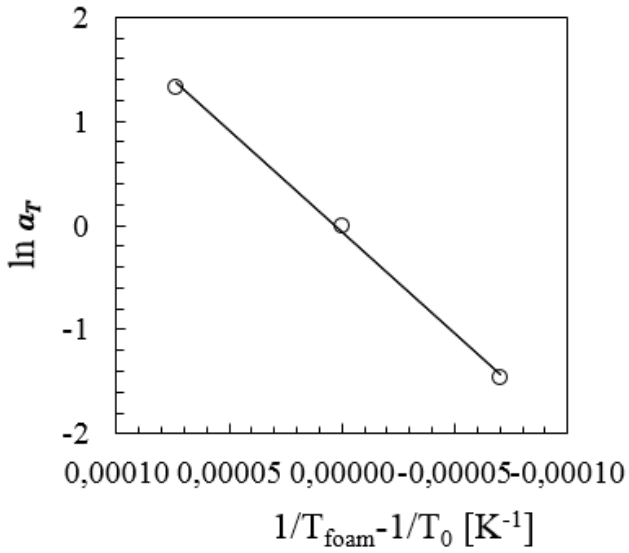

Figure 6. Effect of the T_{foam} on a_T. The solid black line is obtained by interpolation with eq. 4.

As it was explained the use of the shift factor allows to shift data along the *PDR* axis at different T_{foam}:

$$N(T_0, PDR) = N(T_{foam}, PDR * a_T) \quad (5)$$

Figure 7 shows the construction of the master curve. **Figure 7a** shows the relationship between *N* and *PDR* at different T_{foam}, as already discussed in **Figure 1**, and the values of a_T at 90°C and 110°C (100°C has been used as a reference temperature). **Figure 7b** is obtained by shifting the experimental curves of *N* versus *PDR* for neat PS by a_T**PDR*. Hence, data at T_{foam} of 110°C, with a_T less than 1, were shifted towards left and data at T_{foam} of 90°C, with a_T higher than one, were shifted towards right. The master curve for the neat PS foam at 100°C is given by the interpolation of the data at the three different temperatures, as shown in **Figure 7b**. As it is clear in **Figure 7b**, finally, the shifted data based on T_{foam} equal to 100°C, make it possible to increase the range of experimentally accessible PDRs (i.e. grey window) from ca. 10, up to ca. 1000 MPa/s.

Figure 7b shows the variation of *N* on all the extended range of *PDR* and the fitting in terms of the solution of the best equation that has found describing the data in accordance with the behavior of *b* as a function of *PDR*. Herein the slope of *N* as a function of *PDR* at different T_{foam}, *b*, decreases linearly with the *PDR* in a logarithmic scale and, then, a good fitting equation reads:

$$N = c * PDR^{[-d*\ln(PDR/PDR_0)+e]} \quad (6)$$

Where *c*, *d* and *e* are fitting parameters [22] and PDR_0 is the *PDR* at which *N* is equal to $c*PDR^{e-d}$. In particular, the **Table 1** reports the values for neat PS samples and talc-filled PS samples.

fitting parameters	c [s/(cm^3*MPa)]	d	e
neat PS	1500	0.1	2.2
talc-filled PS	26000	0.08	1.4

Table 1. Fitting parameters of the Eq. 6, for neat and talc-filled samples.

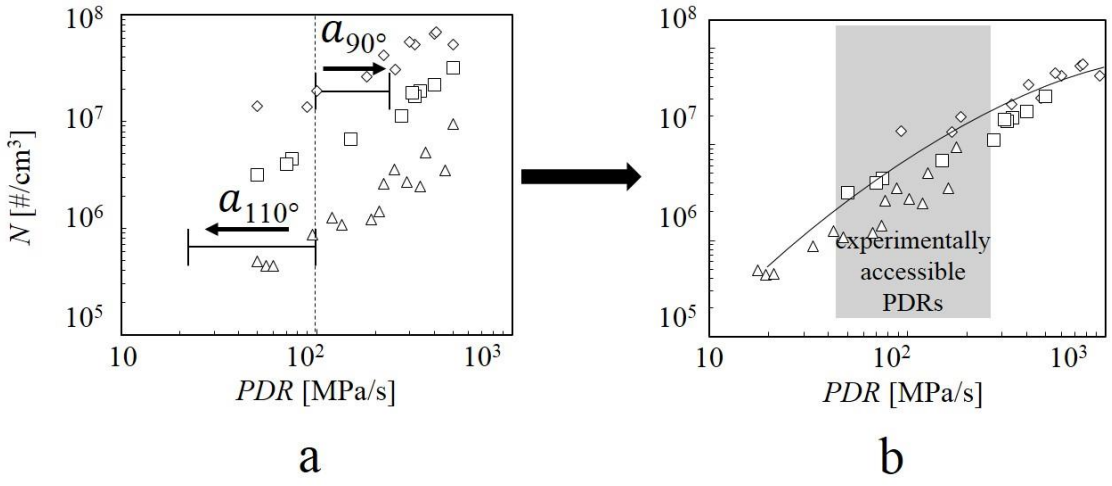

Figure 7. Procedure to build a master curve. a) shows the raw experimental data of *N* versus *PDR* at different T_{foam} (◇ 90°C, □ 100°C, △ 110°C) and how the data at 110 °C and 90 °C were shifted; b) the shifted data are showed and the experimentally accessible *PDR* range is underlined with the grey window. The solid line is the master curve obtained as described in the text.

In the same manner as it was explained for the construction of the master curve for neat PS, a master curve for talc-filled PS was built. In **Figure 8**, talc-filled PS master curve (dashed line) is compared to neat PS master curve. The result is that a lower apparent activation energy (97 kJ/mol) was calculated for talc-filled PS with respect to neat PS [19].

MORPHOLOGY-DESIGN TOOL

In order to verifying any predicting capability of the present approach, and to finally build a design tool to achieve desired foam morphologies (target morphology, $\bar{N}$), we performed an experiment at T_{foam} = 60°C and at *PDR* = 190 MPa/s, that, by scaling to the reference temperature of 100°C, means an extrapolated *PDR* = 1'070 MPa/s (see **Figure 8**), quite far from the accessible experimental window reported in **Figure 7b**. *PDR* extrapolation has been performed based on eq. 4, with a resulting $a_{60°}$ = 5.6. **Figure 9** shows SEM images of neat PS and talc-filled PS foamed at T_{foam} of 60°C and *PDR* = 190 MPa/s. The morphologies are finer than the ones foamed at higher temperature (see **Figure 4**), with smaller cells sizes and ρ = 0.8 g/cm^3 ca. In particular, for the neat PS, *N* = 9.3E10^7 #/cm^3, while for talc-filled PS, *N*=8.4E10^9 #/cm^3 (open symbols in **Figure 8**). To verify the approach, eq. 5 can be used to calculate *N* at 60°C and 190 MPa/s (corresponding to 100°C and 1'070 MPa/s), resulting in 1.5E10^8 #/cm^3 and 9.5E10^9 #/cm^3 for neat and talc-filled PS (closed symbols in **Figure 8**), respectively, which perfectly match the experimental data, proving a good predicting capability of the model at hand, as reported also in **Figure 8.**

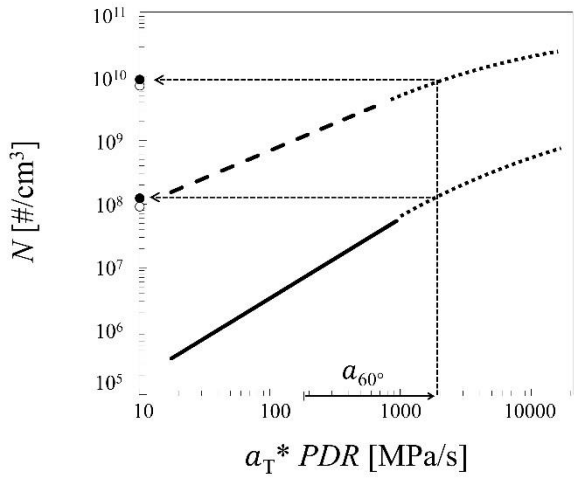

Figure 8. Master curves for neat PS (solid line) and talc-filled PS (dashed line). An extrapolation of the curves (dot lines) can be used to design the foaming process in a larger

PDR range or at different T_{foam} using accessible *PDR*. The open circles (○) represent the experimental *N*, while the closed symbols (●) are the model results.

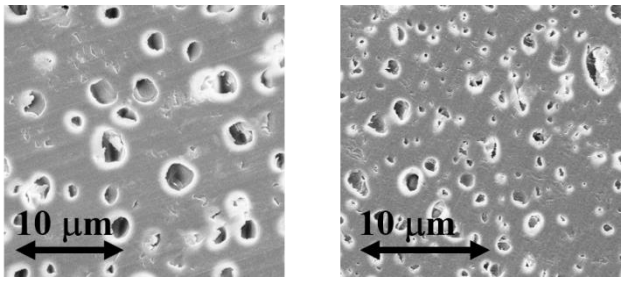

a) b)

Figure 9. SEM images of a) neat PS foams and b) talc-filled PS foams, with P_{sat} = 10MPa and T_{foam} = 60°C.

To conclude, these results prove that, once master curves have been experimentally validated, for the neat polymer or for any polymer-additive mixture, they can be used to design the foaming process to achieve a desired $\overline{N}$. In effect, the horizontal line that intercepts $\overline{N}$ will cross the master curves in two points, giving the $\overline{PDR}$ necessary to achieve $\overline{N}$. Now, if this $\overline{PDR}$ lies outside of the experimentally accessible window, eq. 5 will give the temperature shift factor needed to move horizontally in the experimentally accessible PDR window. It is worth of note that said extrapolation should be performed with caution, since phenomena like polymer vitrification at decreasing temperature may limit the extensibility of the model.

CONCLUSIONS

In this paper, some insight on bubble nucleation at high *PDRs* and at different T_{foam} was gained. In particular, *N* was observed to be linearly increasing with *PDR* in a log-log scale at all of the investigated T_{foam} (i.e. 90°C, 100°C and 110°C), even at very high *PDR*s. The effect of talc as nucleating agent does not qualitatively change the effect of the *PDR* on *N*, however, it reduces the *PDR* influence on *N*, while, at same *PDR*, it induces a 3 orders of magnitude increase in *N*. An experimental approach to predict the *N* at different *PDR* and T_{foam} was presented and validated for the PS/CO_2 system. This easy approach provides a tool to achieve a target morphology by means of master curves describing the combined effect of both T_{foam} and *PDR* on *N*.

CORRESPONDING AUTHOR
edimaio@unina.it, ph. +39 081 768 25 11; f. +39 081 768 24 04

ACKNOWLEDGEMENTS
Rete di Eccellenze Mastri (MAteriali e STRutture Intelligenti, POR Campania FSE 2007/2013, Codice 4-17-3) is acknowledged for partial support of this work.

ABBREVIATIONS
PDR, Pressure drop rate; *N*, cell nucleation density; PS, polystyrene; PP, polypropylene; T_{foam}, foaming temperature; P_{sat}, saturation pressure; T_{sat}, saturation pressure; $\overline{N}$, target morphology; $\overline{PDR}$, target pressure drop rate.

REFERENCES

(1) Colton, J.S.; Suh, N.P. The nucleation of microcellular thermoplastic foam: Process model and experimental results. *Mater. Manuf. Process*, **1986**; 48, 563.

(2) Colton, J. S.; Suh, N. P.; The nucleation of microcellular thermoplastic foam with additives: Part I: Theoretical considerations. *Polym. Eng. Sci.* **1987**; 27, 245.

(3) Park, C. B.; Behravesh, A. H.; Venter, R. D. Low density microcellular foam processing in extrusion using CO_2. *Polym. Eng. Sci.*, **1998**, 38, 1812.

(4) Guo, Q.; Wang, J.; Park, C. B.; Ohshima, M. A microcellular foaming simulation system with a high pressure drop rate. I*nd. Eng. Chem. Res.*, **2006**, 45, 6153.

(5) Taki, K. Experimental and numerical studies on the effects of pressure release rate on number density of bubbles and bubble growth in a polymeric foaming process. *Chem. Eng. Sci.*, **2008**, 63, 3643.

(6) Tsivintzelis, I.; Angelopoulou, A.G.; Panayiotou, C. Foaming of polymers with supercritical CO_2: an experimental and theoretical study. *Polymer*, **2007**, 53, 2563.

(7) Khan, I., Costeux, S.; Adrian, D.; Bunker, S. Numerical studies of nucleation and bubble growth in thermoplastic foams at high nucleation rates, **2013**, Seattle, WA, SPE FOAMS, *Conference proceedings*.

(8) Tammaro, D.; Contaldi, V.; Pastore Carbone, M.G.; Di Maio, E.; Iannace, S. A novel lab scale batch foaming equipment the mini-batch. *J. Cell. Plast.*, **2015**, DOI 10.1177/0021955X15584654.

(9) Muratani, K.; Shimbo, M.; Miyano, Y.; Correlation of decompression time and foaming temperature on the cell density of foamed polystyrene. *Cell. Polym.* **2005**; 24, 198.

(10) Sato, Y.; Takikawa, T.; Takishima, S.; Masuoka, H. Solubilities and diffusion coefficients of carbon dioxide in poly(vinyl acetate) and polystyrene. *J. Supercrit. Fluid.*, **2001**, 19, 187.

(11) Zel′dovich, IAB. Theory of formation of a new phase cavitation, *J. Exp. Theor. Phys*$^{+}$, **1942**, 12, 525.

(12) Chen, L.; Sheth, H.; Wang, X. Effects of shear stress and pressure drop rate on microcellular foaming process. *J. Cell. Plast.*, **2001**, 37, 353.

(13) Arora, K.; A.; Lesser, A. J.; Mccarthy, T. J. Preparation and characterization of microcellular polystyrene foams processed in supercritical carbon dioxide. *Macromolecules*, **1998**, 297, 4620.

(14) Muratani, K.; Shimbo, M.; Miyano, Y. Correlation of decompression time and foaming temperature on the cell density of foamed polystyrene, *Cell. Polym.*, **2005**, 24, 271.

(15) Lee, M.; Park, C.B.; Tzoganakis, C. Measurements and modeling of PS/Supercritical CO_2, solution viscosities, *Polym. Eng. Sci.*, **1999**, 39, 109.

(16) Lee, P. C.; Li, G.; Lee, J. W. S.; Park, C. B. Improvement of cell opening by maintaining a high temperature difference in the surface and core of a foam extrudate, *J. Cell. Plast.*, **2007**, 43, 431.

(17) Alvarez-Idaboy, J. R.; Mora-Diez, N.; Vivier-Bunge, A. A quantum chemical and classical transition state theory explanation of negative activation energies in OH addition to substituted ethenes. *J. Am. Chem. Soc.*, **2000**, 122, 3715.

(18) Lee, M.; Park, C. B.; Tzoganakis, C. Measurements and modeling of PS/supercritical CO, solution viscosities, *Polym. Eng. Sci.*, **1999**, 39, 99.

(19) Wang, C.; Leung, S. N.; Bussmann, M.; Zhai, W. T.; Park, C. B. Numerical investigation of nucleating-agent-enhanced heterogeneous nucleation. *Ind. Eng. Chem. Res.*, **2010**, 49, 12783.

(20) Wong, A.; Park, C. B. The effects of extensional stresses on the foamability of polystyrene–talc composites blown with carbon dioxide, *Chem. Eng. Sci*, **2012**, 75, 49.

(21) Marrazzo, C.; Di Maio, E.; Iannace, S. Conventional and nanometric nucleating agents in poly (ε -caprolactone) foaming : crystals vs bubbles nucleation, *Polym. Eng. Sci.*, **2008**, 56, 216.

(22) Nelder J. A. The fitting of a generalization of the logistic curve, *Biometrics*, **1961**, 17, 89.

GRAPHICAL ABSTRACT (FOR TABLE OF CONTENTS ONLY)

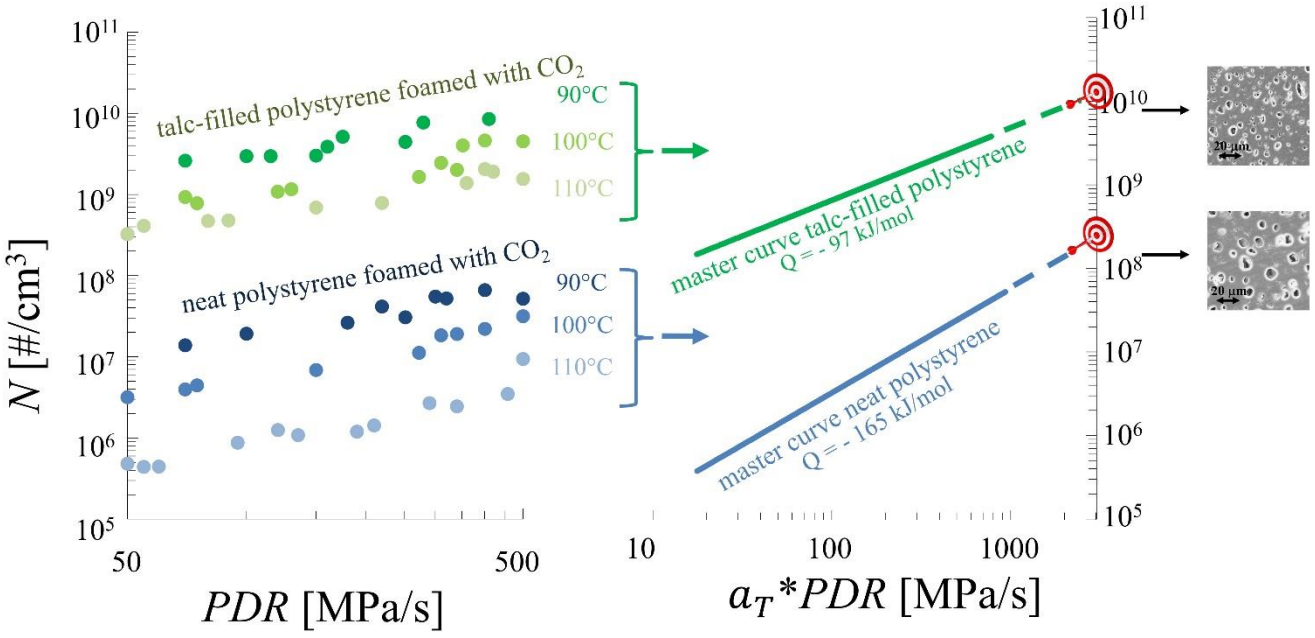

4.3 *Measurements of liquid entrainment between a bubble and an air/liquid interface as a predictor of bulk foam properties*

In the following paragraph, it is reported the work authored by John M. Frostad, Daniele Tammaro, Luciano Santollani, Simone Bochner de Araujo, Gerald G. Fuller, and titled "Measurements of liquid entrainment between a bubble and an air/liquid interface as a predictor of bulk foam properties", submitted in February 2016 to Langmuir, Manuscript ID: ie-2016-01291m.

Measurements of liquid entrainment between a bubble and an air/liquid interface as a predictor of bulk foam properties,

John M. Frostad[1], Daniele Tammaro[2], Luciano Santollani[1], Simone Bochner de Araujo[1], Gerald G. Fuller[1]

[1]Department of chemical enginerring, Stanford University, California, USA
[1]Dipartimento di Ingegneria Chimica, dei Materiali e della Produzione Industriale, University of Naples Federico II, P.le Tecchio 80, I-80125 Napoli, Italy

submitted to *Langmuir* Manuscript ID: ie-2016-01291m

Introduction

Thin liquid films were probably first observed in the form of soap bubbles. The qualitative observations made by Newton (1) and Gibbs (2) revealed that the walls of the soap bubbles grow thinner in time and pass through thicknesses of the order of visible light wavelength. Then different colors appear due to the interference of light reflected from the front and back interfaces. When the thinning process is advanced, thin spots are formed and appear as black spots which are sometimes very unstable. The interest in thin liquid films has kept growing because of their importance to the understanding of dispersed fluid systems. As two drops or bubbles approach one another a film forms between them. The coalescence of the dispersion is directly related to the drainage time and the stability of these films. An emulsion is defined as a liquid phase dispersed in another liquid phase. Emulsions are important in such diverse industrial ' operations as waste water treatment and liquid-liquid extraction (3). A gas phase dispersed in a liquid is called a liquid foam. Foams have various scientific and technological applications (4). For example, because of their low density and their low thermal conductivity, foams have been useful in thermal insulation and fire fighting. Also foaming can be used to

increase fractional conversion in gas-liquid reactions (Triandafilidi, 1958) (5). Recently, in enhanced oil recovery, foam has been used as a mobility control agent. During gas injection recovery process large amounts of oil are bypassed. For example, in steam injection projects, steam channels or fingers through the formation because of its high mobility. In order to alleviate this problem a dilute aqueous surfactant solution is injected with steam. For suitable conditions thin liquid films are generated, retarding flow of steam through certain pathways and therefore reducing its mobility.

In 1961, Fried (6) showed that the injection of aqueous surfactant solutions could reduce drastically gas mobility through porous media. Hirasaki (7), Chambers and Radke (8) have recently reviewed current knowledge of basic mechanisms of foam flow. The mechanism of initial formation and subsequent drainage of thin liquid films leading to their breakage are major inputs to the population balance that predicts the average bubble size or foam texture, a key factor influencing the reduction in gas mobility. Another important parameter is the capillary pressure, i.e., the pressure difference which exists between liquid and gas during foam flow. It depends on, among other things, the surface tension of the liquid and on the relative amounts of liquid and gas present. Khatib et. al. (9) measured capillary pressures in glass bead packs during steady foam flow. They found that drastic foam collapse was occurring at a specified capillary pressure, called "limiting capillary pressure", P1¢. In other words, the coalescence of flowing foam is large for capillary pressure above P1¢ and minimal below P1¢. Aronson et. al. (10) found that the limiting capillary pressure is strongly related to the critical capillary pressure above which a single static liquid film collapses. However Khatib et. al. (9) reported that limiting capillary pressures were also dependent on the gas flow rate and absolute permeability in addition to the critical capillary pressure of a single static liquid film. This last observation indicates that dynamic effects are also important in the stability of foam flowing through porous media. In this thesis, the subject of interest is the drainage of thin films leading to their breakage and thus to the coalescence of dispersions. A thin liquid film consists of two surface layers bounding a liquid interior. The surface active material, present in the liquid phase, is preferentially adsorbed at the surface. A typical diagram of a liquid film is shown Fgure 1a. The thinning of the liquid film is governed by forces within the film which are discussed in the following section.

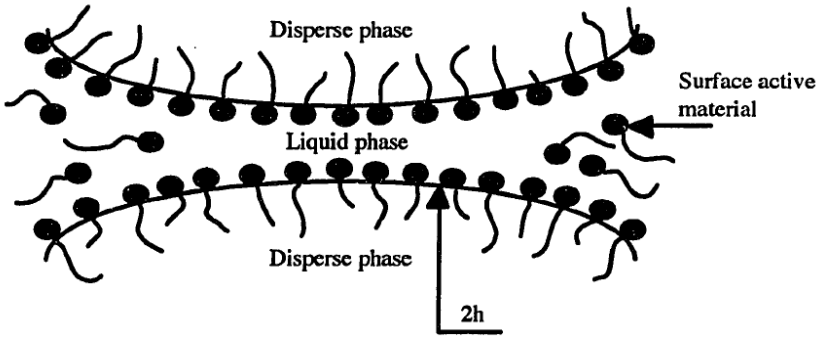

Figure 1a: liquid monolayer with surfactants absorbed.

Understanding the dynamics of foams is has been important to many consumer products and industrial applications [1, 2]. In particular, the influence of surface active compounds on the formation, physical characteristics, and stability of foams continues to be important for new product formulation and process optimization [3]. One important physical characteristic of foams is the volume fraction of air, or "wetness" [3]. Because foams are thermodynamically unstable, the wetness of the foam is a function of time and is influenced by various kinetic processes, many of which have been studied in detail [4].

Foams can be formed in several different ways [5] and in this study, the focus is on the formation of a foam by bubbling a gas into a bulk liquid. This type of foam formation is especially relevant to processes like froth rotation [6] and bubble columns used in scrubbers [7], as well as in consumer products like the foam or "head" that forms on a glass of beer [2]. In this process, the buoyancy of the bubbles causes them to rise to the upper gas/liquid interface where a thin film of liquid are entrained between bubbles and/or between bubbles and the bulk gas phase.

Next, coalescence and other coarsening processes [9] as well as the drainage of liquid out of the thin films [8] determines the wetness of the foam.

One way to study the formation of these foams in this process is to examine the interaction of a single pair of bubbles or a single bubble and a bulk interface. This simplified system has been employed both experimentally [4] and theoretically [10] by previous researchers as a means to understand the fundamental mechanisms involved in foam formation and stability. The same approach is taken here and an experiment was designed to analyze a single bubble which is elevated at a constant velocity until it reaches a particular height relative to the bulk gas/liquid interface.

When the bubble gets close to the bulk interface, hydrodynamic forces will result in the entrainment

of liquid in a thin film in the region of apparent contact. The thickness of the film in this region can be measured using interferometry [5] and can be tracked as a function of time using video microscopy.

Interferometric techniques have been used by many researchers, especially in the well-known Scheludko cell [12], to investigate the dynamics of the liquid drainage out of the film [11].

The majority of these studies were focused on the film stability, measuring the rate of drainage [13] and/or the final stages of drainage where the so-called disjoining pressure becomes important [14]. In this work, the focus is instead on the total amount of liquid that is entrained in the film and how it may relate to the wetness of the resulting bulk foam.

As one would expect, the amount of liquid that is entrained is a function of time. However, the volume of liquid in the "contact" region, where hydrodynamic forces have caused the interfaces to deform, exhibits a maximum value during _lm drainage after the initial contact. The presence of the maximum can be understood by considering a simplified mass balance on the film of liquid:

$$\frac{dV}{dt} = \pi R^2 \frac{dh_{avg}}{dt} + 2\pi R h_{avg} \frac{dR}{dt} \qquad (1)$$

where *V* is the volume of liquid in the thin-film, R is the radial extent of the film, h_{avg} is the average film thickness, and t is the time. In the experiments, *dR/dt* is positive or zero, while dh_{avg}/dt is always negative. Therefore, a maximum in the volume will occur depending on the relative magnitudes of the two terms in equation 1. For larger elevation velocities, this occurs when *dR//dt* changes from positive to zero because the expansion of the film dominates. On the other hand, at lower velocities, the maximum is observed to occur during elevation because the magnitude of the thinning term increases with R^2 compared to the expansion being proportional to *R*.

This under different experimental conditions and with different surfactant systems can then be compared. The fringes produce different colours of reflected light that are well known to correlate to the thickness of the film [11-14]. By measuring the thickness of the film both spatially and temporally, we are able to observe the dynamics of the drainage of the film. This

will enable us to investigate the influence of complex rheology of the bulk fluids as well as the rheology of the interface between the fluid layers.

Methods and Materials

The setup consists of two orthogonally positioned cameras, a capillary for positioning a curved surface (eg. bubble, droplet, or rigid sphere) relative to an interface, a light source for creating Newton fringes, and a motorized stage for translating the curved surface relative to the interface (see figure 1a). For the specific cases of studying drainage from the surface of a bubble or droplet (Figure 1b) a syringe pump and pressure transducer are also included in the setup.

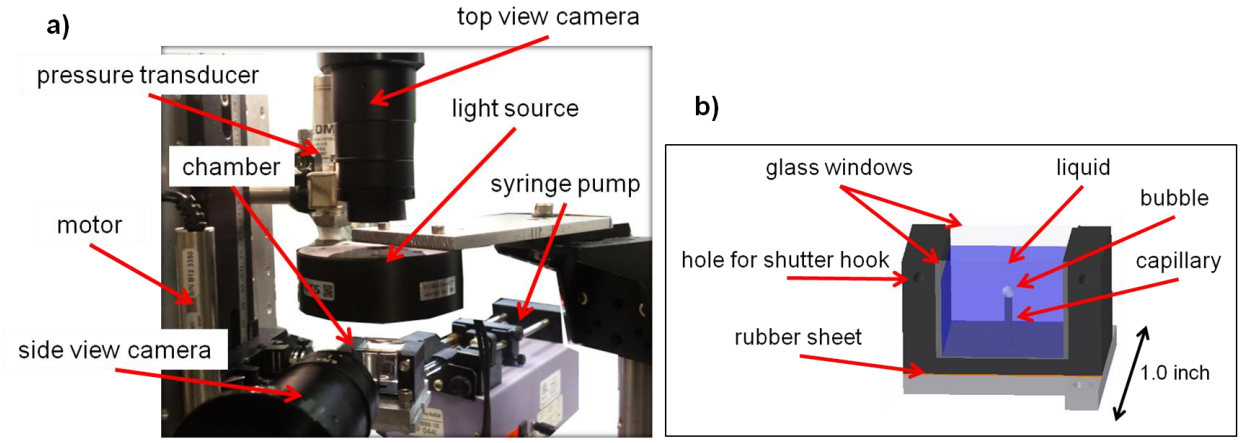

Figure 1: (a) Picture of experimental setup for monitoring thin-film dynamics using interferometry. (b) Schematic of experimental chamber, shown for the case of a liquid/air system.

The pressure transducer enables us to monitor the pressure of the bubble during an experiment, which is related to the instantaneous bubble shape and interfacial tension. The syringe pump is for convenience in carefully generating bubbles or droplets of a particular size. Black Delrin plastic was used to make the chamber containing the fluid of interest in order to reduce the amount of background lighting which adds noise to the observed fringes. Hooks are also added for hanging shutters over the glass windows in the chamber to further reduce background lighting when needed.

The chamber was also designed with a very small volume so that only small amounts of material are needed for testing. This is especially important when testing fluids with expensive or rare materials like monoclonal antibodies or asphaltene surfactants.

A typical experiment is performed by filling the chamber with a fluid, positioning the curved surface at a fixed distance below the upper interface of the fluid, and then translating the curved surface until it protrudes a small amount from the fluid level of the bulk interface. At this point, the fluid drains from the curved surface and when the film is thinner than ~10 μm, fringes can be observed. Figure 2 shows an example of what the fringes look like at various stages of the drainage process for two different fluids. A 10 mM solution of sodiumdodecylsulfate (SDS) responds to gradients in the surface tension and produces chaotic drainage patterns (Figure 2a) while a monoclonal antibody solution (Figure 2b) has an interface with significant rheology that maintains a steady, although irregular, shape of the interface. The irregular shape of the interface is attributed to protein aggregates.

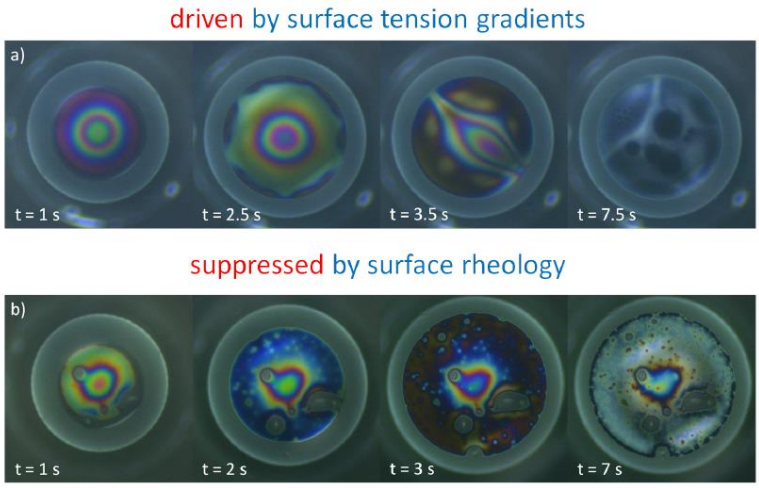

Figure 2: Interference of white light observed during draining of a film of 10 mM SDS solution (a) and monoclonal antibody solution (b) from a curved bubble surface. The drainage can be driven faster by surface tension gradients or supressed by surface rheology.

Figure 3 shows an example of the type of data that is collected. First, the pressure in the bubble is can be recorded during the experiment (Figure 3a). The pressure is steady (with some noise) for the first 10 seconds while the bubble is not moving. Next, the pressure decreases due to decreasing hydrostatic pressure as the bubble translates upwards in the chamber. Eventually, there is a minimum in the pressure where the bubble is level with the bulk interface and then begins to compress due to hydrodynamic resistence. Finally the pressure levels of once the bubble has stopped moving.

At the same time a video is recorded of the interference patterns observed and later post processed to produce the data shown in Figure 3(b) and (c). We observe that the radius of the

film increases as the bubble compresses against the interface and stops increasing once the bubble stops moving. We also observe that the volume of liquid in the film is initially increasing and later decreasing. The maximum in the film volume is taken as a key measurement and discussed in the next section. Finally, statistics of the film thickness such as the maximum and minimum thickness can be plotted and show interesting changes in the rate that are signatures of different phenomena that occur during drainage such as the formation of "plumes" (originally observed by Mysels and described in his book).

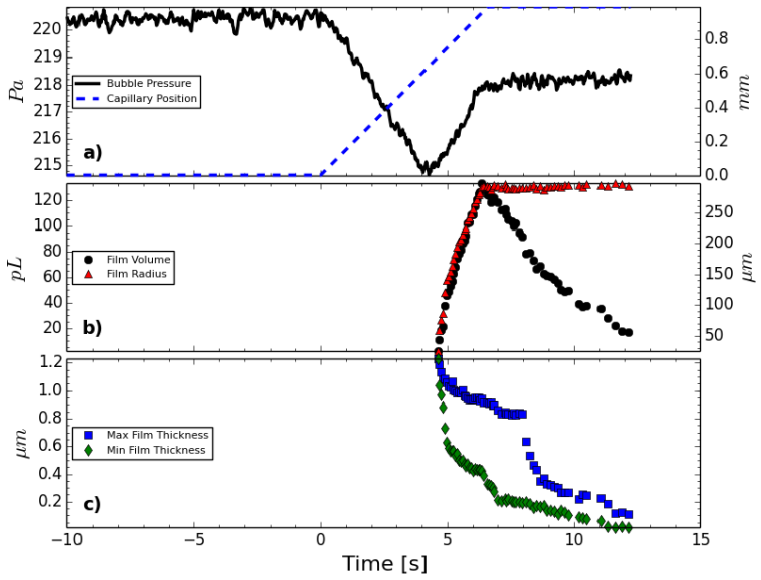

Figure 3: Data for 1.0 μL bubble elevated at 150 μm/s in a solution of 10 mM SDS. (a) Pressure measured inside of the bubble (left) and position of the capillary (right). (b) Volume (left) and radial extent (right) of the thin film of liquid between the bubble and the bulk air as measured via interferometric analysis. (c) Maximum and minimum thicknesses in the thin-film region.

Results and Discussion: drainage from bubbles

We performed a systematic variation of the elevation velocity and the concentration of surfactant in solution while holding the bubble size constant and quantified the results in two ways. The first measurement was to quantify the time required for coalescence, or drainage time. This is measured from the time that the bubble begins to be compressed due to hydrodynamic interaction with the bulk interface until coalescence occurs. The onset of bubble compression is marked by the minimum in the pressure curve (see Figure 3(a)) and coalescence

is observed visually in the video as well as by a very rapid change in the bubble pressure. Figure 4 shows the drainage time as a function of elevation velocity at a fixed surfactant concentration of 10 mM, and as a function of surfactant concentration at a fixed velocity of 150 μm/s.

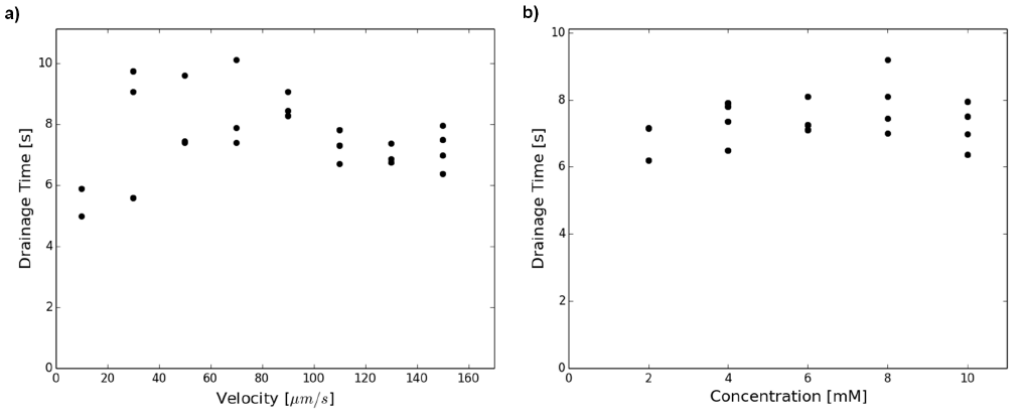

Figure 4: Drainage time as a function of elevation velocity (a) at 10 mM SDS, and surfactant concentration (b) at 150 μm/s.

The second measurement was of the maximum volume entrained in the thin-film.

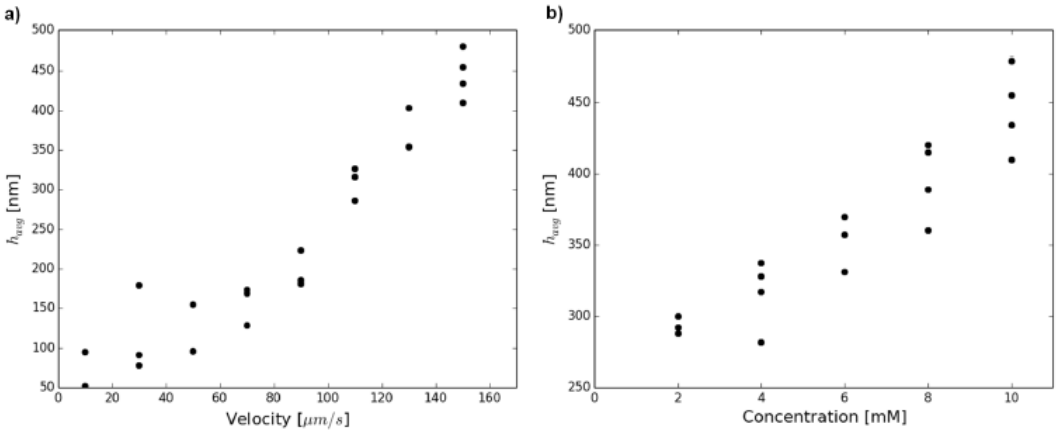

Figure 5: Average film thickness at the point when the film volume has reached a maximum, as a
function of elevation velocity (a) at 10 mM SDS, and surfactant concentration (b) at 150 μm/s.

Interestingly, just measuring these two quantities we immediately found some counter-intuitive results. First, we found that there was no significant variation in the drainage time with varying velocity or surfactant concentration. This is especially surprising when compared to the observation that the amount of liquid entrained in the _lm increases both with increasing velocity and with increasing concentration. Another remarkable point is that both of these trends are agnostic to the critical micelle concentration of the SDS solution which occurs at 6.3 mM (as measured by the pendent drop method), above which the surface tension of the solution is essentially constant.

Conclusions

Bubble columns that produce foam are commonly found in waste water treatment and other industrial processes. The head on a glass of beer is another familiar example of foam formed by bubbles rising through a liquid and collecting on the surface. The characteristics of the foam that is formed in these systems such as the foam height, density and lifetime are all dependent on the properties of the surface-active compounds that are present in the liquid. In the present seminar, a fundamental study of single bubble interactions at a planar air-liquid interface will be discussed. When a single bubble moves upward and reaches the interface, a thin film of liquid is formed that drains and eventually ruptures. The volume of liquid entrained in this film is important in determining the properties of the resulting foam. For example, thicker films will tend to produce more dense foams. A thicker film may also take longer to drain and therefore result in taller foam heights and/or more stable foams. Using interferometry, the volume of liquid entrained in the film is measured for several different surfactant systems. The properties of the surfactants, including interfacial rheological properties, are then related to the volume of fluid entrained in the film.

References

[1] R. J. Pugh. Foaming, foam films, antifoaming and defoaming". In: Advances in Colloid and Interface Science 64 (1996), pp. 67-142.

[2] Elisabeth Steiner, Martina Gastl, and Thomas Becker. \Protein changes during malting and brewing with focus on haze and foam formation: a review". In: European Food Research and

Technology 232.2 (2011), pp. 191-204.

[3] Martin A. Bos and Ton van Vliet. Interfacial rheological properties of adsorbed protein layers and surfactants: a review". In: Advances in Colloid and Interface Science 91.3 (2001), pp. 437- 471.

[4] Stoyan I. Karakashev and Emil D. Manev. Hydrodynamics of thin liquid films: Retrospective and perspectives". In: Advances in Colloid and Interface Science. Reinhard Miller, Honorary Issue 222 (2015), pp. 398-412.

[5] Katsuichi Kitagawa. Thin-film thickness profile measurement by three-wavelength interference color analysis". In: Applied Optics 52.10 (2013), p. 1998.

[6] Newton I. Optics ; London: 1704.

[7] Gibbs J. W. Trans. Connecticut Acad. 1878, 3, 108-343.

[8] Lissant K. J. Emulsions and Emulsion Technology ; M. Dekker: New York, 1984.

[9] Bickerman J. J. Foams: Theory and Industrial Applications ; Reinhold: New York, 1953.

[10] Triandafilidi I. G. Khim. Ihechnol. T opliv. Masel 1958, 3, 27.

[11] Fried A. N. U. S. Dept. of Interior, Bureau of Mines 1961, report 5866.

[12] Hirasaki G. J. J. Petrol. Tech. 1989, 41, 449.

[13] Chambers K. T.; Radke C. J. Interfacial Phenomena in Petroleum Recovery; Morrow, N. R. Ed.; Surfactant Science Series 1991, 23, Ch. 6, 191-255.

[14] Khatib Z. I.; Hirasaki G. J.; Falls A. H. Soc. Petr. Eng. Res. Eng. 1988, 3(3), 919-926.

Chapter 5: summary and key contributions

In this Chapter 5, it is reported the summary of the all thesis and the key contribution given by the research work (i.e. a resume of the results to be published or already published). The next paragraph resume the content of the thesis and the second paragraph resume the key contributions.

5.1 *Summary*

Cell nucleation, growth, deterioration, and collapse phenomena in plastic foaming processes determine the final foam morphology, and hence the foam's application and quality. The successful development of high-quality foams with customizable cell morphology (e.g., closed-cell foams with high cell density, open-cell foams with high porosity, and foams with large volume expansion) for specific applications hinges on the scientific advancement on the knowledge of thermodynamics, kinetics, and rheological behaviours in these phenomena. In this context, this thesis investigated the fundamental mechanisms of cell opening in plastic foaming processes via modeling the entire foaming process and the successful development of a novel experimental apparatus, which is able to reach processing condition difficult to be achieved in typical foaming equipment, was achieved.

5.2 *Key contributions*

Validated modeling of bubble growth, impingement and retraction to predict cell-opening in thermoplastic foaming

We have developed a novel approach to cell opening in thermoplastic foams. The procedure is based on sequential steps. Single bubble growth predictions are used as input for an

impingement model where two (or more) bubbles surrounded by a viscoelastic fluid grow and hydrodynamically interacts. The stresses, deformation rate and film thickness available as output of the model are used in cell wall rupture and cell wall retraction criteria to determine the final structure.

The experiments have shown the correctness of the qualitative nature of the model results developed in this year for the foaming of biodegradable polymer and cell opening. In particular, the developed approach allows designing the processing parameters as well as the material combinations (e.g. in terms of the use of solid additives) to control cell opening and cell wall retraction.

As potential continuations, there are many possibilities for all the parts involved in the project. In the following the main points of possible future discussions are summarized.

1. modeling

- extend to 3D to better define the stress/strain histories in the fluid before opening
- development of a model for bubble opening
- development of a model for film retraction
- define the criteria for cellular structure collapse
- development of a model for cellular structure collapse
- validate the model with other polymer/gas system

2. polymer characterization

- sorption/interfacial/volumetric properties of other polymer/gas solutions
- extended rheological measurements, in shear and elongation, eventually with CO_2
- extended thermal properties, eventually with CO_2

3. foaming attempts

- multiple bubble foaming
- use of different blowing agent (N_2, R134a)
- continuous (extrusion) foaming

A novel lab-scale batch foaming equipment: the mini-batch

A novel batch foaming equipment has been presented, based on the idea of miniaturization of the pressure vessel, in order to maximize the pressure drop rate. The new design, however, is very versatile and cheap and it proved useful as a new tool for studying the foaming process. In fact, we achieved PDR ranging from 30 to 1800 MPa/s, gained the possibility to optically

view the sample while foaming and to expell the sample immidiately at pressure release or retain it in the pressure vessel. Several PS foams were obtained by using CO_2 as the blowing agent in different conditions of PDR and extraction conditions, with a wide range of final foam density and morphologies.

PS foams at high pressure drop rates

In "*PS foams at high pressure drop rates*" paper some insight on bubble nucleation at high *PDR* and at different T_{foam} were discussed. It was discussed, how the increase of *PDR* and the decrease of T_{foam} improve the bubble nucleation obtaining a finer foam morphology. In particular, *N* increases linearly as a function of *PDR* in a log-log scale at all the T_{foam} investigated (i.e. 90°C, 100°C and 110°C) even at very high *PDR*s. The effect of talc as nucleating agent does not change qualitatively the effect of the *PDR* on *N*, however, it reduces the *PDR* influence on *N* while inducing a 3 orders of magnitude increase in *N*. An experimental approach to predict the *N* at different *PDR* and T_{foam} was presented and validated for the PS/CO_2 system. This easy approach supplies a validated tool to design the foaming process from the master curve drawn. In the current work, as an instance, it was presented the possibility to choose an *N* value a priori, and then, set the right parameters (i.e. *PDR*, talc and T_{foam}) from the extrapolation of the master curves.

Measurements of liquid entrainment between a bubble and an air/liquid interface as a predictor of bulk foam properties

Our work this year has focused on developing a new experimental setup that is capable of performing precise, repeatable experiments to quantify the gravity driven drainage of thin films of fluid from curved surfaces. In the previous work, on which the current proposal was based, we observed that when a thin layer of fluid drains off of a solid, curved surface, Newton fringes can be observed due to the interference of light reflected from both sides of the thin film. The fringes produce different colours of reflected light that are well known to correlate to the thickness of the film. By measuring the thickness of the film both spatially and temporally, we are able to observe the dynamics of the drainage of the film. This will enable us to investigate the influence of complex rheology of the bulk fluids as well as the rheology of the interface between the fluid layers. It will also aid in the testing and development of theoretical models.

Now that our setup is completed and we have some initial results for SDS solutions, our next steps will be to perform additional experiments with other surfactant solutions draining from bubbles. We plan to vary the surfactants chosen such that we observe different Marangoni stresses for surfactants with no measurable interfacial rheology and well as several surfactants with significant interfacial rheology. In each of these cases we have will be collecting a rich set of data that upon analysis will lead to additional opportunities to understand the fundamental physics in these systems. For example, we observed something when examining the pressure data that is worth pursuing. The pressure increase during the compression of the bubble was qualitatively observed to be only partially correlated to the interfacial tension of the system. This is interesting because it implies that additional information about the surfactant on the bubble can be obtained from measuring the pressure during bubble compression. We plan to perform a systematic set of experiments to determine what additional information can be gained from this measurement. We also plan to make further refinements to the setup to enable the systematic study of liquid/liquid systems and multilayer systems.

Acknowledgements

Rete di Eccellenze Mastri (MAteriali e STRutture Intelligenti, POR Campania FSE 2007/2013, Codice 4-17-3) is acknowledged for partial support of this work.